

Scalable Ab Initio Electronic Structure Methods with Near Chemical Accuracy for Main Group Chemistry

Wei, Y.,^{†,‡} Debnath, S.,^{†,‡} Weber, J. L.,[†] Mahajan, A.,[†] Reichman, D. R.,[†] and
Friesner, R. A.*[†]

[†]*Department of Chemistry, Columbia University, New York, New York 10027, United
States*

[‡]*Equal contribution*

E-mail: raf8@columbia.edu

Abstract

This study evaluates the precision of widely recognized quantum chemical methodologies, CCSD(T), DLPNO-CCSD(T) and localized ph-AFQMC, for determining the thermochemistry of main group elements. DLPNO-CCSD(T) and localized ph-AFQMC, which offer greater scalability compared to canonical CCSD(T), have emerged over the last decade as pivotal in producing precise benchmark chemical data. Our investigation includes closed-shell, neutral molecules, focusing on their heat of formation and atomization energy sourced from four specific small molecule datasets. Firstly, we selected molecules from the G2 and G3 datasets, noted for their reliable experimental heat of formation data. Additionally, we incorporate molecules from the W4-11 and W4-17 sets, which provide high-level theoretical reference values for atomization energy at 0 K. Our findings reveal that both DLPNO-CCSD(T) and ph-AFQMC methods are capable of achieving a root-mean-square deviation (RMSD) of less than 1 kcal/mol across the combined dataset, aligning with the threshold for chemical accuracy. Moreover, we make efforts to confine the maximum deviations within 2 kcal/mol, a degree of precision that significantly broadens the applicability of these methods in fields such as biology and materials science.

1. Introduction

Quantum chemical methods have seen significant improvements in accuracy and computational efficiency when applied to the chemistry of main group elements over the last three decades. Density functional methods, which scale formally with system size N as N^4 or N^3 and in practice as N^2 or even N (for very large systems), can routinely be applied to systems with hundreds to thousands of atoms, with the best functionals providing an average unsigned error on the order of 2–3 kcal/mol for atomization energies of small molecules.¹ Alternatively, coupled cluster with perturbative triples (CCSD(T)) has been integrated into numerous quantum chemistry software packages in a robust manner, offering average error rates close to 1 kcal/mol for atomization energies of the same category of small molecules; however, the computational cost scales as N^7 .^{2,3} Benchmark methodologies that incorporate higher-order coupled cluster terms and more elaborate treatment of core-valence interactions are capable of producing results reliably within 1 kcal/mol deviation from experimental values.⁴ However, the high computational demand of these approaches limits their application to very small molecular systems.

While the accuracy that can be achieved with modern DFT approaches is extremely impressive, DFT calculations on large data sets reveal a significant number of outliers with errors significantly larger than the 2–3 kcal/mol cited above as the average unsigned error. Importantly, outliers can be obscured when large data sets are used and only the average errors are reported.¹ In a subsequent paper, we will examine in detail the outlier distribution obtained for a range of modern functionals when compared to benchmark methods and curated experimental results. For the present purposes it is sufficient to note that more work remains to be done to improve the robustness of DFT approaches across a wide range of chemistry, even for main group molecules. Moreover, systems containing transition metals can be prone to a higher incidence of outliers.⁵

A consequence of the above observation is that high-level wavefunction-based approaches remain highly relevant in practical applications despite the significantly greater computa-

tional cost as compared to DFT calculations. When addressing the grand challenge of understanding the chemistry of complex systems via quantum chemistry, the initial step typically involves conducting a comprehensive set of DFT calculations to explore various possible structures and reaction mechanisms. However, in refining the results to select the correct reaction mechanism (for example) and in general to achieve chemical accuracy, the ability to do benchmark-level wavefunction-based calculations would be extremely valuable. Furthermore, accurate wavefunction calculations are the best path forward, via the production of benchmark training data sets, to developing improved DFT methods in which the magnitude and frequency of outliers are substantially diminished.

However, in order for wavefunction-based methods to effectively address complex systems, an approach is needed which scales better with system size than the N^7 of conventional CCSD(T). The past decade has seen the development of two notable methods that address this need, both leveraging the concept of orbital localization—a technique tracing back to Pulay’s work in the 1980s.⁶ The first is localized coupled cluster (e.g. L-CCSD(T)), the most widely used implementation of which is the DLPNO algorithm of Neese and coworkers.^{7–9} The formal scaling of DLPNO-CCSD(T) is N^3 ¹⁰ and extremely impressive timing and accuracy numbers over a wide range of systems (and particularly those restricted to main group chemistry) have been published in the past 5 years.^{11–16} DLPNO and related methods (for example other local CCSD(T) methods such as LNO-CCSD(T)¹⁷ and PNO-CCSD(T)¹⁸) represent a revolution in quantum chemical technology as it is now possible to obtain something close to CCSD(T) quality results for systems containing on the order of 100 atoms.

The second approach is auxiliary field quantum Monte Carlo (AFQMC). The AFQMC algorithm was originally developed in the physics community, but it is only in the past 5 years that significant progress has been made in creating a scalable version of the methodology for the *ab initio* study of molecules. There are several different implementations currently in use.^{19–22} In the present paper, we will focus on two of these implementations. The first

is a GPU implementation developed in our groups²³ that exploits localized orbitals²⁴ in a fashion similar to that employed in L-CCSD(T), reducing the formal scaling of AFQMC from N^4 to N^3 . We refer to this approach as L-AFQMC. The second^{25,26} is a CPU-based code optimized to enable systematic convergence of the bias in AFQMC energies to near-exact accuracy by using a large number of determinants in the trial function. We designate this implementation as W-AFQMC since it is based on use of the generalized Wick’s theorem. As yet, this method has not been formulated in a localized representation, although work in that direction is ongoing.²⁷ To avoid high computational costs, here we employ W-AFQMC to resolve discrepancies identified in DLPNO-CCSD(T) and L-AFQMC data.

While the computational cost scaling of L-AFQMC and L-CCSD(T) with system size is similar, L-CCSD(T) is considerably faster due to a smaller prefactor. The advantage of AFQMC is that it is formally exact in the limit of the exact trial wavefunction, and in practice, multireference electronic states can often be readily converged due to the ease of utilizing a multiconfigurational trial function.^{26,28–31} This is more crucial for transition metal containing systems than for main group molecules, but there are still main group cases where AFQMC can achieve demonstrably greater accuracy with scalable trial wavefunctions.^{32,33} While such trials allow systematic convergence of the bias in phaseless AFQMC (ph-AFQMC), this accuracy comes at the cost of greater computational expense. Designing protocols for generating trials that strike a desired balance between accuracy and cost is an active area of research. Based on our testing with the benchmark sets, we present two approaches with different cost-accuracy trade-offs.

We believe that having two scalable benchmark methodologies with distinct theoretical frameworks offers substantial benefits. These benefits extend not only to the generation of data for evaluating and parameterizing DFT functionals but also to their direct application to challenging systems, like the manganese cluster in Photosystem II. As an example, in one of our recent papers we investigated reactions of organolithium systems relevant to lithium ion batteries.³⁴ We performed DLPNO-CCSD(T) and L-AFQMC calculations to look at

both reaction energies and barrier heights. The agreement between the two approaches was remarkably good (a few kcal/mol) across the various reactions that we investigated. We were therefore able to settle on benchmark numbers and use those to evaluate many different DFT functionals, discovering that only a few were able to reproduce the benchmark results reliably. We were then able to use the preferred functionals in computing energies for a large set of organolithium cluster geometries, which we then utilized in parametrizing a machine learning force field (MLFF) for carrying out simulations of lithium ion battery electrolytes.³⁵ While there was no reason, *a priori*, to doubt the performance of DLPNO-CCSD(T) for these systems, there is very little experimental data available for comparisons, and the validation by a second independent benchmark approach provided a much higher degree of confidence in the results than would otherwise have been possible.

In the present paper, our goal is to provide an assessment of the accuracy of both DLPNO-CCSD(T) and L-AFQMC for main group chemistry atomization energies. We have chosen to focus on atomization energies because (a) a relatively large and reliable data set of benchmark experimental and theoretical values is available for a range of small molecules and (b) atomization energies are one of the most difficult properties for electronic structure methods to compute to high precision, due to the large changes in correlation energy upon atomization, and the relatively minimal cancellation of error. We combine four data sets: the G2^{36,37} and G3^{38,39} sets of Pople and coworkers, which claim to have experimental atomization energies that are accurate to 1 kcal/mol or better, and the W4-11⁴⁰ and W4-17⁴¹ (TAE - total atomization energy) data sets of Karton, Martin and coworkers, which employ very high level (and hence expensive) theoretical methods to achieve the same level of reliability. The W4-17 set, the latest iteration of the W4 sets, is an extension of the W4-11 set, as is G3 an extension of G2 with the addition of larger molecules. W4-17, however, is restricted to molecules with no more than 8 heavy atoms. On the other hand, the G3 data set contains larger molecules than the W4-17 heavy atom limit and therefore provides a test of how the quantum chemical methods perform for larger systems. There are (as far as we have

been able to ascertain) no cases where the errors in the W4-11 and W4-17 results exceed the proposed error bars. In contrast, we have had to update a number of the G2 and G3 experimental values with more recent benchmark values.

Our objective with regard to accuracy is to limit the outliers to a maximum of 2 kcal/mol deviation from the experimental or W4 theoretical values. While 2 kcal/mol is not what is generally meant by “chemical accuracy” (that terminology is conventionally reserved for a 1 kcal/mol accuracy level), it is likely to be sufficient accuracy for choosing among alternative reaction mechanisms in complex systems or parametrizing new functionals. An examination of the details of the W4-17 approach suggests that it is going to be difficult if not impossible (at least with current computing capabilities) to construct a *scalable* approach that reliably achieves 1 kcal/mol precision. Our belief is that the maximum 2 kcal/mol level of error that we are aiming for will be good enough not only to analyze chemical reactions in complex systems but also for designing novel chemistries to address a variety of problems in biology and materials science. This is superior to any current DFT functional, where the average errors of the best functional for the current data set are in the range of 2–3 kcal/mol, but the maximum errors are on the order of 8–10 kcal/mol (as we will enumerate in a subsequent publication).

The paper is organized as follows. In Section 2, we discuss the data sets including our updating of a number of the reference values in the G2 and G3 sets. We then discuss computational methods including our scalable formulation of AFQMC, DLPNO-CCSD(T), and CCSD(T) methodology (enabling comparisons for the larger systems), basis sets, core-valence corrections, scalar relativistic corrections, extrapolation to the complete basis set limit, and treatment of atomic energies. Section 3 presents the results for all three methods as compared to the relevant experimental or theoretical benchmarks and discusses their implications. In Section 4, we conclude by summarizing our results and discussing future directions. In general, the performance of both DLPNO-CCSD(T) and L-AFQMC are quite robust, with only a few apparent outliers above our targeted 2 kcal/mol threshold. We

investigate these outliers using more accurate trials with the W-AFQMC method. This enables us to identify outliers arising from the approximations in the methodology, as opposed to cases that are most likely errors or uncertainties in a few of the experimental reference data. Using this targeted convergence of ph-AFQMC, we are able to produce high-quality atomization energies while minimizing cost over a large dataset.

2. Methods

2.1. Datasets

In this study, we have limited our selection to closed-shell, neutral molecules, excluding carbenes. Future work will investigate open-shell systems and ions. In total, 116 molecules are selected from G2 set and 73 molecules from the G3 set respectively. Moreover, the W4 sets also contain significant overlap with molecules from the G2 and G3 sets. After removing duplicates, we are left with 38 molecules from the W4-11 set and 32 molecules from the W4-17 set. The G3 and W4-17 extensions consist of generally larger molecules. Therefore, for the purpose of this study, such separation into “G2”, “G3”, “W4-11”, and “W4-17” is constructive, with the former two sets using experimental heat of formation as reference and the latter two using W4 theory as reference. In total, we have compiled a list of 259 unique molecules across all datasets, with the full list of molecules and the dataset into which each molecule is sorted given in the SI Section 1.

2.2. Reference Values

Reference values for the W4 sets are high-level theoretical atomization energies at 0 K, excluding zero-point energy (ZPE) (labeled as the property TAEe by Karton et al.⁴¹). The reference values for the G2 and G3 sets are experimental heats of formation at 298 K, and the same as those used by Curtiss et al.^{36,38} However, there are some exceptions where we have found conflicting values, as summarized in Table 1, where each of the sources of

Table 1: New vs old reference values for heat of formation. The reference values in the column ‘Previous $\Delta_f H(298\text{ K})$ ’ are the same as used in the original G2/G3 test set papers.^{37,39} All values are reported in kcal/mol. Where the source reports an experiment uncertainty, we have included the uncertainty in the table along with the value.

Molecule	Dataset	Previous $\Delta_f H(298\text{ K})$	Updated $\Delta_f H(298\text{ K})$	Source of update
AlCl ₃	G2	-139.7±0.7	-142.0	W4
AlF ₃	G2	-289±0.6	-290.7	W4
CCl ₂ CCl ₂	G2	-3.0±0.7	-5.1±0.2	ATcT
CF ₂ CF ₂	G2	-157.4±0.7	-161.1±0.1	ATcT
CH ₂ CH-CN	G2	43.2±0.4	44.7±0.2	ATcT
Cyclobutene	G2	37.4±0.4	38.5±0.1	ATcT
Cyclopropene	G2	66.2±0.6	67.8±0.1	ATcT
LiF	G2	-80.1	-81.45±2	CCCBDB
Vinyl chloride	G2	8.9±0.3	5.2±0.06	ATcT
Azulene	G3	69.1±0.8	73.6	CCCBDB
Benzoquinone	G3	-29.4±0.8	-28.7	CCCBDB
Tetramethylsilane	G3	-55.7±0.7	-51.7±0.5	ATcT

the updated reference is listed. The reported reference values from ATcT^{42,43} postdate the G2 and G3 papers. Furthermore, ATcT collates the most recent experiments and theory from various sources using a self-consistent approach and numerous different reactions⁴⁴ and is readily updated.⁴⁵ Therefore, where ATcT data is available and conflicting with the reference used by Curtiss et al., we instead use the ATcT value. In addition, for the cases of AlCl₃ and AlF₃, we found disagreement between the experimental heats of formation and the W4 reported atomization energy. Moreover, the heat of formation values of these molecules are not present in the ATcT database. Thus, for the updated reference values of these molecules, we have converted the W4 atomization values into heats of formation at 298 K using temperature corrections from DFT (refer to Section 2.9 for details). For the three cases of LiF, azulene, and benzoquinone, where no ATcT or W4 value is available, we use the references reported by the NIST database CCCBDB⁴⁶ instead of those reported by Curtiss. As shown in Table 1, the two sources also give conflicting heats of formation for these three molecules. All of our benchmark wavefunction methods yield results that are within 2 kcal/mol of the latter source, rather than the former reference values. Although

this choice is not based on information about the reference alone, CCSD(T) and AFQMC offer independent evaluations of the experimental data, especially in the case of conflict. In particular, we converge AFQMC with respect to the number of determinants for these cases using W-AFQMC. We refer the reader to Section 2.9 for the method of obtaining deviations against reference values.

2.3. Phaseless AFQMC Formulation

Provided that an initial state $|\phi_i\rangle$ has a nonzero overlap with the exact ground state of a system $|\phi_0\rangle$, then the the ground state can be projected from any such trial state as

$$|\phi_0\rangle \propto \lim_{\tau \rightarrow \infty} e^{-\tau \hat{H}} |\phi_i\rangle, \quad (1)$$

where τ is the imaginary time, and \hat{H} is the electronic Hamiltonian under the Born-Oppenheimer approximation which can be written as a sum of one-electron and two-electron terms,

$$\hat{H} = \hat{H}_1 + \hat{H}_2 = \sum_{pq} h_{pq} c_p^\dagger c_q + \frac{1}{2} \sum_{pqrs} V_{pqrs} c_p^\dagger c_q^\dagger c_s c_r. \quad (2)$$

h_{pq} are one-electron integrals and $V_{pqrs} = (pr|qs) = \langle pq|rs\rangle$ (chemists' and physicists' notation respectively) are two-electron integrals. Numerically, we propagate

$$|\phi(\tau + \Delta\tau)\rangle = e^{-\Delta\tau \hat{H}} |\phi(\tau)\rangle, \quad (3)$$

where $|\phi(0)\rangle = |\phi_i\rangle$. The one-body and two-body terms in \hat{H} can be split using the Trotter-Suzuki decomposition,

$$e^{-\Delta\tau(\hat{H}_1 + \hat{H}_2)} \approx e^{-\Delta\tau \hat{H}_1/2} e^{-\Delta\tau \hat{H}_2/2} e^{-\Delta\tau \hat{H}_1/2} + O(\Delta\tau^3), \quad (4)$$

which introduces an error that scales with the timestep. The Hubbard-Stratonovic transformation and the phaseless approximation (see below) also induce timestep errors. We show in SI Section 2 that for this work, the timestep error converges at around $\Delta\tau = 0.005 \text{ Ha}^{-1}$ for frozen-core calculations, and at around 0.001 Ha^{-1} for all-electron calculations. We note that in the calculation of AFQMC energy differences, there is some approximate cancellation of time-step errors.

The two-body operators can be decomposed as the sum of the square of one-body operators through Cholesky decomposition or density fitting. The Hubbard-Stratonovich transformation then converts an exponential with two-body operators into a multidimensional integral over fluctuating auxiliary fields, x_α ,

$$e^{-\Delta\tau(\sum_\alpha \hat{L}_\alpha^2)/2} = \prod_\alpha \int_{-\infty}^{\infty} \frac{1}{\sqrt{2\pi}} e^{-x_\alpha^2/2} e^{\sqrt{\Delta\tau} x_\alpha \hat{L}_\alpha} dx_\alpha + O(\Delta\tau^2), \quad (5)$$

and we arrive at

$$|\phi(\tau + \Delta\tau)\rangle = e^{-\Delta\tau \hat{H}} |\phi(\tau)\rangle = \int d\mathbf{x} p(\mathbf{x}) \hat{B}(\mathbf{x}) |\phi(\tau)\rangle, \quad (6)$$

where $p(\mathbf{x})$ is a Gaussian probability density function and $\hat{B}(\mathbf{x})$ is a one-body propagator depending on the auxiliary fields \mathbf{x} . This multidimensional integral is evaluated using Monte Carlo importance sampling to obtain a stochastic representation of the wave function. For a more in-depth description of AFQMC, we refer the reader to these review articles. [47,48](#)

Due to the fermionic sign problem, the signal-to-noise ratio generally decays exponentially during the imaginary time propagation. It is possible to eliminate the sign problem using a constraint at the expense of a bias in the resulting energies. In this work, we use a constraint referred to as the phaseless approximation (ph-AFQMC), where the phase of the walkers is restricted according to a trial wavefunction. The bias induced by the trial wavefunction can be systematically reduced by improving its quality, for example, by increasing the active space or number of determinants included in the trial. The bias is formally zero in the limit

of the exact trial (see the next subsection, Section 3.3, and SI Section 3 for trial details). We refer the reader to our previous work²⁴ for our approach to localized ph-AFQMC (L-AFQMC) which involves compressing the electron repulsion integrals in the localized orbital basis. Effectively, the scaling for the energy evaluation, the steepest scaling step with system size, is $N^2M + N_{\text{det}}N^2$ (with a prefactor depending on the compressed electron repulsion integral tensor), where M is the number of basis functions, N is the number of electrons, and N_{det} is the number of determinants. See SI Section 4 for an estimate of localization error. For the practical deployment of L-AFQMC, we have developed two protocols, AFQMC 0 and AFQMC I, which are discussed in detail below as well as in Section 3.3. AFQMC I is a scalable AFQMC protocol (scaling $\sim N^3$) that achieves an accuracy comparable to that of DLPNO-CCSD(T), albeit with a significantly larger prefactor for the computation time. AFQMC 0 uses a black-box but less elaborate trial function, but is less accurate, particularly for molecules with significant multireference character.

We also present results for a selected subset of molecules computed with another implementation of AFQMC.^{25,26} This method, which uses a generalized Wick’s theorem approach to efficiently evaluate energies with multideterminantal trials, will be referred to in what follows as W-AFQMC. The advantage of this approach is that it scales as $MN_{\text{det}} + N^2M^2$, which allows the use of a larger number of determinants in the trial wavefunction at an accessible computational cost. It enables one to converge the phaseless bias to the near-exact limit in a given basis set by increasing the number of active space orbitals and determinants included in trial wavefunctions. We use W-AFQMC to calculate energies of the outliers obtained from AFQMC I using on the order of 10,000 determinants and refer to the results in which the L-AFQMC outliers are replaced by the W-AFQMC results as AFQMC II (along with a select few other cases, see SI Section 3). This approach helps us to more confidently address the question, discussed in detail below, as to whether the AFQMC I outliers are due to the phaseless bias or more likely the result of errors in the reference data. We also run apparent DLPNO-CCSD(T) and CCSD(T) outliers with AFQMC II to assess their status.

2.4. AFQMC Trial Generation

In this work, we use a procedure to generate multi-determinant HCI (heat bath configuration interaction) and HCISCF trials for the entire dataset. The CAS family of trials (in this work, we use the HCI solver^{49,50}) provides a robust way of including static correlation in the reference of AFQMC and has been shown^{19,28} to generally perform more accurately than single determinant trials. Nonetheless, the selection of active space for these methods is non-trivial. Akin to multireference perturbation theory methods, a common practice is to use an active space, usually minimal, based on chemical intuition and to pick the leading determinants from the expansion in this active space. However, this does not systematically provide chemically accurate energies. Here, we generally follow a two-step process to select the active space in a relatively automated way that can be applied to large datasets. First, HCI is performed on a “valence” active space, selected based on the atomic composition of the molecule. See SI Section 3 and main text Section 3.3 for the considerations for selecting this active space. Using the spatial 1-RDM of the resulting state, we calculate the natural orbitals and their occupation numbers (NOONs) in the natural orbital basis. We choose a subset of active orbitals from this set based on a NOON threshold (δ) as $\delta \leq \text{NOON} \leq 2 - \delta$. This procedure is often used to flag the more correlated group of orbitals in quantum calculations. A second HCI calculation (or HCISCF for W-AFQMC trials, refer to the SI Section 3) is then performed with the second smaller active space, and this forms the final trial wavefunction. Generally, we choose the number of determinants necessary to retain 99.5% of the CI weight from this final trial wavefunction unless indicated otherwise. Briefly, AFQMC 0 is fully automated and uses L-AFQMC, and thresholds are chosen to be loose, and for the outliers with AFQMC 0, AFQMC I combines trials with larger active spaces, and AFQMC II in turn combines trials with even larger active spaces run with W-AFQMC. This progression gives some indication of the number of determinants required to converge each molecule, but not much more than necessary. For more details, refer to the discussion in Section 3 and SI Section 3.3.

All L-AFQMC trials were generated with the PySCF package⁵¹ where we obtain the Hamiltonian and electron repulsion integrals. The HCI trials are obtained using Dice^{49,50,52} in conjunction with PYSCF. L-AFQMC energy is measured in blocks of size 0.1 Ha^{-1} of 20 timesteps each (each timestep being 0.005 Ha^{-1}). In total, we propagate for between 2000 and 3000 such blocks for each molecule, with 1920 total walkers. W-AFQMC calculations used the same time-step of 0.005 Ha^{-1} for molecules containing only first row atoms, and used a time step of 0.0025 Ha^{-1} for those with heavier atoms. For W-AFQMC, we use 250 walkers and propagate for 1000 blocks of 50 timesteps each.

2.5. CCSD(T) and DLPNO-CCSD(T)

CCSD(T) and DLPNO-CCSD(T) calculations are carried out using the ORCA package⁵³ using restricted Hartree-Fock (RHF) as the reference state. DLPNO-CCSD(T) correlation energies are extrapolated to the complete pair natural space (PNO) using the procedure in Altun et al.⁵⁴ and employing TightPNO thresholds,⁵⁵ between T_{CutPNO} thresholds of 10^{-6} and 10^{-7} for each basis set used. The matching auxiliary basis set is used if available, otherwise, the AutoAux⁵⁶ functionality is used. Where linear dependence is encountered with AutoAux, we increase the even-tempered expansion factor for the s-shell from 1.8 to 2.0.

2.6. Basis Sets

We use the following basis sets: aug-cc-pVXZ-DK ($X = \text{T}, \text{Q}$) for atoms with atomic number less than or equal to that of oxygen, and aug-cc-pCVXZ-DK ($X = \text{T}, \text{Q}$) for fluorine and heavier, obtained using the Basis Set Exchange database.⁵⁷⁻⁶³ This choice is motivated by the documented improvement of basis set convergence when using core-valence or tight-d functions in the basis set for second-row elements (Na-Cl)⁶⁴⁻⁶⁷ as well as fluorine.⁶⁸ While the split-valence aug-cc-pVXZ basis sets are not designed for core-valence correlation,⁶⁹ we find that all-electron calculations using these same basis sets can reach a respectable (especially

for CCSD(T)) albeit overall inferior accuracy (especially for AFQMC) to the frozen core calculations supplemented with MP2 core corrections, as discussed briefly in Section 3, and in more in detail in SI Section 5.

We extrapolate all single point energies to the complete basis set (CBS) limit according to the method of Neese and Valeev⁷⁰ for T/Q extrapolation for both Hartree-Fock and correlation energy, with α and β matching the basis set used. We use the same coefficients α and β for the core-valence sets aug-cc-pCVXZ-DK as the corresponding aug-cc-pVXZ-DK basis sets, where we use the aug-cc-pVXZ coefficients reported by Neese and Valeev. This CBS procedure is used by all the methods investigated, with the exception of the more expensive CCSD(T) and W-AFQMC where we use alternative schemes (see SI Section 3 and Section 6).

2.7. Frozen Core Corrections

Frozen core calculations are carried out according to freezing no orbitals for H-Be, 1s orbitals for B-Mg, and 1s and 2p orbitals for Al-Ar. We correct the core-valence energy using MP2,

$$\Delta_{CV} = E_{CC-MP2}^T - E_{FC-MP2}^T \quad (7)$$

where CC and FC denote core-correlated and frozen-core calculations, respectively. We used the aug-cc-pCVTZ-DK basis set for both calculations. Note that we freeze the 1s electrons in second-row atoms even in the CC calculations. In the following discussion, we focus on the frozen core calculations (along with the MP2 core correction above) for all four methodologies. All electron results for CCSD(T), DLPNO-CCSD(T), and L-AFQMC are presented and compared with the frozen core results in Tables S9 and S10 of the Supplementary Material. In general we do not see any deterioration in accuracy from the use of the frozen core, and recommend that this approach be used going forward for both AFQMC and CCSD(T) based calculations.

2.8. Relativistic Effects

Scalar relativistic effects are included through the DKH2⁷¹⁻⁷³ Hamiltonian for DLPNO-CCSD(T) and CCSD(T), and X2C⁷⁴ for ph-AFQMC, as X2C is not implemented in ORCA and DKH2 is not implemented in PySCF. The MP2 core-valence corrections follow the same relativistic corrections for each method, respectively (MP2 is carried out in ORCA for correcting DLPNO-CCSD(T) and CCSD(T) corrections and in PySCF for ph-AFQMC corrections). The difference between DKH2 and X2C energies are shown to be small for HF and MP2 and mostly cancelled out by atomic energies (see SI Section 7). Spin-orbit corrections to atomic energies are applied using the values from Curtiss et al.³⁶

2.9. Heat of Formation and Atomization

Atomization energies ($\sum E_{\text{atoms},g} - E_{\text{molecule},g}$) and heats of formation are calculated according to the method in Ref.,^{36,75,76} including geometry optimization and thermochemical properties (ZPE, enthalpy, internal energy) using the DFT functional B3LYP^{77,78} and basis set 6-31G*⁷⁹⁻⁸² using the Jaguar software package⁸³ with the maximum available grid point density. A few molecules required a higher-level geometry optimization (see SI Section 8). After optimization, DFT single-point energies were calculated with Jaguar. We note that the first step towards obtaining the heat of formation at 298 K is the atomization at 0 K, and the molecule temperature corrections (from DFT), atom temperature corrections (from experiment) and energy to change the atomic states from gas to standard state (from experiment, i.e. heat of formation of the single atom in the gaseous state) are added to achieve the heat of formation. Experimental values for the atomic heats of formation and temperature corrections are the same as that used by Curtiss et al.,³⁶ with the exception of the sulfur atom heat of formation where we use 66.18 kcal/mol from ATcT⁴² instead of 65.66 kcal/mol.

We emphasize here that as opposed to atomization energy, the heat of formation is defined using standard states of atoms rather than the gas phase state. Nonetheless, these quantities are closely related and in the analysis we convert the W4 atomization energy at 0 K to heat

of formation,

$$\Delta_f H(0 \text{ K}) = \sum_{\text{atoms}} \Delta_f H_{\text{atoms}}(0 \text{ K}) - \Delta_a E(0 \text{ K}), \quad (8)$$

where $\Delta_a E(0 \text{ K})$ is the atomization energy at 0 K. With the addition of aforementioned temperature correction terms from DFT ($H^{298 \text{ K}} - H^{0 \text{ K}}$ for the molecule) and experiment ($H^{298 \text{ K}} - H^{0 \text{ K}}$ for the atom), we obtain $\Delta_f H(298 \text{ K})$. Although these corrections are approximate (even though we expect the errors to be small), they cancel out when obtaining the deviation from the converted W4 heat of formation reference value as the same corrections are applied to the calculated atomization energy of the molecule. Effectively, the deviation D becomes

$$D = \Delta_f H_{\text{expt}}(298 \text{ K}) - \Delta_f H_{\text{calc}}(298 \text{ K}) \quad (9)$$

or

$$D = -(\Delta_a E_{\text{W4}}(0 \text{ K}) - \Delta_a E_{\text{calc}}(0 \text{ K})) \quad (10)$$

for G2/G3 and W4-11/W4-17 sets, respectively, where the only effect of the conversion of the W4 reference values to heat of formation is a change in sign of the deviation from the reference atomization energy. This simple change ensures we are comparing the same quantities.

2.10. Atomic Energies

The treatment of atoms is essential in achieving the targeted accuracy. An explicit near-exact treatment of core-valence correlation on par with valence correlation, as is done in W4-17, requires expensive core-valence corrections. In AFQMC, similar to other projection QMC approaches, the description of core-valence correlations requires onerous convergence of time-step errors. Furthermore, it has been shown that AFQMC atom energies can be difficult to calculate.³³ Hence, we converge the atomic energies with a large number of determinants in W-AFQMC. A less expensive and simpler alternative is to fit the values of the atoms to the

experimental data, which benefits from cancellation of errors. We use this approach for the other benchmark methods. For small molecules, a relatively inexpensive version of the first approach can be shown to work quite well, however, for larger molecules, any difference in molecule versus atom accuracy for a given method is compounded.

Atom energies for all methods are fit as free parameters according to the combined G2/G3 set experimental heats of formation (with the addition of AlCl, AlF, AlH, and AlH₃ in the W4-11 using the converted reference values to heat of formation); for each respective method we obtain a separate least squares multivariate linear regression fit with atomic energies as parameters, calculated heats of formation as dependent variables, and the loss function is the experimental vs calculated heats of formation,

$$\Delta_f H_{\text{expt,molecule}} - \Delta_f H_{\text{calc,molecule}} = \sum_{\text{atom}} N_{\text{atom}} E_{\text{atom}} + c_{\text{molecule}}, \quad (11)$$

where $\Delta_f H_{\text{expt,molecule}}$ and $\Delta_f H_{\text{calc}}$ are the experimental and calculated heats of formation for that molecule, and N_{atom} is the number of the atom constituting the molecule. The energy of the atom, E_{atom} , is the fitting variable, and c_{molecule} are the constant terms (for each molecule, i.e. independent of E_{atom}) such as the temperature terms, energy of the molecule, and heat of formation of the atoms, used when we minimize the left-hand side of the equation above. We have 189 such correlated equations for the 189 molecules in the G2 and G3 sets.

The initial guess for atom energies in the atomic energy fit is the *ab initio* atom energies obtained through each method respectively. It is worth noting that a small error (i.e. slight imperfection in cancellation of error between atom and molecule energy) in the *ab initio* atom energies is multiplied by the number of atoms in the molecule. While we do add spin-orbit corrections to atomic energies using the values from Curtiss et al.,³⁶ this only applies to the initial guess and such atom-related corrections will be encompassed in the final fitted atom energy.

These fitted atom energies are used to calculate the atomization energies for the W4 set. Alternatively, using W-AFQMC, we show that by using around 10^4 determinants in a natural orbital active space the deviation from experiment is near-chemical accuracy without fitting atomic energies. However, we do not expect cancellation of error between molecules and atoms in this case, as we expect both molecular and atomic energies to be close to exact within this method. For the present, for methods that are not asymptotically exact like W-AFQMC, we thus recommend the atom fitting approach, even though i) the efficacy depends on the accuracy of a method across the entire dataset where fitting occurs, ii) the data set must be sufficiently large, and iii) the resultant atom energies are specific to the other conditions of the fit (basis set and electronic structure method). The third point also applies to *ab initio* atom energies but to a less tailored extent. The reader is referred to SI Section 9 for the resulting fitted atomic energies.

3. Results and Discussion

3.1. Overall Performance of CCSD(T) and AFQMC-based Methods

We begin by evaluating the overall performance of the four methods discussed in Section 2: CCSD(T), DLPNO-CCSD(T), AFQMC I, and AFQMC II, across our chosen datasets. Figure 1 displays the root mean square deviation (RMSD) in the enthalpies of formation calculated using these methods, as detailed in Section 2. For the combined dataset (represented by the far-right bar in Figure 1), the RMSD values for all methods fall within 1 kcal/mol, and as we will see below, all four methods have a very small number of outliers with deviations from benchmark experiments or computations greater than 2 kcal/mol. We conclude that for main group chemistry, the localized (and hence scalable) versions of both coupled cluster and AFQMC achieve our target of reliably obtaining near-chemical accuracy for chemical transformations, sufficient for elucidating chemical reaction mechanisms in complex systems. Results along these lines have been presented previously for DLPNO-CCSD(T) (although

not for as large and extensively curated a data set involving experimental and high-level theoretical references), but not for AFQMC. The present exercise establishes AFQMC as a robust alternative benchmark quantum chemical methodology, albeit at a higher computational cost than DLPNO-CCSD(T). For the present systems, we find the scaling exponent with system size to be similar between DLPNO-CCSD(T) and L-AFQMC, and the high prefactor is responsible for the cost of L-AFQMC. See SI Section 10 for examples of the computational costs of each method. We refer the reader to more careful demonstrations of AFQMC and DLPNO-CCSD(T) scaling in these articles.^{10,24,27}

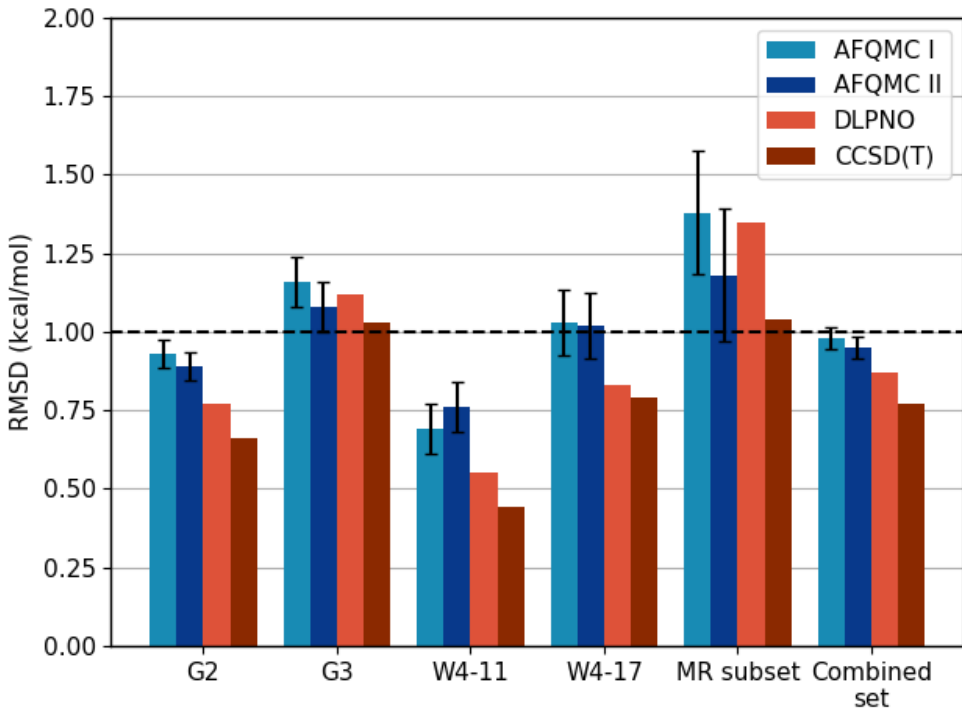


Figure 1: Root-mean-square deviations of the calculated heat of formation of G2, G3 and W4-11/17 datasets with respect to experiment (G2 and G3) or W4 reference values (W4-11, W4-17) for each benchmark method. ‘DLPNO’ refers to DLPNO-CCSD(T). The number of molecules in our mutually exclusive definition of G2, G3, W4-11, and W4-17 are 116, 73, 38, and 32. The separated MR subset refers to the 10 molecules from Table S26, from a combination of G2, W4-11, and W4-17. The combined set consists of the total 259 molecules. The horizontal dashed line at 1 kcal/mol refers to the standard of chemical accuracy.

With regard to the detailed results in Figure 1, a few comments can be made. Firstly, full CCSD(T) displays the smallest RMS error across all four methods. This is most pronounced

for the W4-11 data set, which is not surprising as the benchmark theory used to establish reference values is based on a coupled cluster approach. For the G3 data set, the difference is barely noticeable, reflecting likely performance when comparing with experimental data in practice.

Secondly, the most difficult data set for all methods is, unsurprisingly, but not guaranteed, the subset of 10 cases that we have identified as “multireference” (MR). We classify molecules as multireference based on a set of diagnostics developed by Karton et. al.,^{40,41} as discussed in more detail in Section 11 of the Supplementary Material. For the coupled-cluster based methods, only one molecule, ozone, stands out as displaying an error in excess of 2 kcal/mol. Despite formally being a single reference methodology, the treatment of electron correlation via CCSD(T) appears to be powerful enough to handle many wavefunctions with nontrivial multireference character. DLPNO-CCSD(T) here displays a noticeable (although not large) degradation from full CCSD(T). For AFQMC, an improvement is obtained in the treatment of MR molecules by upgrading the trial function in the AFQMC II approach. Details of results for each quantum chemical method for all of the MR cases can be found in the SI Section 11.

We next analyze the outliers observed across the different data sets and methods, the number of which are summarized in Figure 2 below. A number of interesting points can be made regarding the outliers, which are enumerated along with results for the various computational methods in Table 2. Firstly, neither AFQMC I, AFQMC II nor the two coupled cluster based methods have any outliers for the W4-11 and W4-17 data sets, where the reference values are taken from ultrahigh level computation. Secondly, while CCSD(T) and DLPNO-CCSD(T) have a larger number of outliers than AFQMC II based on our (somewhat arbitrary) cutoff for the deviation from the reference of 2 kcal/mol, a perusal of the data in Table 2 shows that, with the exception of ozone (where we believe that the multireference character is great enough to cause significant errors in CCSD(T) and DLPNO-CCSD(T), which can then be reduced via a large trial function in AFQMC II), the

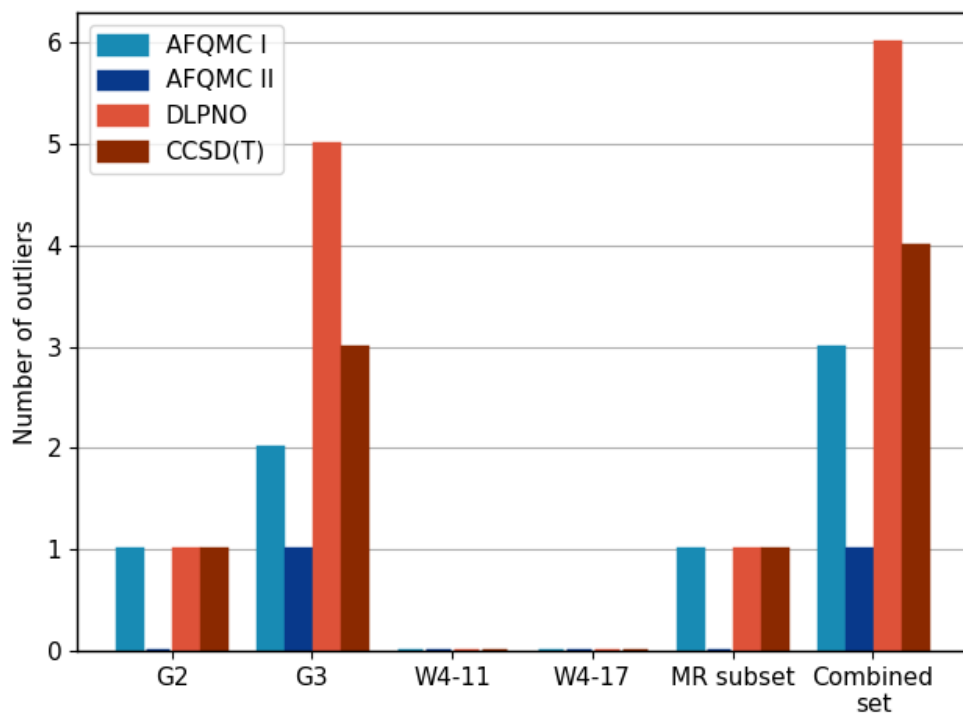


Figure 2: Number of outlier molecules for each method and dataset, where outlier is defined as having larger than 2 kcal/mol deviation in heat of formation from the reference value. ‘DLPNO’ refers to DLPNO-CCSD(T).

computational results for the five remaining molecules are closer to each other than they are to the experimental reference data. A likely interpretation of the results is that the experiments have a residual error of a few kcal/mol (possibly as large as 3-4 kcal/mol for 3-butyn-2-one), and that in fact, the reliability of our scalable benchmark methods is higher than what is suggested in Figure 2. In contrast to a number of other cases that initially appeared to be outliers but were resolved by newer experiments, as discussed in Section 2.2, we were unable to find any relatively recent experimental data. Note that the value of having two distinct computational methods which can be compared, suggested in the Introduction, is already manifested in this analysis. Without the complementary AFQMC I and AFQMC II results, one might conclude that CCSD(T) has occasional outliers even for single-reference main group molecules and that higher-order treatments are required to achieve even the 2 kcal/mol accuracy threshold that we have set.

Table 2: All combined outliers for CCSD(T), DLPNO-CCSD(T), AFQMC I and AFQMC II and their respective deviations against reference heat of formation are reported in kcal/mol.

Molecule	Dataset	CCSD(T)	DLPNO-CCSD(T)	AFQMC I	AFQMC II
Ozone	G2, MR	-2.07	-3.24	-2.57(25)	-0.96(35)
Pyrazine	G3	-1.96	-2.52	-3.11(77)	-1.74(53)
3-Butyn-2-one	G3	-3.35	-3.57	-4.68(55)	-4.60(69)
Cl ₂ O ₂ S	G3	-3.53	-3.43	-1.98(69)	-1.99(78)
Cyclooctatetraene	G3	-1.99	-2.42	-1.43(65)	-1.49(104)
Pyrimidine	G3	2.40	2.49	1.76(55)	1.76(55)

Having summarized the overall performance of our various methodologies, we next examine more carefully the differences between the scalable (DLPNO-CCSD(T) and AFQMC I) and benchmark (CCSD(T) and AFQMC II) versions of our two high level wavefunction based approaches. For the vast majority of molecules in the present data sets, equivalent results are obtained. However, it is useful to examine the cases where there are noticeable differences to see whether a systematic explanation is possible.

3.2. Comparison of CCSD(T) and DLPNO-CCSD(T) Results

Table 3 below presents the 10 molecules with the largest deviations between the CCSD(T) and DLPNO-CCSD(T) results, in order of the size of the deviations (see SI Section 12 for a correlation plot). The interesting point here is that most of these molecules are classified as MR by our diagnostic criteria. This observation suggests that the DLPNO localization scheme may have more difficulties as the MR character of the wavefunction increases. Having said that, the deviations are in general quite small (and in some cases the DLPNO-CCSD(T) results are not clearly inferior to CCSD(T) when comparing with the reference value). We would view the question as to whether the performance of DLPNO-CCSD(T) for main group MR molecules is a significant source of concern (beyond the general question of the accuracy of the underlying CCSD(T) approximation) as a subject for future investigation.

Table 3: DLPNO-CCSD(T) and CCSD(T) deviations in kcal/mol, against the reference heats of formation. The difference between DLPNO-CCSD(T) and CCSD(T) deviations are also reported in kcal/mol. The multireference (MR) criteria is according to Table S26.

Molecule	Dataset	DLPNO-CCSD(T)	CCSD(T)	Difference	MR?
S ₄	W4-11	-1.26	0.66	1.92	Yes
N ₂ O ₄	W4-17	0.03	1.67	1.64	Yes
Ozone	G2	-3.24	-2.07	1.17	Yes
BN	W4-11	-0.53	0.85	1.38	Yes
ClF ₅	W4-17	-0.93	0.12	1.05	Yes
C ₂	W4-11	-1.40	-0.54	0.86	Yes
Ph-Cl	G3	-0.60	0.21	0.81	No
S ₃	W4-11	0.05	0.82	0.77	Yes
Ph-CH ₃	G3	-1.15	-0.42	0.74	No
Benzoquinone	G3	-1.40	-0.69	0.72	No

3.3. Detailed Discussion of ph-AFQMC Methodology

In contrast to our coupled cluster based calculations, for which we utilize well established methods implemented by the Neese group in ORCA, the scalable AFQMC I protocol discussed above required significant novel methodology development. We therefore discuss

AFQMC I development and implementation in detail in what follows. Specification of the AFQMC II protocol given AFQMC I as a starting point is straightforward, using the general procedure described in Section 2.4.

We first perform an initial run of the 259 molecules in our datasets with relatively small initial active spaces (AS), including only the valence electrons and 4 orbitals per atom (excluding hydrogen). Additionally, we set a loose NOON (natural orbital occupation number) cutoff at 0.01, allowing for the selection of active orbitals in the second SHCI step with NOONs ranging from 0.01 to 1.99. The initial and final active spaces chosen for every molecule are listed in the SI and more details about the procedure can be found in SI Section 3. Although this relatively cheap procedure results in around 80% of molecules being run with 1 determinant trials, and on average 2 determinants (maximum 70 determinants), it performs sufficiently well such that 88% of the molecules achieve an unsigned deviation of less than 2 kcal/mol, and achieves an RMSD of 1.67 and MAD (mean absolute deviation) of 1.02 and across the entire combined dataset. We denote this procedure as AFQMC 0.

For the G2 dataset, the RMSD is 1.19 kcal/mol and the MAD is 0.88 kcal/mol. Similarly, for the G3 dataset, the RMSD and MAD are 1.27 kcal/mol and 0.99 kcal/mol, respectively, both of which are quite respectable. However, the performance of AFQMC 0 significantly declines for W4 datasets, with an RMSD of 3.04 kcal/mol for W4-11 and 1.70 kcal/mol for W4-17, with respective MADs of 1.26 kcal/mol and 1.33 kcal/mol. This reduced level of accuracy primarily stems from the enhanced presence of multireference molecules (8/10 from Table S4) in the W4 data sets. The RMSD is furthermore skewed by the presence of a few very large outliers. The 30 outliers for AFQMC 0 are enumerated in detail in Section 13 of the Supplementary Material. A few of the largest errors are listed below in Table 4.

In the AFQMC methodology, the standard approach to address outliers (including those of increasing MR character) is to create a better trial function, using for example an expanded active space as well as more determinants. To address the 17 outliers identified in the G2 and G3 sets and the 13 outliers in the W4-11 and W4-17 sets, we recalculated energies by

Table 4: The top outliers from AFQMC 0 protocol. Deviations ($(\Delta_f H_{\text{expt}}(298 \text{ K}) - \Delta_f H_{\text{calc}}(298 \text{ K}))$ for G2/G3 and $\Delta_a E_{\text{W4}}(0 \text{ K}) - \Delta_a E_{\text{calc}}(0 \text{ K})$ for W4) are listed in kcal/mol with statistical errors in parentheses. After the first CI is performed with an active space (AS) based on orbital maps to the atoms of the molecules (refer Table S4) that returns the ‘First CI AS’ listed, the second AS (shown here as ‘TZ final AS’ and ‘QZ final AS’, as the NOONs have a slight basis set dependency due to approximations such as the SHCI solver) is chosen from those orbitals from the first AS that have NOONs of between 0.01 and 1.99. The final number of determinants is set by the number of determinants required to get to 99.5% saturation of the CI coefficients.

Molecule	Dataset	Deviation	First CI AS	TZ final AS	QZ final AS	TZ final #dets	QZ final #dets
BN	W4-11, MR	-10.51(61)	4e+4e,8o	1e+1e,2o	1e+1e,2o	2	2
C ₂	W4-11, MR	-14.62(43)	4e+4e,8o	1e+1e,2o	1e+1e,2o	2	2
Ozone	G2, MR	-5.05(51)	9e+9e,12o	2e+2e,3o	2e+2e,3o	3	3
3-Butyn-2-one	G3	-4.27(57)	11e+11e,20o	1e+1e,2o	1e+1e,2o	2	2
CICOF	W4-17	3.00(72)	12e+12e,16o	1e+1e,1o	1e+1e,1o	1	1
Dioxetanone	W4-17	3.04(80)	13e+13e,20o	1e+1e,1o	1e+1e,1o	1	1
ClF ₅	W4-17, MR	3.13(104)	21e+21e,24o	1e+1e,2o	1e+1e,1o	2	1
OCS	G2	3.25(67)	8e+8e,12o	1e+1e,1o	1e+1e,1o	1	1
LiF	G2	3.38(39)	4e+4e,5o	1e+1e,1o	1e+1e,1o	1	1
Pyrimidine	G3	3.51(53)	13e+13e,24o	2e+2e,4o	1e+1e,3o	6	1
HClO ₄	W4-17	4.16(82)	15e+15e,20o	1e+1e,1o	1e+1e,1o	1	1

expanding the valence space by one shell and applying a stricter NOON threshold. This approach reduced the number of outliers to 6 in G2/G3 (bicyclobutane, ozone, Li₂, LiF, pyrazine, 3-butyn-2-one) and 4 in W4-11/W4-17 (BN, C₂, N₂O₄, silole).

For these remaining outliers, we apply further modifications, starting with a further increase of the initial active space and the adjusting of the NOON threshold (see SI Section 3 for details). This procedure successfully reduced the list of outliers to only ozone, pyrazine, and 3-butyn-2-one for G2/G3 and none for W4-17. This improves the MAD from 1.02 kcal/mol to 0.78 kcal/mol and RMSD from 1.67 kcal/mol to 0.98 kcal/mol. As noted above, pyrazine and 3-butyn-2-one experimental values are potentially suspect, which suggests that ozone is the only real outlier in AFQMC I, which has among the highest multireference character in the dataset.

In summary, AFQMC I starts from AFQMC 0 and successively increases the active space for the outliers (starting with increasing the initial active space and tightening the NOON threshold if one wants to keep the CI % retained similar) and hence, the number of determinants. The combination of the best trials fall under ‘AFQMC I’ (see SI for a full list).

The aim behind running the dataset in a progressive fashion and only applying larger orbital maps (i.e. orbitals per atom) and stricter thresholds to outliers is a compromise. The goal is achieving useful AFQMC results with close to minimal number of determinants necessary for each molecule, while also reducing manual processes in the selection of active spaces to enable generation of a large amount of benchmark data. AFQMC 0, the fully automated protocol with loose thresholds, performs decently, but by using larger orbital maps for a small percentage of the molecules AFQMC I results in a large improvement of error over the entire dataset.

Under circumstances where the reference is unknown, typically having a converged energy with respect to, for example, determinants²⁸ (See SI Section 3 for an example) gives confidence in the AFQMC benchmark value unless the CI expansion is qualitatively wrong. This process can become expensive, and based on our heuristic we have observed some guidelines for which type of trial and whether convergence is necessary for certain types of molecules. Observing the AFQMC 0 outliers, a few categories of molecules stand out: i) multireference molecules ii) small (< 4 atoms) molecules containing Li, F, or S atoms, iii) conjugated systems, iv) strained systems, and v) halogen oxoacids. The only exceptions to these are diethyl ketone (deviation 2.22 kcal/mol) and HNCO (deviation 2.63 kcal/mol). After an expanded valence space to two instead of one shell, and a 0.001 instead of 0.01 NOON threshold, the remaining real outliers as discussed above mostly fall into the multireference category. Therefore, for main group thermochemistry, for the above categories of outliers (except multireference), we recommend AFQMC 0 with these alternative thresholds. On the other hand, we still recommend that multireference molecules be converged with respect to the active space size and number of determinants.

Where performing calculations with more than 3600 determinants with L-AFQMC does not converge the absolute deviation to < 2 kcal/mol, we perform W-AFQMC calculations, using on the order of 10^4 determinants. As discussed above, we designate the resulting data set, in which the outlier results from AFQMC I are replaced by W-AFQMC derived values,

as AFQMC II (along with a few other molecules with e.g. experimental discrepancies, see SI Section 3 Tables S6 and S7 for a full list). The net result is that only 3-butyne-2-one is an outlier for the entire dataset of 259 molecules with AFQMC II, with a deviation of -4.6 kcal/mol. As this value is within 1.5 kcal/mol of all of the other methods (L-AFQMC, CCSD(T), and DLPNO-CCSD(T)), in addition to this molecule not satisfying any of the multireference criteria, and furthermore having no experimental value from ATcT or theoretical value from W4, it seems highly likely that the experimental value may require updating. Furthermore, as noted above, the fact that CCSD(T), DLPNO-CCSD(T), and AFQMC I results are quite close to W-AFQMC results for the remaining outliers in Table 2 increases confidence that the discrepancies with the experimental reference values for these molecules are also due to experimental error. The ability to perform W-AFQMC calculations for this subset of cases is critical to our suggestion that experimental error is a likely explanation for the deviations of the remaining methods.

Finally, we have investigated the accuracy of the AFQMC I (but not AFQMC II) protocols using all-electron calculations. While this is generally expected to be less accurate due to deficiencies in the aug-cc-pVXZ split-valence Dunning basis sets for correlating core electrons (and to some extent aug-cc-pCVXZ for correlating 1s), we find that overall the all-electron calculations still display an MAD of ~ 1 kcal/mol for the entire dataset, although with more outliers. Interestingly, although the timestep error is much larger for all electron than frozen core and does not cancel between atoms and molecules, the atom-fit for the same timestep (we used 0.005 Ha^{-1}) demonstrates an impressive cancellation of error even though more molecules require larger trials to be run in order to reduce the relative timestep error. We refer the reader to the SI Section 5 for a more detailed discussion of frozen vs non-frozen results, as well as timestep errors in SI Section 2.

4. Conclusion

In this study, we have investigated the performance of three benchmark-level wavefunction approaches — CCSD(T), DLPNO-CCSD(T), and ph-AFQMC—in the context of main group element thermochemistry. The study highlights the ability of the more scalable DLPNO-CCSD(T) and localized ph-AFQMC to achieve accuracies remarkably close to canonical CCSD(T), showcasing their significance in the generation of accurate benchmark chemical data in recent years. The results demonstrate that both DLPNO-CCSD(T) and ph-AFQMC methods consistently deliver RMSDs of below 1 kcal/mol across these selected datasets, adhering to the standard of chemical accuracy, as well as a maximum error of 2 kcal/mol across the entire data set, excepting one or two cases. These above observations highlight the potential of ph-AFQMC as a robust benchmark method that is able to produce accurate results for the small molecules tested here, and is also promising for larger and more challenging systems.

The G2 and G3 test sets and the W4 sets are chosen on account of the readily available and accurate reference values. Further critical investigation of scalable benchmark methods such as DLPNO-CCSD(T) and AFQMC for larger systems is valuable, with the difficulty of such investigation being the lack of accurate experimental references and the computational expense of generating benchmark-level calculations for large datasets of such systems. In particular, having the AFQMC method at disposal would be valuable in cases where one does not expect CCSD(T) to perform well, for example multireference systems or non-equilibrium geometries and bond breaking. Regardless, the current studies in the literature are moving towards that direction.^{28,70} The multireference diagnostic used in this study is by no means exhaustive, and investigation of multireference character for a comparison of DLPNO-CCSD(T), AFQMC and other scalable methods (for example, other L-CCSD(T) methods⁸⁴ and composite methods^{85,86}) is illustrative for the purposes of ascertaining the potential for evaluating challenging systems.

While we have shown that we can achieve an accuracy of < 2 kcal/mol for virtually all the

molecules tested here by increasing the sophistication of the ph-AFQMC trial, finding the most compact trial wavefunction is a challenging multifaceted direction that is ongoing in the ph-AFQMC community. Furthermore, while we have semi-automated the trial generation for ph-AFQMC, there are still non-black-box elements. An algorithm that can find the most compact trial for every molecule in a black-box manner is highly desired but elusive at this point in time. Additionally, alternative AFQMC constraints and algorithms are also being explored in the literature to increase accuracy and decrease the computational cost. AFQMC is developing at a rapid rate, and moving forward, the improvements in implementation and protocol will cement this method as a powerful tool for electronic structure.

Finally, the thorough benchmarking conducted in this study is crucial for establishing benchmark datasets that evaluate the performance of DFT functionals. This will also aid the development of correction schemes aimed at enhancing the accuracy DFT by significantly reducing both the magnitude and frequency of outliers. We discuss this in detail in our subsequent work.

Supporting Information Available

The following files are available free of charge.

- Supporting Information: Molecule list, timestep errors, additional computational details, multireference diagnostics, additional outliers, atom energies, discussion for no frozen core (.pdf)
- Supporting Information: Deviations from experiment for all molecules, trials for AFQMC 0 and AFQMC I for all molecules (.xlsx)
- Supporting Information: xyz coordinates of all molecules (.zip)

Acknowledgement

We thank Hung T. Vuong for valuable discussions and critical contributions to the AFQMC code implementation. We thank Zach K. Goldsmith for assistance with computation and helpful discussions. We thank Hong-Zhou Ye for valuable insights. The computational work was supported by OLCF INCITE 2022 and 2024. The authors acknowledge support by Gates Ventures. A.M. and D.R.R. were partially supported by NSF CHE-2245592. W-AFQMC calculations were performed on the Delta system at the National Center for Supercomputing Applications through allocation CHE230028 from the Advanced Cyberinfrastructure Coordination Ecosystem: Services and Support (ACCESS) program, which is supported by National Science Foundation grants #2138259, #2138286, #2138307, #2137603, and #2138296.

References

- (1) Mardirossian, N.; Head-Gordon, M. Thirty years of density functional theory in computational chemistry: an overview and extensive assessment of 200 density functionals. *Mol. Phys.* **2017**, *115*, 2315–2372.
- (2) Raghavachari, K.; Trucks, G. W.; Pople, J. A.; Head-Gordon, M. A fifth-order perturbation comparison of electron correlation theories. *Chem. Phys. Lett.* **1989**, *157*, 479–483.
- (3) Raghavachari, K. An augmented coupled cluster method and its application to the first-row homonuclear diatomics. *J. Chem. Phys.* **1985**, *82*, 4607–4610.
- (4) Karton, A.; Daon, S.; Martin, J. M. W4-11: A high-confidence benchmark dataset for computational thermochemistry derived from first-principles W4 data. *Chem. Phys. Lett.* **2011**, *510*, 165–178.
- (5) Quintal, M. M.; Karton, A.; Iron, M. A.; Boese, A. D.; Martin, J. M. Benchmark study

- of DFT functionals for late-transition-metal reactions. *J. Phys. Chem. A* **2006**, *110*, 709–716.
- (6) Sæbø, S.; Pulay, P. Local configuration interaction: An efficient approach for larger molecules. *Chem. Phys. Lett.* **1985**, *113*, 13–18.
- (7) Neese, F.; Valeev, E. F. Revisiting the Atomic Natural Orbital Approach for Basis Sets: Robust Systematic Basis Sets for Explicitly Correlated and Conventional Correlated *ab initio* Methods? *J. Chem. Theory Comput.* **2011**, *7*, 33–43.
- (8) Riplinger, C.; Neese, F. An efficient and near linear scaling pair natural orbital based local coupled cluster method. *J. Chem. Phys.* **2013**, *138*, 034106.
- (9) Riplinger, C.; Sandhoefer, B.; Hansen, A.; Neese, F. Natural triple excitations in local coupled cluster calculations with pair natural orbitals. *J. Chem. Phys.* **2013**, *139*, 134101.
- (10) Liakos, D. G.; Neese, F. Is It Possible To Obtain Coupled Cluster Quality Energies at near Density Functional Theory Cost? Domain-Based Local Pair Natural Orbital Coupled Cluster vs Modern Density Functional Theory. *J. Chem. Theory Comput.* **2015**, *11*, 4054–4063.
- (11) Kermani, M. M.; Li, H.; Ottochian, A.; Crescenzi, O.; Janesko, B. G.; Scalmani, G.; Frisch, M. J.; Ciofini, I.; Adamo, C.; Truhlar, D. G. Barrier Heights for Diels–Alder Transition States Leading to Pentacyclic Adducts: A Benchmark Study of Crowded, Strained Transition States of Large Molecules. *J. Phys. Chem. Letters* **2023**, *14*, 6522–6531.
- (12) Ballesteros, F.; Dunivan, S.; Lao, K. U. Coupled cluster benchmarks of large noncovalent complexes: The L7 dataset as well as DNA–ellipticine and buckycatcher–fullerene. *J. Chem. Phys.* **2021**, *154*, 154104.

- (13) Santra, G.; Semidalas, E.; Mehta, N.; Karton, A.; Martin, J. M. S66x8 noncovalent interactions revisited: new benchmark and performance of composite localized coupled-cluster methods. *Phys. Chem. Chem. Phys.* **2022**, *24*, 25555–25570.
- (14) Villot, C.; Ballesteros, F.; Wang, D.; Lao, K. U. Coupled cluster benchmarking of large noncovalent complexes in L7 and S12L as well as the C60 dimer, DNA–ellipticine, and HIV–indinavir. *J. Phys. Chem. A* **2022**, *126*, 4326–4341.
- (15) Calbo, J.; Sancho-García, J. C.; Orti, E.; Arago, J. DLPNO-CCSD (T) scaled methods for the accurate treatment of large supramolecular complexes. *J. Comput. Chem.* **2017**, *38*, 1869–1878.
- (16) Santra, G.; Martin, J. M. Performance of localized-orbital coupled-cluster approaches for the conformational energies of longer n-alkane chains. *J. Phys. Chem. A* **2022**, *126*, 9375–9391.
- (17) Rolik, Z.; Szegedy, L.; Ladjánszki, I.; Ladóczki, B.; Kállay, M. An efficient linear-scaling CCSD(T) method based on local natural orbitals. *The Journal of Chemical Physics* **2013**, *139*, 094105.
- (18) Ma, Q.; Werner, H.-J. Explicitly correlated local coupled-cluster methods using pair natural orbitals. *WIREs Computational Molecular Science* **2018**, *8*, e1371.
- (19) Shee, J.; Weber, J. L.; Reichman, D. R.; Friesner, R. A.; Zhang, S. On the potentially transformative role of auxiliary-field quantum Monte Carlo in quantum chemistry: A highly accurate method for transition metals and beyond. *J. Chem. Phys.* **2023**, *158*, 140901.
- (20) Malone, F. D.; Mahajan, A.; Spencer, J. S.; Lee, J. ipie: A Python-Based Auxiliary-Field Quantum Monte Carlo Program with Flexibility and Efficiency on CPUs and GPUs. *J. Chem. Theory Comput.* **2023**, *19*, 109–121.

- (21) Kim, J.; Baczewski, A. D.; Beaudet, T. D.; Benali, A.; Bennett, M. C.; Berrill, M. A.; Blunt, N. S.; Borda, E. J. L.; Casula, M.; Ceperley, D. M. et al. QMCPACK: an open source ab initio quantum Monte Carlo package for the electronic structure of atoms, molecules and solids. *J. Phys. Condens. Matter* **2018**, *30*, 195901.
- (22) Dice Repository. <https://github.com/sanshar/Dice> (accessed 2024-04-30).
- (23) Shee, J.; Arthur, E. J.; Zhang, S.; Reichman, D. R.; Friesner, R. A. Phaseless Auxiliary-Field Quantum Monte Carlo on Graphical Processing Units. *J. Chem. Theory Comput.* **2018**, *14*, 4109–4121.
- (24) Weber, J. L.; Vuong, H.; Devlaminck, P. A.; Shee, J.; Lee, J.; Reichman, D. R.; Friesner, R. A. A Localized-Orbital Energy Evaluation for Auxiliary-Field Quantum Monte Carlo. *J. Chem. Theory Comput.* **2022**, *18*, 3447–3459.
- (25) Mahajan, A.; Sharma, S. Taming the Sign Problem in Auxiliary-Field Quantum Monte Carlo Using Accurate Wave Functions. *J. Chem. Theory Comput.* **2021**, *17*, 4786–4798.
- (26) Mahajan, A.; Lee, J.; Sharma, S. Selected configuration interaction wave functions in phaseless auxiliary field quantum Monte Carlo. *J. Chem. Phys.* **2022**, *156*, 174111.
- (27) Kurian, J. S.; Ye, H.-Z.; Mahajan, A.; Berkelbach, T. C.; Sharma, S. Toward Linear Scaling Auxiliary-Field Quantum Monte Carlo with Local Natural Orbitals. *J. Chem. Theory Comput.* **2023**, *20*, 134–142.
- (28) Neugebauer, H.; Vuong, H. T.; Weber, J. L.; Friesner, R. A.; Shee, J.; Hansen, A. Toward Benchmark-Quality Ab Initio Predictions for 3d Transition Metal Electrocatalysts: A Comparison of CCSD (T) and ph-AFQMC. *J. Chem. Theory Comput.* **2023**, *19*, 6208–6225.
- (29) Shee, J.; Rudshiteyn, B.; Arthur, E. J.; Zhang, S.; Reichman, D. R.; Friesner, R. A. On achieving high accuracy in quantum chemical calculations of 3 d transition metal-

- containing systems: a comparison of auxiliary-field quantum monte carlo with coupled cluster, density functional theory, and experiment for diatomic molecules. *J. Chem. Theory Comput.* **2019**, *15*, 2346–2358.
- (30) Rudshiteyn, B.; Weber, J. L.; Coskun, D.; Devlaminck, P. A.; Zhang, S.; Reichman, D. R.; Shee, J.; Friesner, R. A. Calculation of metallocene ionization potentials via auxiliary field quantum Monte Carlo: Toward benchmark quantum chemistry for transition metals. *J. Chem. Theory Comput.* **2022**, *18*, 2845–2862.
- (31) Rudshiteyn, B.; Coskun, D.; Weber, J. L.; Arthur, E. J.; Zhang, S.; Reichman, D. R.; Friesner, R. A.; Shee, J. Predicting ligand-dissociation energies of 3d coordination complexes with auxiliary-field quantum Monte Carlo. *J. Chem. Theory Comput.* **2020**, *16*, 3041–3054.
- (32) Weber, J. L.; Churchill, E. M.; Jockusch, S.; Arthur, E. J.; Pun, A. B.; Zhang, S.; Friesner, R. A.; Campos, L. M.; Reichman, D. R.; Shee, J. *In silico* prediction of annihilators for triplet–triplet annihilation upconversion *via* auxiliary-field quantum Monte Carlo. *Chem. Sci.* **2021**, *12*, 1068–1079.
- (33) Lee, J.; Pham, H. Q.; Reichman, D. R. Twenty years of auxiliary-field quantum Monte Carlo in quantum chemistry: An overview and assessment on main group chemistry and bond-breaking. *J. Chem. Theory Comput.* **2022**, *18*, 7024–7042.
- (34) Debnath, S.; Neufeld, V. A.; Jacobson, L. D.; Rudshiteyn, B.; Weber, J. L.; Berkelbach, T. C.; Friesner, R. A. Accurate quantum chemical reaction energies for lithium-mediated electrolyte decomposition and evaluation of density functional approximations. *J. Phys. Chem. A* **2023**, *127*, 9178–9184.
- (35) Stevenson, J.; Agarwal, G.; Jacobson, L. Machine learning force field ranking of candidate solid electrolyte interphase structures in Li-ion batteries. *ChemRxiv* **2023**, DOI:10.26434/chemrxiv-2023-gwnl8 (2023-12-07 Version 1).

- (36) Curtiss, L. A.; Raghavachari, K.; Redfern, P. C.; Pople, J. A. Assessment of Gaussian-2 and density functional theories for the computation of enthalpies of formation. *J. Chem. Phys.* **1997**, *106*, 1063–1079.
- (37) Curtiss, L. A.; Raghavachari, K.; Trucks, G. W.; Pople, J. A. Gaussian-2 theory for molecular energies of first- and second-row compounds. *J. Chem. Phys.* **1991**, *94*, 7221–7230.
- (38) Curtiss, L. A.; Raghavachari, K.; Redfern, P. C.; Pople, J. A. Assessment of Gaussian-3 and density functional theories for a larger experimental test set. *J. Chem. Phys.* **2000**, *112*, 7374–7383.
- (39) Curtiss, L. A.; Raghavachari, K. Gaussian-3 and related methods for accurate thermochemistry. *Theor. Chem. Acc.* **2002**, *108*, 61–70.
- (40) Karton, A.; Daon, S.; Martin, J. M. W4-11: A high-confidence benchmark dataset for computational thermochemistry derived from first-principles W4 data. *Chem. Phys. Lett.* **2011**, *510*, 165–178.
- (41) Karton, A.; Sylvetsky, N.; Martin, J. M. L. W4-17: A diverse and high-confidence dataset of atomization energies for benchmarking high-level electronic structure methods. *J. Comput. Chem.* **2017**, *38*, 2063–2075.
- (42) Active Thermochemical Tables. <https://atct.anl.gov/> (accessed 2024-04-30).
- (43) Ruscic, B.; Bross, D. Active Thermochemical Tables (ATcT) Thermochemical Values ver. 1.130. <https://atct.anl.gov/Thermochemical%20Data/version%201.130/index.php> (accessed 2024-04-30).
- (44) Ruscic, B.; Pinzon, R. E.; Morton, M. L.; von Laszewski, G.; Bittner, S. J.; Nijssure, S. G.; Amin, K. A.; Minkoff, M.; Wagner, A. F. Introduction to Active Ther-

- mochemical Tables: Several “Key” Enthalpies of Formation Revisited. *J. Phys. Chem. A* **2004**, *108*, 9979–9997.
- (45) Welch, B. K.; Dawes, R.; Bross, D. H.; Ruscic, B. An Automated Thermochemistry Protocol Based on Explicitly Correlated Coupled-Cluster Theory: The Methyl and Ethyl Peroxy Families. *The Journal of Physical Chemistry A* **2019**, *123*, 5673–5682, PMID: 31244124.
- (46) Computational Chemistry Comparison and Benchmark DataBase. <https://cccbdb.nist.gov/> (accessed 2024-04-30).
- (47) Shi, H.; Zhang, S. Some recent developments in auxiliary-field quantum Monte Carlo for real materials. *J. Chem. Phys.* **2021**, *154*, 024107.
- (48) Motta, M.; Zhang, S. Ab initio computations of molecular systems by the auxiliary-field quantum Monte Carlo method. *Wiley Interdiscip. Rev.: Comput. Mol. Sci.* **2018**, *8*, e1364.
- (49) Sharma, S.; Holmes, A. A.; Jeanmairet, G.; Alavi, A.; Umrigar, C. J. Semistochastic Heat-Bath Configuration Interaction Method: Selected Configuration Interaction with Semistochastic Perturbation Theory. *J. Chem. Theory Comput.* **2017**, *13*, 1595–1604.
- (50) Holmes, A. A.; Tubman, N. M.; Umrigar, C. J. Heat-Bath Configuration Interaction: An Efficient Selected Configuration Interaction Algorithm Inspired by Heat-Bath Sampling. *J. Chem. Theory Comput.* **2016**, *12*, 3674–3680.
- (51) Sun, Q.; Zhang, X.; Banerjee, S.; Bao, P.; Barbry, M.; Blunt, N. S.; Bogdanov, N. A.; Booth, G. H.; Chen, J.; Cui, Z.-H. et al. Recent developments in the PySCF program package. *J. Chem. Phys.* **2020**, *153*, 024109.
- (52) Smith, J. E. T.; Mussard, B.; Holmes, A. A.; Sharma, S. Cheap and Near Exact CASSCF with Large Active Spaces. *J. Chem. Theory Comput.* **2017**, *13*, 5468–5478.

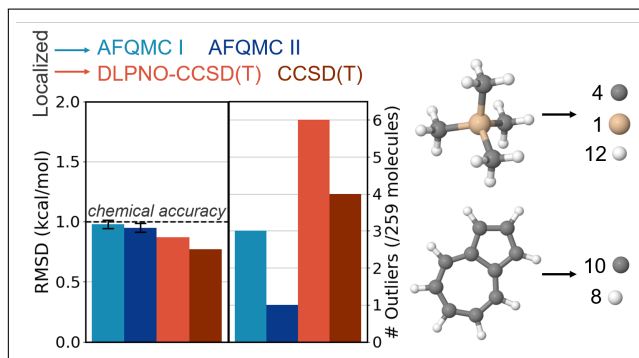
- (53) Neese, F. The ORCA program system. *Wiley Interdiscip. Rev.: Comput. Mol. Sci.* **2012**, *2*, 73–78.
- (54) Altun, A.; Neese, F.; Bistoni, G. Extrapolation to the Limit of a Complete Pair Natural Orbital Space in Local Coupled-Cluster Calculations. *J. Chem. Theory Comput.* **2020**, *16*, 6142–6149.
- (55) Liakos, D. G.; Sparta, M.; Kesharwani, M. K.; Martin, J. M. L.; Neese, F. Exploring the Accuracy Limits of Local Pair Natural Orbital Coupled-Cluster Theory. *J. Chem. Theory Comput.* **2015**, *11*, 1525–1539.
- (56) Stoychev, G. L.; Auer, A. A.; Neese, F. Automatic Generation of Auxiliary Basis Sets. *J. Chem. Theory Comput.* **2017**, *13*, 554–562.
- (57) Dunning, T. H. Gaussian basis sets for use in correlated molecular calculations. I. The atoms boron through neon and hydrogen. *J. Chem. Phys.* **1989**, *90*, 1007–1023.
- (58) de Jong, W. A.; Harrison, R. J.; Dixon, D. A. Parallel Douglas-Kroll energy and gradients in NWChem: Estimating scalar relativistic effects using Douglas-Kroll contracted basis sets. *J. Chem. Phys.* **2001**, *114*, 48.
- (59) Kendall, R. A.; Dunning, T. H.; Harrison, R. J. Electron affinities of the first-row atoms revisited. Systematic basis sets and wave functions. *J. Chem. Phys.* **1992**, *96*, 6796–6806.
- (60) Prascher, B. P.; Woon, D. E.; Peterson, K. A.; Dunning, T. H.; Wilson, A. K. Gaussian basis sets for use in correlated molecular calculations. VII. Valence, core-valence, and scalar relativistic basis sets for Li, Be, Na, and Mg. *Theor. Chem. Acc.* **2011**, *128*, 69–82.
- (61) Woon, D. E.; Dunning, T. H. Gaussian basis sets for use in correlated molecular calculations. III. The atoms aluminum through argon. *J. Chem. Phys.* **1993**, *98*, 1358–1371.

- (62) Schuchardt, K. L.; Didier, B. T.; Elsethagen, T.; Sun, L.; Gurumoorthi, V.; Chase, J.; Li, J.; Windus, T. L. Basis Set Exchange: A Community Database for Computational Sciences. *J. Chem. Inf. Model.* **2007**, *47*, 1045–1052.
- (63) Pritchard, B. P.; Altarawy, D.; Didier, B.; Gibsom, T. D.; Windus, T. L. A New Basis Set Exchange: An Open, Up-to-date Resource for the Molecular Sciences Community. *J. Chem. Inf. Model.* **2019**, *59*, 4814–4820.
- (64) Martin, J. M.; Uzan, O. Basis set convergence in second-row compounds. The importance of core polarization functions. *Chem. Phys. Lett.* **1998**, *282*, 16–24.
- (65) Martin, J. M. L. Basis set convergence study of the atomization energy, geometry, and anharmonic force field of SO₂: The importance of inner polarization functions. *J. Chem. Phys.* **1998**, *108*, 2791–2800.
- (66) Bauschlicher, C. W.; Ricca, A. Atomization Energies of SO and SO₂: Basis Set Extrapolation Revisited. *J. Phys. Chem. A* **1998**, *102*, 8044–8050.
- (67) Bauschlicher, C. W.; Partridge, H. The sensitivity of B3LYP atomization energies to the basis set and a comparison of basis set requirements for CCSD(T) and B3LYP. *Chem. Phys. Lett.* **1995**, *240*, 533–540.
- (68) Feller, D.; Dixon, D. A. Coupled Cluster Theory and Multireference Configuration Interaction Study of FO, F₂O, FO₂, and FOOF. *J. Phys. Chem. A* **2003**, *107*, 9641–9651.
- (69) Peterson, K. A.; Dunning, J., Thom H. Accurate correlation consistent basis sets for molecular core–valence correlation effects: The second row atoms Al–Ar, and the first row atoms B–Ne revisited. *J. Chem. Phys.* **2002**, *117*, 10548–10560.
- (70) Neese, F.; Valeev, E. F. Revisiting the Atomic Natural Orbital Approach for Basis Sets:

- Robust Systematic Basis Sets for Explicitly Correlated and Conventional Correlated ab initio Methods? *J. Chem. Theory Comput.* **2011**, *7*, 33–43.
- (71) Nakajima, T.; Hirao, K. The higher-order Douglas–Kroll transformation. *J. Chem. Phys.* **2000**, *113*, 7786–7789.
- (72) Mayer, M.; Krüger, S.; Rösch, N. A two-component variant of the Douglas–Kroll relativistic linear combination of Gaussian-type orbitals density-functional method: Spin–orbit effects in atoms and diatomics. *J. Chem. Phys.* **2001**, *115*, 4411–4423.
- (73) Wolf, A.; Reiher, M.; Hess, B. A. The generalized Douglas–Kroll transformation. *J. Chem. Phys.* **2002**, *117*, 9215–9226.
- (74) Liu, W.; Peng, D. Exact two-component Hamiltonians revisited. *J. Chem. Phys.* **2009**, *131*, 031104.
- (75) Friesner, R. A.; Knoll, E. H.; Cao, Y. A localized orbital analysis of the thermochemical errors in hybrid density functional theory: Achieving chemical accuracy via a simple empirical correction scheme. *J. Chem. Phys.* **2006**, *125*, 124107.
- (76) Goldfeld, D. A.; Bochevarov, A. D.; Friesner, R. A. Localized orbital corrections applied to thermochemical errors in density functional theory: The role of basis set and application to molecular reactions. *J. Chem. Phys.* **2008**, *129*, 214105.
- (77) Becke, A. D. Density-functional thermochemistry. III. The role of exact exchange. *J. Chem. Phys.* **1993**, *98*, 5648–5652.
- (78) Lee, C.; Yang, W.; Parr, R. G. Development of the Colle-Salvetti correlation-energy formula into a functional of the electron density. *Phys. Rev. B* **1988**, *37*, 785–789.
- (79) Ditchfield, R.; Hehre, W. J.; Pople, J. A. Self-Consistent Molecular-Orbital Methods. IX. An Extended Gaussian-Type Basis for Molecular-Orbital Studies of Organic Molecules. *J. Chem. Phys.* **1971**, *54*, 724–728.

- (80) Frisch, M. J.; Trucks, G. W.; Schlegel, H. B.; Scuseria, G. E.; Robb, M. A.; Cheeseman, J. R.; Scalmani, G.; Barone, V.; Mennucci, B.; Petersson, G. A. et al. Gaussian 09 Revision E.01. Gaussian, Inc., Wallingford, CT, 2009.
- (81) Hariharan, P. C.; Pople, J. A. The influence of polarization functions on molecular orbital hydrogenation energies. *Theor. Chim. Acta* **1973**, *28*, 213–222.
- (82) Francl, M. M.; Pietro, W. J.; Hehre, W. J.; Binkley, J. S.; Gordon, M. S.; DeFrees, D. J.; Pople, J. A. Self-consistent molecular orbital methods. XXIII. A polarization-type basis set for second-row elements. *J. Chem. Phys.* **1982**, *77*, 3654–3665.
- (83) Bochevarov, A. D.; Harder, E.; Hughes, T. F.; Greenwood, J. R.; Braden, D. A.; Philipp, D. M.; Rinaldo, D.; Halls, M. D.; Zhang, J.; Friesner, R. A. Jaguar: A high-performance quantum chemistry software program with strengths in life and materials sciences. *Int. J. Quantum Chem* **2013**, *113*, 2110–2142.
- (84) Semidalas, E.; Martin, J. M. The MOBH35 Metal–Organic Barrier Heights Reconsidered: Performance of Local-Orbital Coupled Cluster Approaches in Different Static Correlation Regimes. *Journal of Chemical Theory and Computation* **2022**, *18*, 883–898, PMID: 35045709.
- (85) Chan, B.; Ho, J. Simple Composite Approach to Efficiently Estimate Basis Set Limit CCSD(T) Harmonic Frequencies and Reaction Thermochemistry. *The Journal of Physical Chemistry A* **2023**, *127*, 10026–10031, PMID: 37970798.
- (86) Semidalas, E.; Martin, J. M. L. Can G4-like composite Ab Initio methods accurately predict vibrational harmonic frequencies? *Molecular Physics* **2024**, *122*, e2263593.

TOC Graphic



Supplementary Information: ‘Scalable Ab Initio Electronic Structure Methods with Near Chemical Accuracy for Main Group Chemistry’

Wei, Y.,^{†,†} Debnath, S.,^{‡,†} Weber, J. L.,[‡] Mahajan, A.,[‡] Reichman, D. R.,[‡] and
Friesner, R. A.*[‡]

[†]*Equal contribution*

[‡]*Department of Chemistry, Columbia University, New York, New York 10027, United
States*

E-mail: raf8@columbia.edu

Contents

1. List of Molecules	S3
2. Timestep Errors	S12
3. AFQMC Procedure in Detail	S14
4. AFQMC Localization	S25
5. Frozen Core vs. All Electron Performance	S26
6. Composite CCSD(T) CBS	S27
7. Effect of DKH2 or X2C	S29
8. Alternative Geometries	S32
9. Atom Energies	S33
10. Computational Timings	S36
11. Multireference Diagnostics	S43
12. CCSD(T) DLPNO-CCSD(T) Correlation	S53
13. AFQMC 0 Outliers	S55

1. List of Molecules

Table S1: Full list of molecules, the name in SI tables and xyz file name (.xyz files provided in a separate .zip along with the SI), the mutually exclusive datasets sorted in reporting for this work, the common chemical name, and the chemical formula.

Name in SI Tables	Dataset	Common Name	Formula
2-butyne	G2	2-Butyne	C ₄ H ₆
Acetaldehyde	G2	Acetaldehyde	CH ₃ CHO
Acetylene	G2	Ethyne	C ₂ H ₂
Acetone	G2	Acetone	CH ₃ COCH ₃
AlCl ₃	G2	Aluminum trichloride	AlCl ₃
AlF ₃	G2	Aluminum trifluoride	AlF ₃
Allene	G2	Allene	CH ₂ =C=CH ₂
Aziridine	G2	Aziridine	C ₂ H ₄ NH
BCl ₃	G2	Trichloroborane	BCl ₃
Benzene	G2	Benzene	C ₆ H ₆
BF ₃	G2	Trifluoroborane	BF ₃
Bicyclo-1-1-0-butane	G2	Bicyclo-1-1-0-butane	C ₄ H ₆
CCl ₂ CCl ₂	G2	Perchloroethene	CCl ₂ CCl ₂
CCl ₄	G2	Perchloromethane	CCl ₄
CF ₂ CF ₂	G2	Perfluoroethene	CF ₂ CF ₂
CF ₃ -CN	G2	2,2,2-Trifluoroacetonitrile	CF ₃ -CN
CF ₄	G2	Perfluoromethane	CF ₄
CH ₂ CH-CN	G2	Acrylonitrile	CH ₂ CH-CN
CH ₂ Cl ₂	G2	Dichloromethane	CH ₂ Cl ₂
CH ₂ F ₂	G2	Difluoromethane	CH ₂ F ₂
CH ₃ -CH ₂ -CH ₂ -Cl	G2	Propyl chloride	CH ₃ -CH ₂ -CH ₂ -Cl
CH ₃ -CH ₂ -Cl	G2	Ethyl chloride	CH ₃ -CH ₂ -Cl
CH ₃ -CH ₂ -O-CH ₃	G2	Methoxyethane	CH ₃ -CH ₂ -O-CH ₃
CH ₃ -CH ₂ -SH	G2	Ethanethiol	CH ₃ -CH ₂ -SH
CH ₃ -CN	G2	Acetonitrile	CH ₃ -CN
CH ₃ -O-CH ₃	G2	Methoxymethane	CH ₃ -O-CH ₃
CH ₃ -O-NO	G2	Methyl nitrite	CH ₃ -O-NO
CH ₃ -S-CH ₃	G2	Dimethyl sulfphide	CH ₃ -S-CH ₃

CH3-SH	G2	Methanethiol	CH3-SH
CH3-SiH3	G2	Methyl silane	CH3-SiH3
CH3CFO	G2	Acetyl fluoride	CH3CFO
CH3Cl	G2	Chloromethane	CH3Cl
CH3COCl	G2	Acetyl chloride	CH3COCl
CH3CONH2	G2	Acetamide	CH3CONH2
CH3COOH	G2	Acetic acid	CH3COOH
CH3NO2	G2	Nitromethane	CH3NO2
CH4	G2	Methane	CH4
CHCl3	G2	Chloromethane	CHCl3
Cl2	G2	Dichlorine	Cl2
ClF	G2	Fluorine chloride	ClF
ClF3	G2	Chloride trifluoride	ClF3
ClNO	G2	Nitrosyl chloride	ClNO
CO	G2	Carbon monoxide	CO
CO2	G2	Carbon dioxide	CO2
CS	G2	Carbon monosulfide	CS
CS2	G2	Carbon disulfide	CS2
Cyanogen	G2	Cyanogen	NCCN
Cyclobutane	G2	Cyclobutane	C4H8
Cyclobutene	G2	Cyclobutene	C4H6
Cyclopropane	G2	Cyclopropane	C3H6
Cyclopropene	G2	Cyclopropene	C3H4
Dimethylamine	G2	Dimethylamine	(CH3)2NH
Dimethylsulfoxide	G2	Dimethylsulfoxide	(CH3)2SO
Ethane	G2	Ethane	C2H6
Ethanol	G2	Ethanol	CH3CH2OH
Ethenone	G2	Ethenone	H 2C=C=O
Ethylene	G2	Ethylene	C2H4
F2	G2	Difluorine	F2
F2O	G2	Hypofluorous anhydride	F2O
Furan	G2	Furan	C4H4O

Glyoxal	G2	Oxaldehyde	HCOCOH
H2	G2	Dihydrogen	H2
H2CO	G2	Formaldehyde	H2CO
H2NNH2	G2	Hydrazine	H2NNH2
H2O	G2	Water	H2O
HCF3	G2	Trifluoromethane	HCF3
HCl	G2	Hydrogen chloride	HCl
HCN	G2	Hydrogen cyanide	HCN
HCOOCH3	G2	Methyl formate	HCOOCH3
HCOOH	G2	Formic acid	HCOOH
HF	G2	Hydrofluoric acid	HF
HOCl	G2	Hypochlorous acid	HOCl
HOOH	G2	Hydrogen peroxide	HOOH
Isobutane	G2	Isobutane	C4H10
Isobutene	G2	Isobutene	C4H8
Isopropyl-alcohol	G2	Isopropanol	(CH3)2CHOH
Ketene	G2	Ketene	C2H2O
Li2	G2	Dilithium	Li2
LiF	G2	Lithium fluoride	LiF
LiH	G2	Lithium hydride	LiH
Methanol	G2	Methanol	H3COH
Methylamine	G2	Methylamine	CH3NH2
Methylene-cyclopropane	G2	Methylene-cyclopropane	C4H6
N2	G2	Dinitrogen	N2
Na2	G2	Disodium	Na2
NaCl	G2	Sodium chloride	NaCl
NF3	G2	Nitrogen trifluoride	NF3
NH3	G2	Ammonia	NH3
NNO	G2	Nitrous oxide	NNO
OCS-m1	G2	Carbon oxide sulfide	OCS-m1
Oxirane	G2	Oxirane	C2H4O
Ozone	G2	Ozone	O3

P2	G2	Diphosphorus	P2
PF3	G2	Trifluorophosphorus	PF3
PH3	G2	Phosphine	PH3
Propane	G2	Propane	C3H8
Propene-CS	G2	Propylene	CH3CH=CH2
Propyne	G2	Propyne	CH3CCH
Pyridine	G2	Pyridine	C5H5N
Pyrole	G2	Pyrrole	C4H5N
SH2	G2	Hydrogen sulfide	SH2
Si2H6	G2	Disilane	Si2H6
SiCl4	G2	Silicon tetrachloride	SiCl4
SiF4	G2	Silicon tetrafluoride	SiF4
SiH4	G2	Silane	SiH4
SiO	G2	Silicon monoxide	SiO
SO2	G2	Sulfur dioxide	SO2
Spiropentane	G2	Spiropentane	C5H8
Thiooxirane	G2	Thiirane	C2H4S
Thiophene	G2	Thiophene	C4H4S
Trans-1-3-butadiene	G2	1-3-butadiene	C4H6
Trans-butane	G2	Butane	C4H10
Trans-ethylamine	G2	Ethylamine	CH3CH2NH2
Trimethyl-amine	G2	Trimethyl amine	N(CH3)3
Vinyl-chloride	G2	Vinyl chloride	H2C=CHCl
Vynil-fluoride	G2	Vinyl fluoride	H2C=CHF
1,3-cyclohexadiene	G3	1,3-Cyclohexadiene	(C2H4)(CH)4
1,3-DiFluorobenzene	G3	1,3-Difluorobenzene	C6H4F2
1,4-DiFluorobenzene	G3	1,4-Difluorobenzene	C6H4F2
2-methyl	G3	2-Methylthiophene	CH3C4H3S
2,5-Dihydrothiophene	G3	2,5-dihydrothiophene	C6H6S
3-methyl	G3	3-methylpentane	C6H14
Acetic	G3	Acetic anhydride	C4H6O3
azulene	G3	Azulene	C10H8

benzoquinone	G3	Benzoquinone	C6H4O2
c2f6	G3	Hexafluoroethane	C2F6
C4H4N2	G3	Pyrazine	C4H4N2
C4H6	G3	Methyl allene	CH3-CH=C=CH2
C4H6O	G3	Divinyl ether	O(CH=CH2)2
C4H8O2	G3	1,4-Dioxane	C4H8O2
C5H8	G3	Isoprene	C5H8
C6H12	G3	Cyclohexane	C6H12
C6H5-CH3	G3	Toluene	PhCH3
C6H5-NH2	G3	Aniline	PhNH2
C6H5-OH	G3	Phenol	PhOH
cf3cl	G3	Chlorotrifluoromethane	CF3Cl
CH3_2CH-CHO	G3	Isobutanal	(CH3)2CH-CHO
CH3_2CH-CN	G3	Isobutane nitrile	(CH3)2CH-CN
CH3_2CH-O- CH_CH3_2	G3	Diisopropyl ether	(CH3)2CH-O-CH(CH3)2
CH3_3C-NH2	G3	t-Butyl amine	(CH3)3C-NH2
CH3_3C-O-CH3	G3	t-Butyl methyl ether	(CH3)3C-O-CH3
CH3_3C-SH	G3	t-Butanethiol	(CH3)3C-SH
CH3-C_O_-CCH	G3	3-butyne-2-one	C4H4O
CH3-C_O_-O- CH_CH3_2	G3	Isopropyl acetate	CH3-COOCH(CH3)2
CH3-C_O_-OCH3	G3	Methyl acetate	CH3-COOCH3
CH3-CH_OCH3_2	G3	1,1-dimethoxy ethane	CH3-CH(OCH3)2
CH3-CH2-CH_CH3_- NO2	G3	Nitro-s-butane	CH3-CH2-CH(CH3)-NO2
CH3-CH2-CO-CH2-CH3	G3	Diethyl ketone	CH3-CH2-CO-CH2-CH3
CH3-CH2-O-CH2-CH3	G3	Diethyl ether	CH3-CH2-O-CH2-CH3
CH3-CH2-S-S-CH2-CH3	G3	Diethyl disulfide	CH3-CH2-S-S-CH2-CH3
CH3-CHCH-CHO	G3	Crotonaldehyde	CH3-CHCH-CHO
CH3-CO-CH2-CH3	G3	Methyl ethyl ketone	CH3-CO-CH2-CH3
Chlorobenzene	G3	Chlorobenzene	PhCl

Cl2O2S	G3	Chlorosulfinyl hypochlorite	Cl2O2S
Cl2S2	G3	Disulfur dichloride	Cl2S2
cyclooctatetraene	G3	1,3,5,7-Cyclooctatetraene	C8H8
cyclopentane	G3	Cyclopentane	C5H10
cyclopentanone	G3	Cyclopentanone	C5H8O
dimethyl	G3	Dimethyl sulfone	(CH3)2SO2
Fluorobenzene	G3	Fluorobenzene	PhF
n-Butyl	G3	n-Butyl chloride	CH3(CH2)3Cl
n-heptane	G3	n-Heptane	C7H16
n-hexane	G3	n-Hexane	C6H14
N-methyl	G3	N-Methyl pyrrole	C5H7N
n-octane	G3	n-Octane	C8H18
n-pentane	G3	n-Pentane	C5H12
Naphthalene	G3	Naphthalene	C10H8
NC-CH2-CH2-CN	G3	Succinonitrile	NC-CH2-CH2-CN
Neopentane	G3	Neopentane	C(CH3)4
P4	G3	Tetraphosphorus	P4
para-cyclohexadiene	G3	1,4-Cyclohexadiene	C6H8
PCl3	G3	Phosphorus trichloride	PCl3
PCl5	G3	Phosphorus pentachloride	PCl5
Perhydropyridine	G3	Piperidine	C5H10NH
pf5	G3	Phosphorus pentafluoride	PF5
POCl3	G3	Phosphorus oxychloride	POCl3
pyrimidine	G3	Pyrimidine	C4H4N2
SCl2	G3	Sulfur dichloride	SCl2
sf6	G3	Sulfur hexafluoride	SF6
SiCl2	G3	Dichlorosilane	SiCl2
SO3	G3	Sulfur trioxide	SO3
t-butanol	G3	t-Butanol	(CH3)3COH
t-Butyl	G3	t-Butyl chloride	(CH3)3CCl
tetrahydrofuran	G3	Tetrahydrofuran	C4H8O

Tetrahydropyran	G3	Tetrahydropyran	C ₅ H ₁₀ O
Tetrahydropyrrole	G3	Tetrahydropyrrole	C ₄ H ₈ NH
Tetrahydrothiophene	G3	Tetrahydrothiophene	C ₄ H ₈ S
Tetrahydrothiopyran	G3	Tetrahydrothiopyran	C ₅ H ₁₀ S
Tetramethylsilane	G3	Tetramethylsilane	(CH ₃) ₄ Si
alcl	W4-11	Aluminum monochloride	AlCl
alf	W4-11	Aluminum monofluoride	AlF
alh	W4-11	Aluminum monohydride	AlH
alh3	W4-11	Aluminum trihydride	AlH ₃
b2h6	W4-11	Diborane	B ₂ H ₆
bf	W4-11	Beryllium monofluoride	BF
bh	W4-11	Beryllium monohydride	BH
bh3	W4-11	Borane	BH ₃
bhf2	W4-11	Difluoroborane	BHF ₂
c-hono	W4-11	cis-Nitrous acid	c-HONO
c-n2h2	W4-11	cis-Diazine	c-N ₂ H ₂
ch2nh	W4-11	Methanimine	CH ₂ NH
ch3f	W4-11	Fluoromethane	CH ₃ F
clcn	W4-11	Nitryl chloride	ClCN
dioxirane	W4-11	Dioxirane	CH ₂ O ₂
f2co	W4-11	Carbonyl fluoride	F ₂ CO
fccf	W4-11	Difluoroacetylene	FCCF
hccf	W4-11	Fluoroacetylene	HCCF
hcn	W4-11	Formonitrile oxide	HCNO
hcof	W4-11	Formyl fluoride	HCOF
hnco	W4-11	Isocyanic acid	HNCO
hnnn	W4-11	Hydrogen azide	HNNN
hno	W4-11	Nitrosyl hydride	HNO
hocn	W4-11	Cyanic acid	HOCN
hof	W4-11	Hypofluorous acid	HOF
nh2cl	W4-11	Chloramine	NH ₂ Cl
oxirene	W4-11	Oxirene	C ₂ H ₂ O

s2o	W4-11	Disulfur monoxide	S2O
sih3f	W4-11	Fluorosilane	SiH3F
t-hono	W4-11	trans-Nitrous acid	t-HONO
t-n2h2	W4-11	trans-Diazine	t-N2H2
c2h5f	W4-11	Fluoroethane	C2H5F
bn	W4-11	Boron nitride	BN
c2	W4-11	Dicarbon	C2
cl2o	W4-11	Dichlorine monoxide	Cl2O
foof	W4-11	Dioxygen difluoride	FOOF
s3	W4-11	Trisulfur	S3
s4-c2v	W4-11	Tetrasulfur (C2v)	S4 (C2v)
beta-lactim	W4-17	Beta-lactim	(C3H4N)OH
borole	W4-17	Borole	C4H5B
c2cl2	W4-17	Dichloroacetylene	C2Cl2
c2cl6	W4-17	Hexachloroethane	C2Cl6
c2clh	W4-17	Chloroethyne	C2ClH
ccl2o	W4-17	Phosgene	CCl2O
cf2cl2	W4-17	Dichlorodifluoromethane	CF2Cl2
ch2clf	W4-17	Chlorofluoromethane	CH2ClF
ch3ph2	W4-17	Methylphosphine	CH2PH2
cis-c2f2cl2	W4-17	cis-Dichlorodifluoroethene	c-CF2Cl2
clcof	W4-17	Carbonyl chloride fluoride	ClCOF
cyclobutadiene	W4-17	Cyclobutadiene	C4H4
cyclopentadiene	W4-17	Cyclopentadiene	H6C5
dioxetan2one	W4-17	1,3-Dioxetan-2-one	H2C2O3
dioxetane	W4-17	Dioxetane	H4C2O2
dithiotane	W4-17	1,3-Dithiotane	H4C2S2
fno	W4-17	Nitrosyl fluoride	FNO
formamide	W4-17	Formamide	CH3NO
formic-anhydride	W4-17	Formic-anhydride	H2C2O3
hclo4	W4-17	Perchloric acid	HClO4
hoclo2	W4-17	Chloric acid	HOClO2

hoclo	W4-17	Chlorous acid	HOCIO
n2o4	W4-17	Dinitrogen tetraoxide	N2O4
nh2f	W4-17	Fluoroamine	NH2F
nh2oh	W4-17	Hydroxylamine	NH2OH
oxadiazole	W4-17	Oxadiazole	H2C2N2O
oxetane	W4-17	Oxetane	H6C3O
silole	W4-17	Silole	H6C4Si
tetrahedrane	W4-17	Tetrahedrane	C4H4
trans-c2f2cl2	W4-17	trans- Dichlorodifluoroethene	t-CF2Cl2
clf5	W4-17	Chlorine pentafluoride	ClF5
cloocl	W4-17	Chlorine peroxide	ClOOCl

2. Timestep Errors

Table S2: AFQMC atomization energies in kcal/mol for the molecule FOOF with all electron calculation. Bottom of the table shows various reference atomization energy values in kcal/mol.

Time step (a.u.)	Atomization energy	\sim Core hrs cost
0.0050	142.5(4)	2500
0.0025	144.1(4)	5000
0.0010	145.3(6)	10500
<hr/>		
ATcT reference	146.4	
W4	146.0	

As a demonstration, we show the timestep error for the molecule FOOF, where we calculate both the atom and molecule energies using W-AFQMC with 10000 determinants for the molecule and 10000 determinants for the atoms. Instead of the MP2 basis correction to get to the CBS limit from aug-cc-pVTZ-DK and aug-cc-pVQZ-DK (see main text Section 2.6), for this exercise this molecule is small enough to run aug-cc-pVTZ-DK and aug-cc-pVQZ-DK directly. The convergence with timestep is shown in Table S2. The computational scaling with timestep is linear.

Looking at Figure S1, all electron atomic energies display a less pronounced dependence on the AFQMC time-step compared to the molecular energy. This results in a notable time-step error in atomization energies. Note that there are multiple sources of time step errors in AFQMC: Trotter decomposition, Hubbard-Stratonovich transformation, hybrid and phaseless approximations, with the last two being trial dependent. Calculations with frozen core electrons or those using basis sets without tight core functions exhibit a much weaker time-step dependence. Indeed, the timestep error for the molecule can reach the order of 10 kcal/mol by using 0.005 Ha⁻¹ instead of 0.0025 Ha⁻¹ when using a single determinant trial without frozen core. In contrast, for most cases a timestep of 0.005 Ha⁻¹ is sufficient when freezing core electrons. For example, Table S3 shows the single point energies using L-AFQMC all-electron calculation, with a 1 determinant trial for CCl4. Real space methods, like diffusion Monte Carlo, also struggle with time step issues, and the field often resorts to pseudopotentials to avoid substantial costs. AFQMC, as an orbital space method, offers the convenient option of freezing core electrons (not possible in DMC) and adding composite perturbative corrections from cheaper methods.

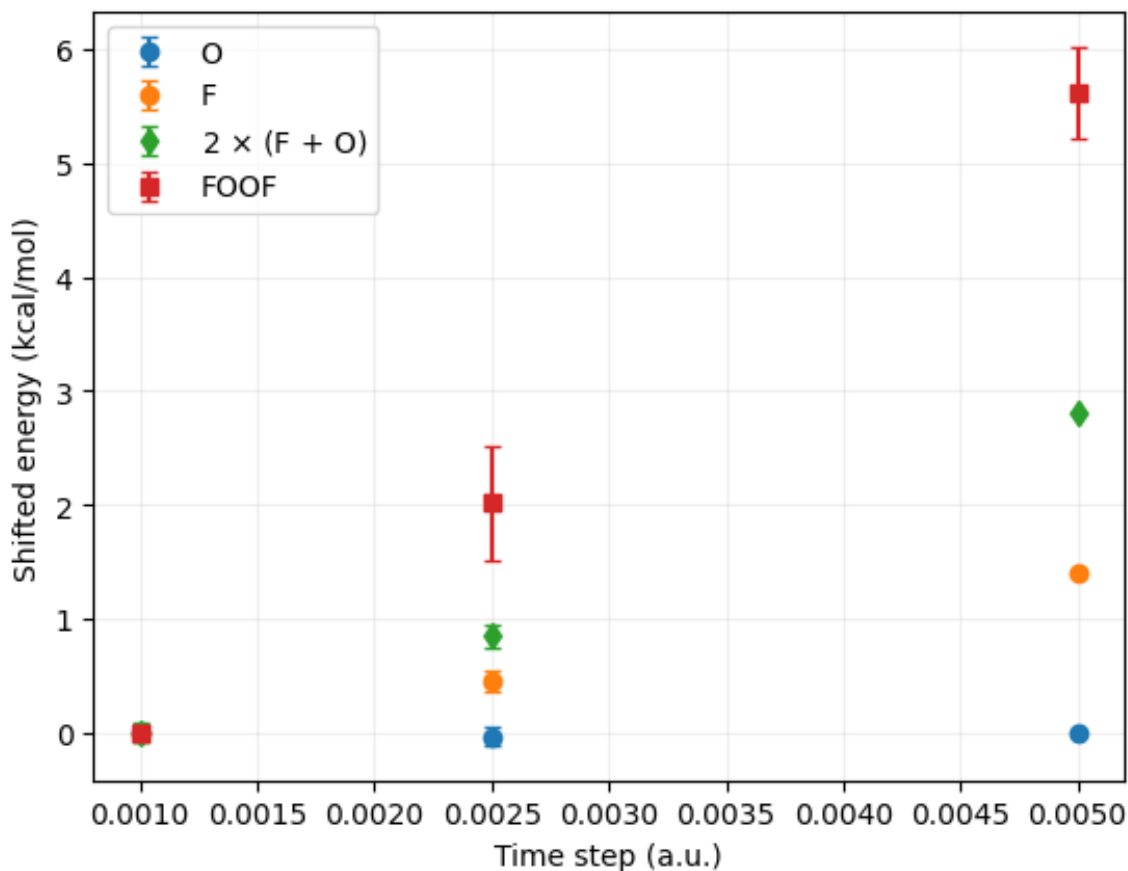


Figure S1: All electron AFQMC CBS energies (with respect to the corresponding time step 0.001 a.u. values) as a function of time step for FOOF.

Table S3: Single point energies (SPEs) for CCl₄ L-AFQMC run with a 1 determinant trial for all-electron and frozen-core (without MP2 core-valence corrections), for the "TZ" basis set as used in the main text. For comparison, SPE with a 200 determinant trial is also shown for all-electron, displaying slightly lower timestep error. All values are reported in atomic units.

Timestep	SPE all-electron 1 det	SPE frozen core 1 det	SPE all-electron 200 dets
0.00125	-1884.01412(60)	-1882.64117(63)	-1884.01443(66)
0.0025	-1884.01220(78)	-1882.64127(48)	-1884.01136(59)
0.0050	-1883.99762(61)	-1882.64129(58)	-1883.99929(53)
0.010	-1883.96231(74)	-1882.64146(45)	-1883.96526(56)

3. AFQMC Procedure in Detail

L-AFQMC — AFQMC 0, AFQMC I

In selecting the first active space, the number of orbitals for each atom is chosen according to one of the schemes in Table S4, and for the molecule the number of active orbitals is the sum of that for the constituent atoms. The number of active electrons per atom is the number of valence electrons starting from the last noble gas (H:1, He:2, Li:1, Be:2, B:3 ...). This automated procedure mimics "chemical intuition", where the orbital maps represent "electron shells" — for example, 4 orbitals from the last noble gas constitute the s and p shells in the first and second rows (where the 1st row starts at Li, as commonly denoted in the literature). We find that this first choice of active space also often results in a relatively large energy separation between the active and inactive orbitals in the canonical restricted Hartree Fock basis, which is another way that has been used in the literature to choose active orbitals^{1,2} and which we consider for manual selection of active spaces for some molecules in the all-electron calculations (see SI Section 5), but not for AFQMC 0 which is fully automated. For AFQMC 0, orbital map I from Table S4 is used for every molecule.

Table S4: Number of active orbitals that are chosen for each constituent atom in the molecule, for the first round of SHCI. 1st row refers to atoms from lithium to neon, and 2nd row refers to atoms from sodium to argon. AFQMC 0 is fully automated and only uses orbital map I. AFQMC I aims to achieve an economical balance between orbital maps I, II, III, and in a small number of cases, IV or V, as well as the NOON thresholds that determine the active space to run a second and final SHCI.

First AS Orbital Maps	H	1st row	2nd row
I	0	4	4
II	1	8	10
III	1	17	19
IV	1	23	23
V	1	27	23

AFQMC 0 selects the second active space from orbitals that are between 0.01 and 1.99 occupancy from NOONs. We used a SHCI threshold of $\epsilon_1 = 10^{-4}$ for the first CASCI, and an $\epsilon_1 = 10^{-5}$ for the second CASCI.

In cases where we seek to obtain a large final active space, we use a larger number of orbitals for the

Table S5: Convergence of C2 with respect to active space and number of determinants. Refer to Table S4 for orbital map meanings. Deviation is reported in kcal/mol from the reference heat of formation (see main text Section 2.9 for details).

Valence orbital map	NOON	Initial AS	Final AS	Dets	CI %	CBS Energy (Ha)	Sterr (kcal/mol)	Deviation (kcal/mol)
I	0.01	4e+4e, 8o	1e+1e, 2o	2	99.50%	-75.82118	0.43	-14.62
II	0.001	4e+4e, 16o	4e+4e, 8o	62	99.50%	-75.834882	0.34	-6.02
III	0.005	4e+4e, 34o	4e+4e, 12o	289	99.50%	-75.84212	0.20	-1.48
III	0.001	4e+4e, 34o	4e+4e, 17o	771	99.50%	-75.84274	0.13	-1.09

first SHCI. We take the outliers from AFQMC 0 and use orbital map II, and if that does not converge the result then we move on to orbital map III. The systematic progression is as follows: AFQMC 0 (orbital map I, NOON threshold 0.01) \rightarrow orbital map II, NOON threshold 0.001 \rightarrow orbital map III, NOON threshold 0.005. Only BN, LiF and Li₂ required orbital maps IV and V. AFQMC 0 is deliberately chosen to be loose, while the following progressions prioritize using a larger first active space and the NOON threshold were chosen based on how many determinants can be realistically used with L-AFQMC (which for this work we cap at 2000 or 3000) where we still maintain close to 99% of the CI weight. Table S6 shows the trials required for each molecule, where "I, 0.01" is always the AFQMC 0 trial, and for AFQMC I and AFQMC II, the outliers are replaced with more sophisticated trials, where available. The trial shown is the smallest orbital map required (out of the list in Table S4) to achieve < 2 kcal/mol deviation, and the combination of these trials comprise AFQMC I. The few molecules which have thresholds that deviate from the "default" NOON thresholds of 0.001 or 0.005 for orbital map II and III respectively are either limited by the number of determinants that our computational resources allow (if higher) or require more determinants (if lower). See Table S5 for an example. As mentioned in the main text, we run a few additional W-AFQMC trials other than the AFQMC I outliers, to check the updated experimental values or geometry discrepancies (see main text Section 2.2 and Table S7 below).

Table S6: The full list of molecules and trials (valence orbital map, NOON threshold, and CI% retained if not 99.5%) are reported, as well as if the molecule is an outlier (> 2 kcal/mol deviation from the reference value), and the number of determinants for each trial. Unless indicated otherwise, the trials shown are for L-AFQMC, and "I, 0.01" is the AFQMC 0 protocol, while AFQMC I uses more sophisticated trials for the outliers of AFQMC 0. The number of determinants shown are for the TZ basis set.

Molecule	Datasets	AFQMC 0	AFQMC I	AFQMC II	AFQMC 0	AFQMC I	AFQMC II	AFQMC 0	AFQMC I	AFQMC II
					outlier?	outlier?	outlier?	dets	dets	dets
2-butyne	G2	I, 0.01	I, 0.01	I, 0.01				1	1	1
Acetaldehyde	G2	I, 0.01	I, 0.01	I, 0.01				1	1	1

Acetylene	G2	I, 0.01	I, 0.01	I, 0.01		1	1	1
Acetone	G2	I, 0.01	I, 0.01	I, 0.01		1	1	1
AlCl3	G2	I, 0.01	I, 0.01	W-AFQMC		1	1	10000
AlF3	G2	I, 0.01	I, 0.01	W-AFQMC		1	1	10000
Allene	G2	I, 0.01	I, 0.01	I, 0.01		1	1	1
Aziridine	G2	I, 0.01	I, 0.01	I, 0.01		1	1	1
BCl3	G2	I, 0.01	I, 0.01	I, 0.01		1	1	1
Benzene	G2	I, 0.01	I, 0.01	I, 0.01		5	5	5
BF3	G2	I, 0.01	I, 0.01	I, 0.01		1	1	1
Bicyclo-1-1-0-butane	G2	I, 0.01	III, 0.005	W-AFQMC	Yes	1	234	10000
CCl2CCl2	G2	I, 0.01	I, 0.01	I, 0.01		2	2	2
CCl4	G2	I, 0.01	I, 0.01	I, 0.01		1	1	1
CF2CF2	G2	I, 0.01	I, 0.01	W-AFQMC		1	1	10000
CF3-CN	G2	I, 0.01	I, 0.01	I, 0.01		1	1	1
CF4	G2	I, 0.01	I, 0.01	I, 0.01		1	1	1
CH2CH-CN	G2	I, 0.01	I, 0.01	W-AFQMC		2	2	10000
CH2Cl2	G2	I, 0.01	I, 0.01	I, 0.01		1	1	1
CH2F2	G2	I, 0.01	I, 0.01	I, 0.01		1	1	1
CH3-CH2-CH2-Cl	G2	I, 0.01	I, 0.01	I, 0.01		1	1	1
CH3-CH2-Cl	G2	I, 0.01	I, 0.01	I, 0.01		1	1	1
CH3-CH2-O-CH3	G2	I, 0.01	I, 0.01	I, 0.01		1	1	1
CH3-CH2-SH	G2	I, 0.01	I, 0.01	I, 0.01		1	1	1
CH3-CN	G2	I, 0.01	I, 0.01	I, 0.01		1	1	1
CH3-O-CH3	G2	I, 0.01	I, 0.01	I, 0.01		1	1	1
CH3-O-NO	G2	I, 0.01	I, 0.01	I, 0.01		2	2	2
CH3-S-CH3	G2	I, 0.01	I, 0.01	I, 0.01		1	1	1
CH3-SH	G2	I, 0.01	I, 0.01	I, 0.01		1	1	1
CH3-SiH3	G2	I, 0.01	I, 0.01	I, 0.01		1	1	1
CH3CFO	G2	I, 0.01	I, 0.01	I, 0.01		1	1	1
CH3Cl	G2	I, 0.01	I, 0.01	I, 0.01		1	1	1
CH3COCl	G2	I, 0.01	I, 0.01	I, 0.01		1	1	1
CH3CONH2	G2	I, 0.01	I, 0.01	I, 0.01		1	1	1
CH3COOH	G2	I, 0.01	I, 0.01	I, 0.01		1	1	1
CH3NO2	G2	I, 0.01	I, 0.01	I, 0.01		3	3	3
CH4	G2	I, 0.01	I, 0.01	I, 0.01		1	1	1
CHCl3	G2	I, 0.01	I, 0.01	I, 0.01		1	1	1
Cl2	G2	I, 0.01	I, 0.01	I, 0.01		2	2	2
ClF	G2	I, 0.01	I, 0.01	I, 0.01		2	2	2
CLF3	G2, MR	I, 0.01	II, 0.001	II, 0.001	Yes	2	1971	1971
ClNO	G2	I, 0.01	I, 0.01	I, 0.01		13	13	13
CO	G2	I, 0.01	I, 0.01	I, 0.01		1	1	1
CO2	G2	I, 0.01	I, 0.01	I, 0.01		1	1	1
CS	G2	I, 0.01	I, 0.01	I, 0.01		12	12	12
CS2	G2	I, 0.01	I, 0.01	I, 0.01		13	13	13
Cyanogen	G2	I, 0.01	I, 0.01	I, 0.01		12	12	12
Cyclobutane	G2	I, 0.01	I, 0.01	I, 0.01		1	1	1
Cyclobutene	G2	I, 0.01	I, 0.01	W-AFQMC		1	1	10000
Cyclopropane	G2	I, 0.01	I, 0.01	I, 0.01		1	1	1
Cyclopropene	G2	I, 0.01	I, 0.01	I, 0.01		1	1	1
Dimethylamine	G2	I, 0.01	I, 0.01	I, 0.01		1	1	1
Dimethylsulfoxide	G2	I, 0.01	I, 0.01	I, 0.01		1	1	1
Ethane	G2	I, 0.01	I, 0.01	I, 0.01		1	1	1

Ethanol	G2	I, 0.01	I, 0.01	I, 0.01			1	1	1
Ethenone	G2	I, 0.01	I, 0.01	I, 0.01			1	1	1
Ethylene	G2	I, 0.01	I, 0.01	I, 0.01			1	1	1
F2	G2	I, 0.01	II, 0.001	II, 0.001	Yes		2	13	13
F2O	G2	I, 0.01	II, 0.001	II, 0.001	Yes		1	257	257
Furan	G2	I, 0.01	I, 0.01	I, 0.01			1	1	1
Glyoxal	G2	I, 0.01	I, 0.01	I, 0.01			3	3	3
H2	G2	I, 0.01	I, 0.01	I, 0.01			1	1	1
H2CO	G2	I, 0.01	I, 0.01	I, 0.01			1	1	1
H2NNH2	G2	I, 0.01	I, 0.01	I, 0.01			1	1	1
H2O	G2	I, 0.01	I, 0.01	I, 0.01			1	1	1
HCF3	G2	I, 0.01	I, 0.01	I, 0.01			1	1	1
HCl	G2	I, 0.01	I, 0.01	I, 0.01			2	2	2
HCN	G2	I, 0.01	I, 0.01	I, 0.01			1	1	1
HCOOCH3	G2	I, 0.01	I, 0.01	I, 0.01			1	1	1
HCOOH	G2	I, 0.01	I, 0.01	I, 0.01			1	1	1
HF	G2	I, 0.01	I, 0.01	I, 0.01			1	1	1
HOCl	G2	I, 0.01	I, 0.01	I, 0.01			1	1	1
HOOH	G2	I, 0.01	I, 0.01	I, 0.01			1	1	1
Isobutane	G2	I, 0.01	I, 0.01	I, 0.01			1	1	1
Isobutene	G2	I, 0.01	I, 0.01	I, 0.01			1	1	1
Isopropyl-alcohol	G2	I, 0.01	I, 0.01	I, 0.01			1	1	1
Ketene	G2	I, 0.01	I, 0.01	I, 0.01			1	1	1
Li2	G2	I, 0.01	V, 1e-5	V, 1e-5	Yes		1	5	5
LiF	G2	I, 0.01	V, 1e-5	W-AFQMC	Yes		1	48	10000
LiH	G2	I, 0.01	I, 0.01	I, 0.01			1	1	1
Methanol	G2	I, 0.01	I, 0.01	I, 0.01			1	1	1
Methylamine	G2	I, 0.01	I, 0.01	I, 0.01			1	1	1
Methylene-cyclopropane	G2	I, 0.01	I, 0.01	I, 0.01			1	1	1
N2	G2	I, 0.01	I, 0.01	I, 0.01			1	1	1
Na2	G2	I, 0.01	I, 0.01	I, 0.01			2	2	2
NaCl	G2	I, 0.01	I, 0.01	I, 0.01			1	1	1
NF3	G2	I, 0.01	I, 0.01	I, 0.01			1	1	1
NH3	G2	I, 0.01	I, 0.01	I, 0.01			1	1	1
NNO	G2	I, 0.01	I, 0.01	I, 0.01			1	1	1
OCS-m1	G2	I, 0.01	II, 0.001	II, 0.001	Yes		1	439	439
Oxirane	G2	I, 0.01	I, 0.01	I, 0.01			1	1	1
Ozone	G2, MR	I, 0.01	III, 0.002, 98.5%	W-AFQMC	Yes	Yes	3	2234	10000
P2	G2	I, 0.01	I, 0.01	I, 0.01			15	15	15
PF3	G2	I, 0.01	I, 0.01	I, 0.01			1	1	1
PH3	G2	I, 0.01	I, 0.01	I, 0.01			1	1	1
Propane	G2	I, 0.01	I, 0.01	I, 0.01			1	1	1
Propene-CS	G2	I, 0.01	I, 0.01	I, 0.01			1	1	1
Propyne	G2	I, 0.01	I, 0.01	I, 0.01			1	1	1
Pyridine	G2	I, 0.01	I, 0.01	I, 0.01			5	5	5
Pyrole	G2	I, 0.01	I, 0.01	I, 0.01			1	1	1
SH2	G2	I, 0.01	I, 0.01	I, 0.01			1	1	1
Si2H6	G2	I, 0.01	I, 0.01	I, 0.01			1	1	1
SiCl4	G2	I, 0.01	I, 0.01	I, 0.01			1	1	1
SiF4	G2	I, 0.01	I, 0.01	I, 0.01			1	1	1
SiH4	G2	I, 0.01	I, 0.01	I, 0.01			1	1	1
SiO	G2	I, 0.01	I, 0.01	I, 0.01			1	1	1
SO2	G2	I, 0.01	I, 0.01	W-AFQMC			3	3	10000

Spiropentane	G2	I, 0.01	I, 0.01	I, 0.01				1	1	1
Thiooxirane	G2	I, 0.01	II, 0.001	II, 0.001	Yes			1	24	24
Thiophene	G2	I, 0.01	I, 0.01	I, 0.01				1	1	1
Trans-1-3-butadiene	G2	I, 0.01	II, 0.001	II, 0.001	Yes			1	15	15
Trans-butane	G2	I, 0.01	I, 0.01	I, 0.01				1	1	1
Trans-ethylamine	G2	I, 0.01	I, 0.01	I, 0.01				1	1	1
Trimethyl-amine	G2	I, 0.01	I, 0.01	I, 0.01				1	1	1
Vinyl-chloride	G2	I, 0.01	I, 0.01	W-AFQMC				1	1	10000
Vinyl-fluoride	G2	I, 0.01	I, 0.01	I, 0.01				1	1	1
1,3-cyclohexadiene	G3	I, 0.01	II, 0.001	II, 0.001	Yes			1	131	131
1,3-DiFluorobenzene	G3	I, 0.01	I, 0.01	I, 0.01				2	2	2
1,4-DiFluorobenzene	G3	I, 0.01	I, 0.01	I, 0.01				6	6	6
2-methyl	G3	I, 0.01	I, 0.01	I, 0.01				1	1	1
2,5-Dihydrothiophene	G3	I, 0.01	I, 0.01	I, 0.01				1	1	1
3-methyl	G3	I, 0.01	I, 0.01	I, 0.01				1	1	1
Acetic	G3	I, 0.01	II, 0.001	II, 0.001	Yes			1	1166	1166
azulene	G3	I, 0.01	II, 0.001, 98%	W-AFQMC	Yes			12	2347	10000
benzoquinone	G3	I, 0.01	I, 0.01	W-AFQMC				6	6	10000
c2f6	G3	I, 0.01	I, 0.01	W-AFQMC				1	1	10000
C4H4N2	G3	I, 0.01	II, 0.001	W-AFQMC	Yes	Yes		7	736	10000
C4H6	G3	I, 0.01	I, 0.01	I, 0.01				1	1	1
C4H6O	G3	I, 0.01	I, 0.01	I, 0.01				1	1	1
C4H8O2	G3	I, 0.01	I, 0.01	I, 0.01				1	1	1
C5H8	G3	I, 0.01	I, 0.01	I, 0.01				1	1	1
C6H12	G3	I, 0.01	I, 0.01	I, 0.01				1	1	1
C6H5-CH3	G3	I, 0.01	I, 0.01	I, 0.01				1	1	1
C6H5-NH2	G3	I, 0.01	I, 0.01	I, 0.01				1	1	1
C6H5-OH	G3	I, 0.01	I, 0.01	I, 0.01				1	1	1
cf3cl	G3	I, 0.01	I, 0.01	I, 0.01				1	1	1
CH3_2CH-CHO	G3	I, 0.01	I, 0.01	I, 0.01				1	1	1
CH3_2CH-CN	G3	I, 0.01	I, 0.01	I, 0.01				1	1	1
CH3_2CH-O-CH-CH3_2	G3	I, 0.01	I, 0.01	I, 0.01				1	1	1
CH3_3C-NH2	G3	I, 0.01	I, 0.01	I, 0.01				1	1	1
CH3_3C-O-CH3	G3	I, 0.01	I, 0.01	I, 0.01				1	1	1
CH3_3C-SH	G3	I, 0.01	I, 0.01	I, 0.01				1	1	1
CH3-C_O_-CCH	G3	I, 0.01	III, 0.005,98.5%	W-AFQMC	Yes	Yes	Yes	2	1701	10000
CH3-C_O_-O-CH-CH3_2	G3	I, 0.01	I, 0.01	I, 0.01				1	1	1
CH3-C_O_-OCH3	G3	I, 0.01	I, 0.01	I, 0.01				1	1	1
CH3-CH-CH-CH3_2	G3	I, 0.01	I, 0.01	I, 0.01				1	1	1
CH3-CH2-CH-CH3-NO2	G3	I, 0.01	I, 0.01	I, 0.01				3	3	3
CH3-CH2-CO-CH2-CH3	G3	I, 0.01	II, 0.001	II, 0.001	Yes			1	2	2
CH3-CH2-O-CH2-CH3	G3	I, 0.01	I, 0.01	I, 0.01				1	1	1

CH3-CH2-S-S- CH2-CH3	G3	I, 0.01	I, 0.01	I, 0.01		1	1	1
CH3-CHCH-CHO	G3	I, 0.01	I, 0.01	I, 0.01		2	2	2
CH3-CO-CH2- CH3	G3	I, 0.01	I, 0.01	I, 0.01		1	1	1
Chlorobenzene	G3	I, 0.01	I, 0.01	I, 0.01		5	5	5
Cl2O2S	G3	I, 0.01	I, 0.01	W-AFQMC		2	2	10000
Cl2S2	G3	I, 0.01	I, 0.01	I, 0.01		6	6	6
cyclooctatetraene	G3	I, 0.01	I, 0.01	W-AFQMC		1	1	10000
cyclopentane	G3	I, 0.01	I, 0.01	I, 0.01		1	1	1
cyclopentanone	G3	I, 0.01	I, 0.01	I, 0.01		1	1	1
dimethyl	G3	I, 0.01	I, 0.01	I, 0.01		1	1	1
Fluorobenzene	G3	I, 0.01	I, 0.01	I, 0.01		1	1	1
n-Butyl	G3	I, 0.01	I, 0.01	I, 0.01		1	1	1
n-heptane	G3	I, 0.01	I, 0.01	I, 0.01		1	1	1
n-hexane	G3	I, 0.01	I, 0.01	I, 0.01		1	1	1
N-methyl	G3	I, 0.01	I, 0.01	I, 0.01		1	1	1
n-octane	G3	I, 0.01	I, 0.01	I, 0.01		1	1	1
n-pentane	G3	I, 0.01	I, 0.01	I, 0.01		1	1	1
Naphthalene	G3	I, 0.01	I, 0.01	W-AFQMC		7	7	10000
NC-CH2-CH2- CN	G3	I, 0.01	I, 0.01	I, 0.01		1	1	1
Neopentane	G3	I, 0.01	I, 0.01	I, 0.01		1	1	1
P4	G3	I, 0.01	I, 0.01	I, 0.01		1	1	1
para- cyclohexadiene	G3	I, 0.01	I, 0.01	I, 0.01		1	1	1
PCl3	G3	I, 0.01	I, 0.01	I, 0.01		1	1	1
PCl5	G3	I, 0.01	I, 0.01	I, 0.01		1	1	1
Perhydropyridine	G3	I, 0.01	I, 0.01	I, 0.01		1	1	1
pf5	G3	I, 0.01	I, 0.01	I, 0.01		1	1	1
POCl3	G3	I, 0.01	I, 0.01	I, 0.01		1	1	1
pyrimidine	G3	I, 0.01	II, 0.001	II, 0.001	Yes	6	1054	1054
SCl2	G3	I, 0.01	I, 0.01	I, 0.01		1	1	1
sf6	G3	I, 0.01	I, 0.01	W-AFQMC		1	1	10000
SiCl2	G3	I, 0.01	I, 0.01	I, 0.01		2	2	2
SO3	G3	I, 0.01	I, 0.01	I, 0.01		3	1	1
t-butanol	G3	I, 0.01	I, 0.01	I, 0.01		1	1	1
t-Butyl	G3	I, 0.01	I, 0.01	I, 0.01		1	1	1
tetrahydrofuran	G3	I, 0.01	I, 0.01	I, 0.01		1	1	1
Tetrahydropyran	G3	I, 0.01	I, 0.01	I, 0.01		1	1	1
Tetrahydropyrrole	G3	I, 0.01	I, 0.01	I, 0.01		1	1	1
Tetrahydrothiophene	G3	I, 0.01	I, 0.01	I, 0.01		1	1	1
Tetrahydrothiopyran	G3	I, 0.01	I, 0.01	I, 0.01		1	1	1
Tetramethylsilane	G3	I, 0.01	I, 0.01	I, 0.01		1	1	1
alcl	W4-11	I, 0.01	I, 0.01	I, 0.01		1	1	1
alf	W4-11	I, 0.01	I, 0.01	I, 0.01		1	1	1
alh	W4-11	I, 0.01	I, 0.01	I, 0.01		1	1	1
alh3	W4-11	I, 0.01	I, 0.01	I, 0.01		1	1	1
b2h6	W4-11	I, 0.01	I, 0.01	I, 0.01		1	1	1
bf	W4-11	I, 0.01	I, 0.01	I, 0.01		1	1	1
bh	W4-11	I, 0.01	I, 0.01	I, 0.01		1	1	1
bh3	W4-11	I, 0.01	I, 0.01	I, 0.01		1	1	1
bhf2	W4-11	I, 0.01	I, 0.01	I, 0.01		1	1	1
c-hono	W4-11	I, 0.01	I, 0.01	I, 0.01		2	2	2
c-n2h2	W4-11	I, 0.01	I, 0.01	I, 0.01		2	2	2

ch2nh	W4-11	I, 0.01	I, 0.01	I, 0.01		1	1	1
ch3f	W4-11	I, 0.01	I, 0.01	I, 0.01		1	1	1
clcn	W4-11	I, 0.01	I, 0.01	I, 0.01		1	1	1
dioxirane	W4-11	I, 0.01	I, 0.01	I, 0.01		1	1	1
f2co	W4-11	I, 0.01	II, 0.001	II, 0.001	Yes	1	25	25
fccf	W4-11	I, 0.01	I, 0.01	I, 0.01		1	1	1
hccf	W4-11	I, 0.01	I, 0.01	I, 0.01		1	1	1
hcno	W4-11	I, 0.01	I, 0.01	I, 0.01		1	1	1
hcof	W4-11	I, 0.01	I, 0.01	I, 0.01		1	1	1
hnco	W4-11	I, 0.01	II, 0.001	II, 0.001	Yes	1	50	50
hnnn	W4-11	I, 0.01	I, 0.01	I, 0.01		1	1	1
hno	W4-11	I, 0.01	I, 0.01	I, 0.01		2	2	2
hocn	W4-11	I, 0.01	I, 0.01	I, 0.01		1	1	1
hof	W4-11	I, 0.01	I, 0.01	I, 0.01		1	1	1
nh2cl	W4-11	I, 0.01	I, 0.01	I, 0.01		1	1	1
oxirene	W4-11	I, 0.01	I, 0.01	I, 0.01		1	1	1
s2o	W4-11	I, 0.01	I, 0.01	W-AFQMC		2	2	10000
sih3f	W4-11	I, 0.01	I, 0.01	I, 0.01		1	1	1
t-hono	W4-11	I, 0.01	I, 0.01	I, 0.01		2	2	2
t-n2h2	W4-11	I, 0.01	I, 0.01	I, 0.01		1	1	1
c2h5f	W4-11	I, 0.01	I, 0.01	I, 0.01		1	1	1
bn	W4-11, MR	I, 0.01	IV, 0.001	IV, 0.001	Yes	2	1597	1597
c2	W4-11, MR	I, 0.01	III, 0.001	III, 0.001	Yes	2	771	771
cl2o	W4-11	I, 0.01	I, 0.01	I, 0.01		1	1	1
foof	W4-11, MR	I, 0.01	I, 0.01	W-AFQMC		13	13	10000
s3	W4-11, MR	I, 0.01	I, 0.01	W-AFQMC		3	3	10000
s4-c2v	W4-11, MR	I, 0.01	I, 0.01	W-AFQMC		10	10	10000
clf5	W4-17, MR	I, 0.01	II, 0.001, 98.5%	II, 0.001, 98.5%	Yes	2	2187	2187
cloocl	W4-17, MR	I, 0.01	I, 0.01	I, 0.01		5	5	5
beta-lactim	W4-17	I, 0.01	I, 0.01	I, 0.01		1	1	1
borole	W4-17	I, 0.01	I, 0.01	I, 0.01		1	1	1
c2cl2	W4-17	I, 0.01	I, 0.01	I, 0.01		1	1	1
c2cl6	W4-17	I, 0.01	I, 0.01	I, 0.01		1	1	1
c2clh	W4-17	I, 0.01	I, 0.01	I, 0.01		1	1	1
ccl2o	W4-17	I, 0.01	I, 0.01	I, 0.01		1	1	1
cf2cl2	W4-17	I, 0.01	I, 0.01	I, 0.01		1	1	1
ch2clf	W4-17	I, 0.01	I, 0.01	I, 0.01		1	1	1
ch3ph2	W4-17	I, 0.01	I, 0.01	I, 0.01		1	1	1
cis-c2f2cl2	W4-17	I, 0.01	I, 0.01	I, 0.01		1	1	1
clcof	W4-17	I, 0.01	II, 0.001	II, 0.001	Yes	1	481	481
cyclobutadiene	W4-17	I, 0.01	II, 0.001	II, 0.001	Yes	1	52	52
cyclopentadiene	W4-17	I, 0.01	I, 0.01	I, 0.01		1	1	1
dioxetan2one	W4-17	I, 0.01	II, 0.001	II, 0.001	Yes	1	191	191
dioxetane	W4-17	I, 0.01	I, 0.01	I, 0.01		1	1	1
dithiotane	W4-17	I, 0.01	I, 0.01	I, 0.01		1	1	1
fno	W4-17	I, 0.01	I, 0.01	I, 0.01		2	2	2
formamide	W4-17	I, 0.01	I, 0.01	I, 0.01		1	1	1
formic-anhydride	W4-17	I, 0.01	I, 0.01	I, 0.01		1	1	1

hclo4	W4-17	I, 0.01	II, 0.001, 99%	II, 0.001, 99%	Yes	1	2428	2428
hoclo2	W4-17	I, 0.01	II, 0.001	II, 0.001	Yes	1	3086	3086
hoclo	W4-17	I, 0.01	II, 0.001	II, 0.001	Yes	1	553	553
n2o4	W4-17, MR	I, 0.01	II, 0.002	W-AFQMC	Yes	70	3506	10000
nh2f	W4-17	I, 0.01	I, 0.01	I, 0.01		1	1	1
nh2oh	W4-17	I, 0.01	I, 0.01	I, 0.01		1	1	1
oxadiazole	W4-17	I, 0.01	I, 0.01	I, 0.01		3	3	3
oxetane	W4-17	I, 0.01	I, 0.01	I, 0.01		1	1	1
silole	W4-17	I, 0.01	III, 0.005, 99%	III, 0.005, 99%	Yes	2	1621	1621
tetrahydrane	W4-17	I, 0.01	I, 0.01	I, 0.01		1	1	1
trans-c2f2cl2	W4-17	I, 0.01	I, 0.01	I, 0.01		1	1	1

W-AFQMC

The procedure for the W-AFQMC is similar to that for the trials run using L-AFQMC discussed above, with differences accounting for the ability to run with more determinants. We also attempt to converge atom energies with this implementation rather than use the fitted atom energies, due to the ability to run upwards of 10 thousand determinants and in account of atomic energies being difficult to calculate with AFQMC.³ Firstly, we use an active space with all valence electrons and the 100 lowest energy valence Hartree Fock orbitals for the first HCI calculation, rather than selecting based on a (generally smaller) orbital map as above. This space can be enlarged further for bigger or more correlated molecules, but we found our choice to be sufficient for the mostly single-reference molecules studied here. We used an $\epsilon_1 = 10^{-4}$ threshold for the variational HCI calculations for molecules, while a tighter threshold of $\epsilon_1 = 5 \times 10^{-5}$ for atoms. To choose active space for the second calculation, we use a NOON threshold of 0.001 for molecules and 0.0001 for atoms. For this study, this procedure produced active spaces of up to 60 orbitals. Finally, rather than HCI calculation as above, we perform an HCISCF calculation using this active space with the same ϵ_1 as in the first step. The goal here is not to converge the HCISCF calculation very well, but to generate a good set of orbitals to allow compact HCI expansions. We use up to 10^4 leading determinants from the HCI expansion in these optimized orbitals as trial states in AFQMC. This choice for the number of determinants was made based on tests of convergence for a set of molecules from the multireference subset, which requires more determinants for convergence. As an illustrative example, we show the convergence trace with respect to the number of determinants for the ozone molecule in Fig. S2. The energy is converged within stochastic error bars at 10^3 determinants in this case.

Table S7: All of the molecules run using the W-AFQMC (these, combined with the rest of the molecules run using AFQMC I, form AFQMC II) and their deviations in kcal/mol, and statistical error in parentheses. The "AFQMC I" results are shown for comparison, a combination of AFQMC 0 and better trial wavefunctions. DLPNO-CCSD(T) and CCSD(T) deviations are also shown for comparison. Azulene and naphthalene CCSD(T) results are unavailable due to limitations in disk space.

Molecule	Dataset	AFQMC I	AFQMC II	DLPNO	CCSD(T)
AlCl3	G2	1.10(48)	-1.95(43)	0.77	0.73
AlF3	G2	1.78(58)	-1.41(35)	0.11	0.14
Bicyclo-1-1-0-butane	G2	-1.74(42)	-1.50(43)	-1.92	-1.92
CF2CF2	G2	0.33(58)	-1.28(69)	0.32	0.40
CH2CH-CN	G2	0.61(73)	-0.83(35)	-0.79	-0.74
Cyclobutene	G2	-0.52(46)	-0.38(36)	-0.19	-0.14
LiF	G2	0.91(11)	0.47(9)	1.17	1.18
Ozone	G2, MR	-2.57(25)	-0.96(35)	-3.24	-2.07
SO2	G2	-1.88(74)	-0.76(43)	-1.62	-1.24
Vinyl-chloride	G2	-1.17(47)	-1.26(27)	-0.13	-0.11
azulene	G3	1.73(99)	0.99(105)	0.53	N/A
benzoquinone	G3	-1.77(70)	-1.92(85)	-1.40	-0.69
c2f6	G3	1.72(85)	0.55(91)	1.19	1.22
3-butyn-2-one	G3	-4.68(55)	-4.60(69)	-3.57	-3.35
C4H4N2	G3	-3.11(77)	-1.74(53)	-2.52	-1.96
Cl2O2S	G3	-1.98(69)	-1.99(78)	-3.43	-3.53
cyclooctatetraene	G3	-1.43(65)	-1.49(104)	-2.42	-1.99
Naphthalene	G3	-0.37(89)	-1.15(113)	-1.02	N/A
sf6	G3	-1.46(89)	-0.60(88)	-1.61	-1.71
foof	W4-11, MR	-0.69(78)	0.60(52)	-1.12	-0.57
s2o	W4-11	0.17(52)	-1.48(35)	-0.21	0.52
S3	W4-11, MR	-0.71(47)	-0.34(86)	0.05	0.82
S4	W4-11, MR	0.07(79)	-1.44(88)	-1.26	0.66
n2o4	W4-17, MR	-1.47(79)	-1.09(79)	0.03	1.67
RMSD		1.74(14)	1.54(15)	1.67	1.55

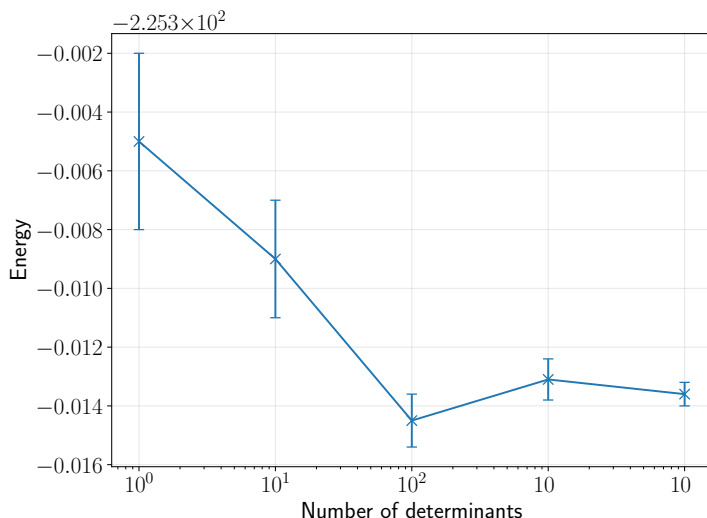


Figure S2: Convergence of the ground state energy of ozone with respect to the number of determinants in the trial calculated using W-AFQMC. We used the aug-cc-pVTZ-DK basis set and froze the core electrons. The trial active space obtained using the natural orbital procedure has the size (18e, 37o).

We used the following formula, due to Martin,⁴ for performing two-point CBS extrapolations:

$$E_n = E_\infty + \frac{A}{(n + \frac{1}{2})^4}, \quad (\text{S1})$$

where n is the cardinality of the basis set. We denote the CBS limit obtained using basis sets of cardinality n_1 and n_2 using method M as $E_M^{n_1 n_2}$. aug-cc-pVnZ-DK basis sets were used for frozen core AFQMC and MP2 calculations. We add the MP2 basis set correction to AFQMC energies as

$$E_{\text{AFQMC},\infty} \approx E_{\text{AFQMC}}^{DT} + E_{\text{MP2}}^{Q5} - E_{\text{MP2}}^{DT}. \quad (\text{S2})$$

In a few cases where the 5Z basis set HF calculations could not be converged, we used the E_{MP2}^{QT} energy instead.

The AFQMC II results involve taking select molecules (e.g. outliers, or molecules with experimental uncertainty) and running using the aforementioned protocol, and combining these results with the AFQMC I of molecules not run using this second implementation (see Table S6). Again, AFQMC II progressively builds on AFQMC I. Note that these basis sets and CBS extrapolation schemes only apply to W-AFQMC, where we prioritize running with a large number of determinants. For AFQMC 0, AFQMC I, CCSD(T), and DLPNO-CCSD(T), see the main text for the basis sets and CBS. The full list of trials run using

W-AFQMC is shown in Table S7. For this subspace of data, AFQMC, CCSD(T), and DLPNO-CCSD(T) perform very similarly.

4. AFQMC Localization

For all molecules and trials for L-AFQMC, we use the compression threshold of T_{SVD} 0.0001, which is shown to be close to convergence (of energy) to the non-compressed implementation.⁵ For a representative molecule, CCl₄, as shown in Table S8, with AFQMC 0 (1 determinant in this case), the compression rate is 60% for frozen core and 80% for all-electron. The CBS energy difference between L-AFQMC with and without compression is -0.06 kcal/mol, for the frozen core calculation, which is one tenth of the statistical error. On the other hand, the all-electron compression error is on the order of -3 kcal/mol. For reference, the energy of the 200 determinant CCl₄ trial also mentioned in the above section is -1884.5075(11), which is closer to the no LO value. As with the timestep error, we expect the LO error to decrease with increasing the active space in the trial. However, this is at the expense of less compression.

Table S8: CBS energy for frozen vs no frozen core for CCl₄ single determinant trial.

	LO CBS Energy (Ha)	No LO CBS Energy (Ha)	Difference (kcal/mol)
Frozen core	-1882.7855(10)	-1882.7856(10)	-0.06
All electron	-1884.5015(12)	-1884.5062(12)	-2.98

5. Frozen Core vs. All Electron Performance

As discussed in Section 2 above, the all electron calculations display a larger timestep error, which requires a larger number of determinants to converge and is not fully cancelled out by the atoms, even with atom fitting. Here, we look at the differences in overall performance between frozen core (with MP2 core-valence correction) and all-electron calculations. Table S9 lists the RMSD for the combined dataset for each method, with frozen and all-electron. Table S10 lists the number of outliers for each method. While the RMSD using all-electron calculation is decent across the dataset, the number of outliers significantly increases compared to frozen core.

Table S9: RMSD for the combined dataset of 259 molecules for frozen vs all electron calculations for each method, reported in kcal/mol.

Method	AFQMC 0	AFQMC I	CCSD(T)	DLPNO-CCSD(T)
Frozen	1.67	0.98	0.77	0.87
All electron	2.16	1.25	0.84	1.04

Table S10: Total number of outliers for frozen vs all electron calculation for each method.

Method	AFQMC 0	AFQMC I	CCSD(T)	DLPNO-CCSD(T)
Frozen	30	3	4	6
All electron	58	15	8	15

For a detailed list of all deviations, frozen and all electron, as well as the statistical errors, the AFQMC 0 and AFQMC I details (trial, active space, determinants for both TZ and QZ basis sets), as well as lists of the atomic energies, refer to the .xlsx spreadsheet also provided. Due to the difficulty of converging the all-electron trials, there are many cases where manual trials were selected in the way of chemical intuition and looking at orbital energies and symmetries to confirm the relatively larger deviation values are not due to the NOON selection procedure selecting qualitatively wrong CI expansions (AFQMC 0 remains as is without manual selection). For these manual selections, only one round of SHCI/SHCISCF is run with $\epsilon_1 = 5 \times 10^{-5}$, and the orbitals are selected from the HOMO-LUMO gap in the canonical (RHF) basis.

6. Composite CCSD(T) CBS

For the majority of G3 molecules and some G2 molecules (benzene, spiropentane, butane, trimethyl-amine), we are unable to run full CCSD(T) at the aug-cc-pVQZ-DK level due to limitations in disk space of the temporary directory of each of our computational nodes (2 TB). Therefore, we settle for a composite scheme where the CCSD(T) energy for aug-cc-p(C)VQZ-DK is extrapolated from DLPNO and cc-p(C)VQZ-DK CCSD(T).

$$E_{\text{CCSD(T)}}^{\text{aug-cc-p(C)VXZ}} \approx E_{\text{CCSD(T)}}^{\text{cc-p(C)VXZ}} + E_{\text{DLPNO 6/7}}^{\text{aug-cc-p(C)VXZ}} - E_{\text{DLPNO 6/7}}^{\text{cc-p(C)VXZ}} \quad (\text{S3})$$

where DLPNO 6/7 means DLPNO-CCSD(T) extrapolated with TCut6 and TCut7 PNO thresholds as discussed in main text Section 2.5 and 2.6. Overall, we do not get a significant difference using this composite CBS compared to full CCSD(T) aug-cc-p(C)VTZ/aug-cc-p(C)VQZ extrapolation. Table S11 shows the difference in single point energy between regular T/Q and this composite scheme. The composite scheme is consistently higher in energy, which means for calculating atomization energy the atom fit will cancel out the difference further.

Table S11: Difference in energy between the regular CCSD(T) T/Q CBS and CCSD(T) using the composite CBS scheme for the W4-17 set, reported in kcal/mol.

Molecule	CBS energy (kcal/mol)	diff
beta-lactim	-0.20	
borole	-0.15	
c2cl2	-0.12	
c2cl6	N/A	
c2clh	-0.09	
ccl2o	-0.08	
cf2cl2	-0.16	
ch2clf	-0.15	
ch3ph2	-0.10	
cis-c2f2cl2	-0.24	
clcof	-0.15	
clf5	-0.82	
cloocl	0.00	
cyclobutadiene	-0.20	

cyclopentadiene	-0.21
dioxetan2one	-0.27
dioxetane	-0.22
dithiotane	-0.22
fno	-0.24
formamide	-0.10
formic-anhydride	-0.15
hclo4	-0.09
hoclo2	-0.14
hoclo	-0.12
n2o4	-0.04
nh2f	-0.12
nh2oh	-0.13
oxadiazole	-0.41
oxetane	-0.12
silole	-0.18
tetrahydrane	-0.17
trans-c2f2cl2	-0.31

7. Effect of DKH2 or X2C

Table S12: HF energies for aug-cc-pCVTZ-DK basis set with frozen core, without relativistic Hamiltonian, with X2C, and with DKH2..

Molecule	HF no relham (Ha)	HF X2C (Ha)	HF DKH2 (Ha)	HF DKH2 - no relham (kcal/mol)	HF DKH2 - X2C (kcal/mol)
beta-lactim	-245.86732	-245.99934	-245.99941	-82.88765	-0.04
borole	-179.06580	-179.13416	-179.13419	-42.91142	-0.01
c2cl2	-994.03679	-997.54946	-997.55081	-2,205.04688	-0.84
c2cl6	-2,830.82156	-2,841.29977	-2,841.30379	-6,577.59784	-2.52
c2clh	-535.44360	-537.21538	-537.21606	-1,112.21485	-0.43
cc2o	-1,031.13482	-1,034.68839	-1,034.68977	-2,230.73158	-0.86
cf2cl2	-1,155.18237	-1,158.86763	-1,158.86911	-2,313.43201	-0.93
ch2clf	-597.69627	-599.54651	-599.54725	-1,161.48998	-0.47
ch3ph2	-381.36740	-382.37077	-382.37144	-630.03995	-0.42
cis-c2f2cl2	-1,193.01529	-1,196.71563	-1,196.71712	-2,322.89740	-0.93
clcof	-671.42697	-673.33284	-673.33362	-1,196.42645	-0.49
clf5_MR	-956.06111	-958.27092	-958.27195	-1,387.30234	-0.64
cloocl_MR	-1,067.90024	-1,071.49489	-1,071.49630	-2,256.52842	-0.88
cyclobutadiene	-153.69507	-153.75658	-153.75660	-38.60874	-0.01
cyclopentadiene	-192.85604	-192.93287	-192.93289	-48.22382	-0.02
dioxetan2one	-301.57987	-301.77693	-301.77705	-123.72616	-0.08
dioxetane	-227.81242	-227.95389	-227.95398	-88.82412	-0.05
dithiotane	-872.67266	-875.34988	-875.35130	-1,680.84919	-0.90
fno	-228.69739	-228.87767	-228.87779	-113.20593	-0.08
formamide	-168.99829	-169.09958	-169.09964	-63.59908	-0.04
formic-anhydride	-301.58866	-301.78581	-301.78593	-123.78963	-0.08
hclo4	-758.97780	-760.93752	-760.93834	-1,230.23922	-0.51
hoclo2	-684.15782	-686.06447	-686.06525	-1,196.91129	-0.49
hoclo	-609.34468	-611.19691	-611.19765	-1,162.73901	-0.47
n2o4	-408.18080	-408.46418	-408.46436	-177.93450	-0.11
nh2f	-155.01807	-155.14244	-155.14252	-78.09545	-0.05
nh2oh	-131.03832	-131.12431	-131.12436	-53.98654	-0.03
oxadiazole	-260.63036	-260.77797	-260.77805	-92.67488	-0.05
oxetane	-191.97620	-192.07760	-192.07765	-63.65914	-0.03
silole	-443.80478	-444.58867	-444.58927	-492.26886	-0.38
tetrahedrane	-153.65087	-153.71213	-153.71215	-38.45463	-0.01
trans-c2f2cl2	-1,193.01679	-1,196.71705	-1,196.71853	-2,322.84354	-0.93

Displayed in Tables S12 and S13 are the difference in total Hartree-Fock energies and MP2 energies for the basis set aug-cc-pCVTZ-DK i) without the use of a relativistic Hamiltonian, ii) with the use of the X2C Hamiltonian, and iii) with the use of the DKH2 Hamiltonian for the W4-17 dataset. The difference between the use of DKH2 and X2C in the total energy is small, especially for first-row atoms. For the second-row atoms, the difference between the use of DKH2 and X2C is approximately proportional to the

Table S13: MP2 energies for aug-cc-pCVTZ-DK basis set with frozen core without relativistic Hamiltonian, with X2C, and with DKH2.

Molecule	MP2 no relham (Ha)	MP2 X2C (Ha)	MP2 DKH2 (Ha)	MP2 DKH2 - no relham (kcal/mol)	MP2 DKH2 - X2C (kcal/mol)
beta-lactim	-246.81800	-246.95052	-246.95059	-83.20	-0.04
borole	-179.79723	-179.86582	-179.86585	-43.06	-0.01
c2cl2	-994.73057	-998.24384	-998.24519	-2,205.42	-0.85
c2cl6	-2,832.35764	-2,842.83774	-2,842.84175	-6,578.78	-2.52
c2clh	-535.94811	-537.72024	-537.72092	-1,112.44	-0.43
ccl2o	-1,031.92423	-1,035.47865	-1,035.48003	-2,231.27	-0.86
cf2cl2	-1,156.26245	-1,159.94898	-1,159.95047	-2,314.23	-0.93
ch2clf	-598.33102	-600.18192	-600.18267	-1,161.91	-0.47
ch3ph2	-381.71729	-382.72089	-382.72156	-630.18	-0.42
cis-c2f2cl2	-1,194.24248	-1,197.94411	-1,197.94560	-2,323.71	-0.93
clcof	-672.27791	-674.18465	-674.18543	-1,196.97	-0.49
clf5_MR	-957.70307	-959.91529	-959.91632	-1,388.81	-0.64
cloocl_MR	-1,068.79946	-1,072.39521	-1,072.39662	-2,257.22	-0.88
cyclobutadiene	-154.33868	-154.40041	-154.40043	-38.75	-0.01
cyclopentadiene	-193.67577	-193.75286	-193.75289	-48.39	-0.02
dioxetan2one	-302.61700	-302.81485	-302.81497	-124.23	-0.08
dioxetane	-228.63342	-228.77545	-228.77554	-89.18	-0.05
dithiotane	-873.37337	-876.05125	-876.05268	-1,681.27	-0.90
fno	-229.42315	-229.60414	-229.60426	-113.65	-0.08
formamide	-169.61996	-169.72165	-169.72171	-63.85	-0.04
formic-anhydride	-302.62283	-302.82077	-302.82089	-124.28	-0.08
hclo4	-760.72019	-762.17228	-762.17310	-911.70	-0.51
hoclo2	-685.60341	-687.05390	-687.05468	-910.67	-0.49
hoclo	-610.47327	-611.92055	-611.92129	-908.63	-0.47
n2o4	-409.94073	-409.91656	-409.91673	15.06	-0.11
nh2f	-155.51095	-155.63576	-155.63585	-78.37	-0.05
nh2oh	-131.52091	-131.60722	-131.60727	-54.20	-0.03
oxadiazole	-261.61319	-261.76146	-261.76153	-93.09	-0.05
oxetane	-192.73816	-192.83994	-192.84000	-63.91	-0.03
silole	-444.57097	-445.35522	-445.35583	-492.49	-0.38
tetrahydrane	-154.30672	-154.36822	-154.36824	-38.60	-0.01
trans-c2f2cl2	-1,194.24329	-1,197.94484	-1,197.94633	-2,323.66	-0.93

number of each atom (for example, Cl atom contributes 0.4 to 0.5 kcal/mol to the difference) which will become cancelled out with the atom fitting procedure as described in the main text.

8. Alternative Geometries

DFT geometry optimization with a small basis set and single point energy calculation with a higher-level theory is a popular approach and is used successfully to derive accurate thermochemistry in numerous methods such as G2/G3/G4 and ccCA, and is shown to provide accurate total energies^{6,7} as well as vibrational properties.^{7,8} While we do not use accurate wavefunction methods to optimize geometry for the entire dataset as this is generally limited to only very small systems,⁹⁻¹¹ there are cases where we have found that an alternative geometry is useful which we list here.

To assist SCF convergence, for the W4 "multireference" (TAEMR, which is separate from our MR subset, refer Section 11) molecules (BN, C2, Cl2O, FOOF, S3, S4, ClF5, F2O and ClOOC1), as well as a few other exceptions that help converge either AFQMC, CCSD(T) or DLPNO-CCSD(T) (CCl2CCl2, SO3, HClO4, HOClO2, HOClO, S2O, and N2O4), we use the CCSD(T)/cc-pV(Q+d)Z geometries provided by the W4-11¹² and W4-17¹³ sources for CCSD(T), DLPNO-CCSD(T) and AFQMC. In particular, we note, as shown in Table S14, cases where the CCSD(T) energy is noticeably improved (by > 2 kcal/mol) after using the CCSD(T)-optimized geometry. All geometries used in the correlated methods are provided in a .zip file.

Table S14: Comparison of CCSD(T) deviations from experiment for the molecules where the B3LYP/6-31G* optimized geometry shows a difference of > 2 kcal/mol in energy from that optimized by CCSD(T)/cc-pV(Q+d)Z.¹³

Molecule	B3LYP/6-31G* CCSD(T) deviation	CCSD(T)/cc-pV(Q+d)Z CCSD(T) deviation
SO3	-1.87	0.23
HClO4	-6.75	1.11
HOClO2	-3.88	0.73
HOClO	-1.91	0.28

9. Atom Energies

Table S15: Frozen core atom energy without MP2 core correction for CCSD(T). Ab initio energies are obtained the same way as for molecules in the main text (T/Q CBS extrapolation, see main text Section 2.6). Atomic energies fit to G2/G3 as discussed in Section 2.10. The difference between these energies is shown in kcal/mol.

CCSD(T) atom	Fitted atom energies (Ha)	Ab initio atom energies (Ha)	Diff (kcal/mol)
C	-37.80495	-37.80485	-0.059
O	-75.05708	-75.05855	0.919
S	-398.75915	-398.75935	0.124
F	-99.75609	-99.75658	0.304
N	-54.55929	-54.55991	0.387
B	-24.60865	-24.60916	0.321
Na	-162.39546	-162.39489	-0.357
Al	-242.37215	-242.37132	-0.517
Si	-289.54608	-289.54398	-1.318
P	-341.64853	-341.64883	0.188
Cl	-461.12061	-461.11929	-0.827
Li	-7.45643	-7.45327	-1.986

Atom energies before and after fitting to G2/G3 for the CCSD(T) and DLPNO-CCSD(T) methods are shown in Tables S15 and S16. *Ab initio* atom energies are obtained using the same method as for molecules (TZ/QZ CBS, see main text), and in addition with spin-orbit corrections.¹⁴ Atoms such as O and Si can be different on the order of 1 kcal/mol, while Li has a 2 kcal/mol in difference. Shown in Table S17 are the CCSD(T) RMSDs of the W4-11 and W4-17 datasets using the fitted atom energies (only using G2/G3 data) and using *ab initio* atom energies. There are no outliers (> 2kcal/mol) using the fitted atomic energies, while the outliers using *ab initio* atom energies are N2O4 (2.78 kcal/mol), C2Cl6 (-6.95 kcal/mol) and FOOF (3.01 kcal/mol).

We also note that the cases where AFQMC I and AFQMC 0 have different fitted atom energies, as shown in Tables S18 and S19. The all-electron (no frozen core) atom energies show more difference upon improving the results with AFQMC I, possibly due to the reduction of timestep error with using larger trials. The carbon atom energy being the most robust reflects the relative abundance of carbon in the G2/G3 datasets.

Table S16: Frozen core atom energy without MP2 core correction for DLPNO-CCSD(T). Ab initio energies are obtained the same way as for molecules in the main text (T/Q CBS extrapolation with TCutPNO 6/7, see main text Section 2.5 and 2.6). Atomic energies fit to G2/G3 as discussed in Section 2.10. The difference between these energies is shown in kcal/mol.

DLPNO atom	Fitted atom energies (Ha)	Ab initio atom energies (Ha)	Diff (kcal/mol)
C	-37.80453	-37.80477	0.152
O	-75.05634	-75.05763	0.806
S	-398.75851	-398.75867	0.101
F	-99.75562	-99.75537	-0.153
N	-54.55851	-54.55947	0.605
B	-24.60857	-24.60927	0.442
Na	-162.39518	-162.39485	-0.208
Al	-242.37209	-242.37148	-0.381
Si	-289.54591	-289.54389	-1.272
P	-341.64780	-341.64814	0.208
Cl	-461.12023	-461.11867	-0.980
Li	-7.45643	-7.45325	-1.996

Table S17: CCSD(T) RMSD of the W4 datasets in kcal/mol, using atom energies fitted from the G2/G3 experimental data compared to using *ab initio* atom energies from CCSD(T) with spin-orbit coupling and CBS extrapolation (see main text Section 2).

CCSD(T) Atom	W4-11	W4-17
Fitted	0.44	0.79
Ab initio	0.94	1.71

Table S18: Frozen core atom energy without MP2 core correction for AFQMC 0 and AFQMC I, fitted to G2/G3 heats of formation. The difference between these energies is shown in kcal/mol.

AFQMC atom, frozen	Fitted atom energies AFQMC 0 (Ha)	Fitted atom energies AFQMC I (Ha)	Diff (kcal/mol)
C	-37.80593	-37.80592	-0.009
O	-75.05872	-75.05884	0.079
S	-398.76035	-398.76024	-0.066
F	-99.75762	-99.75756	-0.039
N	-54.56073	-54.56062	-0.068
B	-24.60945	-24.60962	0.104
Na	-162.39617	-162.39618	0.006
Al	-242.37202	-242.37209	0.046
Si	-289.54708	-289.54712	0.028
P	-341.64971	-341.64975	0.022
Cl	-461.12163	-461.12158	-0.030
Li	-7.45746	-7.45650	-0.605

Table S19: All-electron atom energy without MP2 core correction for AFQMC 0 and AFQMC I, fitted to G2/G3 heats of formation. The difference between these energies is shown in kcal/mol.

AFQMC atom, no frozen	Fitted atom energies AFQMC 0 (Ha)	Fitted atom energies AFQMC I (Ha)	Diff (kcal/mol)
C	-37.84282	-37.84281	-0.008
O	-75.10131	-75.10148	0.107
S	-399.17722	-399.17728	0.040
F	-99.81872	-99.81892	0.128
N	-54.60029	-54.60011	-0.110
B	-24.64709	-24.64622	-0.547
Na	-162.45462	-162.45432	-0.189
Al	-242.77266	-242.77236	-0.191
Si	-289.95449	-289.95407	-0.260
P	-342.06083	-342.06072	-0.069
Cl	-461.54156	-461.54194	0.236
Li	-7.45773	-7.45707	-0.412

10. Computational Timings

Table S20: Timings of different benchmark methods for three molecules, for the basis aug-cc-pVTZ-DK.

Molecule	CCSD(T)	DLPNO	AFQMC 0	AFQMC I	W-AFQMC	AFQMC 0 dets	AFQMC I dets	W-AFQMC dets
Unit	CPU	CPU	GPU	GPU	CPU			
Bicyclobutane	1.20	1.44	35.4	347	530	1	1098	10000
N2O4	2.48	1.68	42.4	904	1175	80	3506	10000
Azulene	>176	30.9	111	3840	5440	12	2347	10000

Shown in Table S20 is the number of computational hours required for each benchmark method for a select few molecules. DLPNO refers to DLPNO-CCSD(T). Units are reported in hours. The CPU models we use are AMD EPYC 7643 48-Core Processor with 2 threads per core (96 threads) and run with 8 threads per calculation. GPU calculations are run with AMD Instinct MI250X GPU which have 2 GCDs each and each calculation is run with 80 or 160 "GPUs" (GCDs). Therefore one CPU hour refers to one hour on one thread and one GPU hour refers to one hour on one GCD. The total walltime of the calculation is the CPU or GPU hour divided by the number of parallel processes which is 8 for CPU calculations and 80 or 160 for GPU calculations with AFQMC 0. For AFQMC I, we use up to 960 parallel processes resulting in a real-world wall-time of under 4 hours. In Table S20, the azulene CCSD(T) time is the time elapsed before the calculation exhausts the temporary storage in the compute node and as a result we do not have a finished calculation for CCSD(T) energy. While we have not attempted to convert GPU hours and CPU hours to the same unit due to variations in hardware, GPU hours are usually much more expensive (on the order of $50\times$ ¹⁵). Therefore, for large determinant trials, W-AFQMC displays a cost advantage, although L-AFQMC runs much faster in real time due to GPU parallelization. However, we only use 250 walkers with W-AFQMC while we use 1920 walkers for L-AFQMC, and we reduce the amount of energy evaluation times by $2.5\times$ for W-AFQMC compared to L-AFQMC. While the larger active space and determinants for the W-AFQMC trial compensates for the statistical error to an extent, to achieve the same statistical error as L-AFQMC (Table S21) requires more sampling which will increase the computational time significantly. These factors make a quantitative comparison difficult. What is clear is the advantage of CCSD(T) and DLPNO-CCSD(T) for small systems, which is not surprising because of the prefactor in AFQMC as a statistical method that requires averaging over imaginary time. CCSD(T) however, scales prohibitively, as

can be seen for azulene.

Table S21: Statistical errors for the AFQMC protocols in only aug-cc-pVTZ-DK basis, reported in Hartrees.

St. err (Ha)	AFQMC 0	AFQMC I	W-AFQMC
Bicyclobutane	0.0004	0.0004	0.0005
n2o4	0.0007	0.0005	0.0009
azulene	0.0007	0.0007	0.0012

Although fluctuations in hardware (for example, filesystem load) make these timings approximate, the rough scaling of the DLPNO and L-AFQMC methods can be demonstrated. For example, we show the CPU and GPU hours for the entire W4-17 dataset in Tables S22 and S23. While DLPNO scales as approximately N^3 or N^2 (if we compare the same system with the TZ and QZ basis sets), and L-AFQMC does not appear to scale worse than this with system size from TZ to QZ. However, the prefactor makes the difference in absolute computational cost very noticeable from DLPNO-CCSD(T) to AFQMC. On the other hand, CCSD(T) shows larger fluctuations in timings.

Table S22: W4-17 dataset TZ (as used in the main text) timings (excluding Hartree-Fock times) in CPU hours for the coupled-cluster methods and GPU hours for AFQMC 0 and AFQMC I (AFQMC timings scaled to fixed 1 mHa statistical error). DLPNO-CCSD(T) was parallelized with 8 proceses and AFQMC 0 with 80 GPUs. AFQMC I is only shown if the trial was different from AFQMC 0.

W4-17 TZ	Electrons	Basis functions	DLPNO 7	DLPNO 6	CCSD(T)	AFQMC 0	AFQMC I
beta-lactim	38	345	1.52	0.56	2.89	5.16	
borole	34	345	1.42	0.55	2.38	5.71	
c2cl2	46	242	0.38	0.17	0.5	6.02	
c2cl6	114	542	7.45	4.21	44.35	13.00	
c2clh	30	190	0.2	0.07	0.16	2.90	
ccl2o	48	242	0.48	0.2	0.66	3.19	
cf2cl2	58	314	0.89	0.59	2.34	4.07	
ch2clf	34	226	0.24	0.1	0.38	1.35	
ch3ph2	26	236	0.2	0.07	0.29	1.47	
cis-c2f2cl2	64	360	1.84	0.87	4.98	6.99	
clcof	40	226	0.33	0.17	0.42	4.76	8.93

clf5_MR	62	370	2.55	1.27	8.32	11.87	315.75
cloocl_MR	50	242	0.53	0.22	0.7	5.05	
cyclobutadiene	28	276	0.73	0.24	0.75	3.84	4.51
cyclopentadiene	36	368	1.72	0.67	3.84	3.88	
dioxetan2one	38	276	0.88	0.38	1.22	5.87	13.95
dioxetane	32	276	0.61	0.25	1	3.79	
dithiotane	48	334	0.98	0.46	2.18	2.87	
fno	24	151	0.18	0.05	0.09	2.93	
formamide	24	207	0.29	0.09	0.26	1.54	
formic-anhydride	38	276	0.79	0.33	1.14	4.96	
hclo4	50	282	1.14	0.48	1.62	6.17	123.91
hoclo2	42	236	0.67	0.23	0.7	5.42	85.46
hoclo	34	190	0.3	0.14	0.25	4.95	15.64
n2o4	46	276	1.12	0.57	2.48	8.91	109.30
nh2f	18	151	0.11	0.05	0.07	1.36	
nh2oh	18	161	0.1	0.04	0.08	1.50	
oxadiazole	36	276	1.18	0.4	1.09	5.07	
oxetane	32	322	0.77	0.43	1.8	4.38	
silole	44	397	1.82	0.89	5.14	3.07	48.05
tetrahydrane	28	276	0.63	0.23	0.76	2.83	
trans-c2f2cl2	64	360	1.9	0.95	5.61	7.42	

Table S23: W4-17 dataset QZ (as used in the main text) timings (excluding Hartree-Fock times) in CPU hours for the coupled-cluster methods and GPU hours for AFQMC 0 and AFQMC I (AFQMC timings scaled to fixed 1 mHa statistical error). DLPNO-CCSD(T) was parallelized with 8 proceses and AFQMC 0 with 160 GPUs. AFQMC I is only shown if the trial was different from AFQMC 0.

W4-17 QZ	Electrons	Basis functions	DLPNO 7	DLPNO 6	CCSD(T)	AFQMC 0	AFQMC I
beta-lactim	38	630	6.04	2.61	36.18	14.31	
borole	34	630	5.37	2.24	33.65	22.84	
c2cl2	46	428	1.68	0.65	7.99	10.03	

c2cl6	114	964	35.74	23.25	N/A	66.02		
c2clh	30	340	0.7	0.25	10.02	4.97		
ccl2o	48	428	1.78	0.76	106.64	4.63		
cf2cl2	58	566	4.03	2.18	5.65	9.96		
ch2clf	34	415	1.01	0.42	11.92	3.78		
ch3ph2	26	444	0.9	0.32	49.67	5.67		
cis-c2f2cl2	64	646	7.82	4.3	5.52	24.46		
clcof	40	403	1.34	0.6	86.72	12.63	4.40	
clf5_MR	62	679	9.99	4.95	9.13	73.68	266.89	
cloocl_MR	50	428	1.97	0.78	34.75	12.44		
cyclobutadiene	28	504	2.51	0.93	72.91	15.75	7.74	
cyclopentadiene	36	676	6.86	3.6	6.91	12.86		
dioxetan2one	38	492	3.29	1.48	39.06	22.19	13.92	
dioxetane	32	504	2.3	1.02	237.1	10.53		
dithiotane	48	612	4.04	2.22	0.79	12.08		
fno	24	269	0.59	0.18	3.11	5.88		
formamide	24	378	1	0.34	28.26	6.15		
formic-anhydride	38	492	2.88	1.21	41.62	12.54		
hclo4	50	500	3.9	1.75	8.95	23.66	78.80	
hoclo2	42	420	2.12	0.82	2.44	12.84	102.42	
hoclo	34	340	0.98	0.3	34.54	7.45	34.87	
n2o4	46	480	5.22	2.12	28.52	22.23	45.96	
nh2f	18	281	0.39	0.11	0.83	3.04		
nh2oh	18	298	0.47	0.12	33.38	2.71		
oxadiazole	36	492	4.35	1.48	22.44	13.48		
oxetane	32	596	3.57	1.68	155.49	18.10		
silole	44	730	7.41	3.67	47.21	10.49	22.62	
tetrahydrane	28	504	2.66	1.03	49.44	9.48		
trans-c2f2cl2	64	646	8.03	4.34	51.49	13.35		

Table S24: Linear hydrocarbons TZ (as used in the main text) timings (excluding Hartree-Fock times) in CPU hours for the coupled-cluster methods and GPU hours for AFQMC 0 (scaled to fixed 1 mHa statistical error). DLPNO-CCSD(T) was parallelized with 8 proceses and AFQMC 0 with 80 GPUs.

TZ	Correlated electrons	Basis functions	DLPNO 7	DLPNO 6	CCSD(T)	AFQMC 0
methane	8	138	0.04	0.01	0.01	0.35
ethane	14	230	0.12	0.04	0.12	1.20
propane	20	322	0.31	0.13	7.74	1.62
butane	26	414	0.77	0.43	11.86	3.13
pentane	32	506	1.51	0.81	19.97	3.74
hexane	38	598	2.45	1.63	34.90	10.44
heptane	44	690	4.14	2.65	N/A	14.01
octane	50	782	5.27	3.31	N/A	9.12

Table S25: Linear hydrocarbons QZ (as used in the main text) timings (excluding Hartree-Fock times) in CPU hours for the coupled-cluster methods and GPU hours for AFQMC 0 (scaled to fixed 1 mHa statistical error). DLPNO-CCSD(T) was parallelized with 8 processes (except octane which uses 4) and AFQMC 0 with 160 GPUs.

QZ	Correlated electrons	Basis functions	DLPNO 7	DLPNO 6	CCSD(T)	AFQMC 0
methane	8	264	0.15	0.03	8.90	0.45
ethane	14	436	0.42	0.16	17.19	1.97
propane	20	608	1.39	0.73	279.44	2.42
butane	26	780	3.48	2.26		5.57
pentane	32	952	7.97	4.42		14.23
hexane	38	1124	14.11	10.15		38.66
heptane	44	1296	21.96	13.57		75.81
octane	50	1468	16.46	9.90		191.78

Tables S24 and S25 show CPU and GPU hours for a series of linear hydrocarbons of increasing size using the TZ and QZ basis set as described in the main text. DLPNO-CCSD(T) scales approximately cubically with respect to the number of basis functions (as shown in Figures S3 and S4). CCSD(T) shows a less smooth scaling trajectory possibly due to disk or memory requirement differences. In particular, for hexane we had to reduce the number of parallel processes from 8 to 2 to allow for more memory per process which is expected to decrease the total CPU hours taken. The AFQMC scaling is also more noisy as compression and batching of walkers can cause non-linear changes in calculation speed.

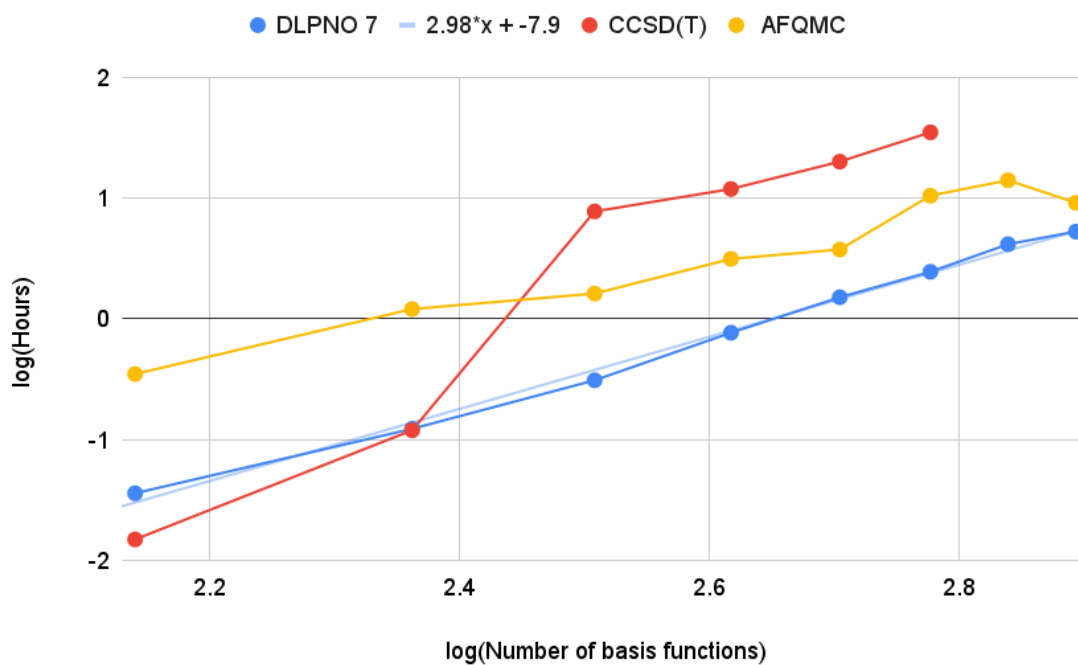


Figure S3: Timings (on a \log_{10} scale) of DLPNO-CCSD(T) with $\text{TCutPNO} = 7$, CCSD(T), and AFQMC 0 in hours (CPU or GPU hours), excluding HF reference generation, of a the series of linear hydrocarbons as written in Table S24. DLPNO-CCSD(T) shows approximately cubic scaling.

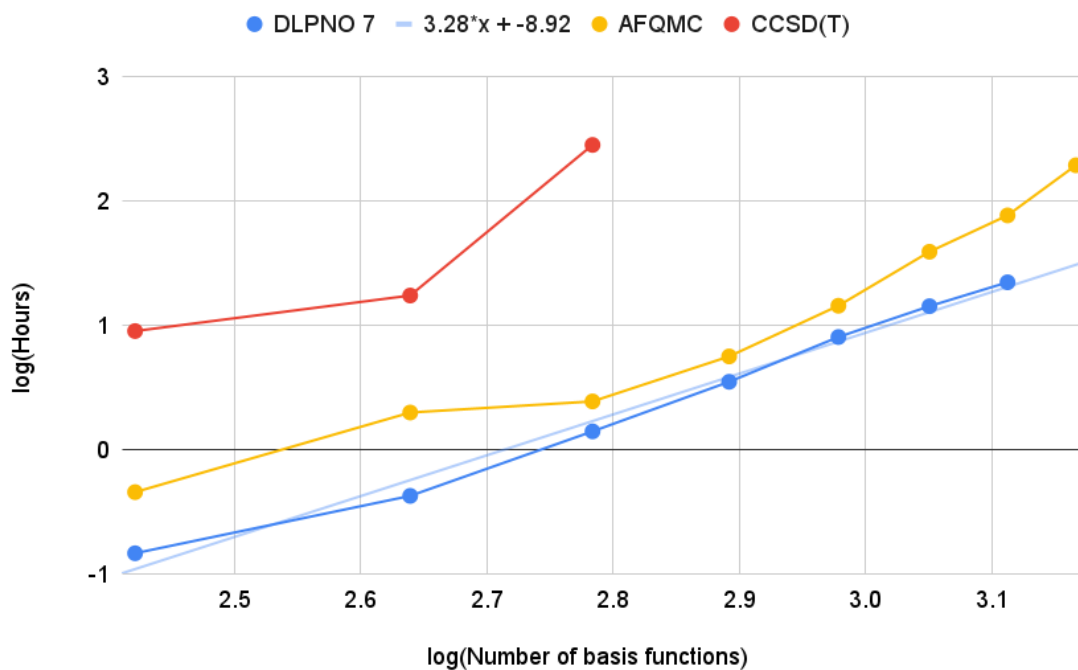


Figure S4: Timings (on a \log_{10} scale) of DLPNO-CCSD(T) with $\text{TCutPNO} = 7$, CCSD(T), and AFQMC 0 in hours (CPU or GPU hours), excluding HF reference generation, of a the series of linear hydrocarbons as written in Table S25. DLPNO-CCSD(T) shows approximately cubic scaling. Octane is not included in the DLPNO-CCSD(T) fit because it required more memory per process so we used 4 parallel threads instead of 8 (as for the rest) as well as allocated more memory.

11. Multireference Diagnostics

In categorizing our datasets, as described in main text Section 2.1, we further identify a multireference (MR) subset from the collection of 259 molecules. The criteria for classifying molecules into the MR subset incorporate a suite of diagnostics: the TAE(T) diagnostic as cited by Karton et al.,¹³ the T_1 ¹⁶ and D_1 ¹⁷ diagnostics, the measure of spin contamination (expressed as $\Delta\langle S^2 \rangle = \langle S^2 \rangle_{\text{unrestricted calculation}} - \langle S^2 \rangle_{\text{exact}}$),^{1,18,19} and the $1 - c_0^2$ ²⁰ metric from CASCI calculations. A molecule is typically classified into the MR category if it demonstrates a $\text{TAE(T)} > 10$, $T_1 > 0.02$, $D_1 > 0.05$, regularized $\Delta\langle S^2 \rangle > 0.05$ ¹ and $1 - c_0^2 > 0.1$. Although no single diagnostic can be solely relied upon to identify the multireference character of a molecule, together, these diagnostics offer detailed insight, with each one emphasizing unique aspects. For example, for the coupled cluster based diagnostics, while T_1 and D_1 are both based on single excitations and are well correlated,²¹ D_1 emphasizes correlation in more local regions of the molecule. Meanwhile, TAE(T) correlates better with CCSDTQ5 energy from connected quadruple and quintuple excitations.¹² On the other hand, spin contamination refers to the mixing of low-lying excited states with higher multiplicity into the ground state, and $1 - c_0^2$ is an indication of the insufficiency of the reference wavefunction for capturing static correlation in CAS methods but limited by the active space. T_1 and D_1 multireference diagnostics are calculated with CCSD and the aug-cc-pVTZ-DK/aug-cc-pCVTZ-DK basis set with frozen core (the same as mentioned in main text Section 2.6 for "TZ"). Spin contamination, $\Delta\langle S^2 \rangle = \langle S^2 \rangle_{\text{PBE0}} - \langle S^2 \rangle_{\text{exact}}$, is carried out using unrestricted Kohn-Sham DFT using the PBE0 functional²² and def2-SVP²³ basis set, as shown by Neugebauer et. al.¹ to be negligibly different from that obtained by a larger basis set. We use the same regularization as Neugebauer, which for closed shell is a factor of $\frac{1}{0.75}$. The $1 - c_0^2$ diagnostic is obtained from the AFQMC 0 leading CI coefficient contribution (c_0) calculated using aug-cc-pVTZ-DK/aug-cc-pCVTZ-DK basis sets (same basis set combination as mentioned in the main text Section 2.6).

To identify the multireference (MR) subset, we initially utilized the TAEMR set as defined by Karton et al.^{12,13}, having a threshold of $\text{TAE(T)} > 10$. From this set, we excluded F2O and Cl2O due to their failure to meet the specified thresholds for across diagnostics, exhibiting relatively low values. Conversely, we included N2O4 in the set because it demonstrated high values for the other criteria. Table S26 presents the finalized MR subset comprising 10 molecules. It details the original dataset to which each molecule

Table S26: List of the molecules we have determined to be MR, their deviations in each respective method AFQMC I, AFQMC II, DLPNO-CCSD(T), and CCSD(T) against reference heat of formation, in kcal/mol. In comparison, the Multireference diagnostics TAE(T), T_1 , D_1 , $\Delta\langle S^2 \rangle$ (regularized),¹ and $1 - c_0^2$ are also shown for each molecule. Multireference molecules are considered as TAE(T) > 10,¹³ $T_1 > 0.02$, $D_1 > 0.05$, regularized $\Delta\langle S^2 \rangle > 0.05$ and $1 - c_0^2 > 0.1$. The list is ordered according to TAE(T) as in Karton et al.¹³

Molecule	Dataset	AFQMC I	AFQMC II	DLPNO	CCSD(T)	TAE(T)	T_1	D_1	$\Delta\langle S^2 \rangle$	$1 - c_0^2$
BN	W4-11	-1.13	-1.13	-0.53	0.85	18.8	0.072	0.197	1.36	0.09
O3	G2	-2.57	-0.96	-3.24	-2.07	17.4	0.027	0.075	0.59	0.10
FOOF	W4-11	-0.69	0.60	-1.12	-0.57	16.9	0.027	0.090	0.00	0.08
ClF5	W4-17	-1.30	-1.30	-0.93	0.12	14.8	0.017	0.054	0	0.01
C2	W4-11	-1.07	-1.07	-1.40	-0.54	13.3	0.038	0.085	1.27	0.18
ClF3	G2	-1.80	-1.80	-1.25	-0.85	12.8	0.018	0.056	0	0.01
ClOOC1	W4-17	-1.38	-1.38	0.47	0.66	12.2	0.019	0.058	0	0.01
S4	W4-11	0.07	-1.44	-1.26	0.66	12.2	0.023	0.089	0.79	0.15
S3	W4-11	-0.71	-0.34	0.05	0.82	10.2	0.022	0.053	0.09	0.07
N2O4	W4-17	-1.47	-1.09	0.03	1.67	9.1	0.021	0.069	0	0.12

belongs (categorized as explained in main text Section 2.1 and listed in the .xlsx document provided), the deviations observed using wavefunction methods, and the values for each MR diagnostic. Although TAE(T) was our primary diagnostic in alignment with the approach of Karton et al., for three molecules in our MR subset (ClF5, ClF3, and ClOOC1), only one additional diagnostic (D_1) surpassed the threshold. For the remainder, at least two diagnostics exceeded the established thresholds. Table S27 lists the MR diagnostics for the entire molecule list.

Table S27: MR diagnostics for the entire combined dataset.

Molecule	T_1	D_1	$\Delta\langle S^2 \rangle$	$1 - c_0^2$
2-butyne	0.0106	0.026	0	0
Acetaldehyde	0.0146	0.047	0	0
Acetylene	0.0130	0.028	0	0
Acetone	0.0136	0.049	0	0
AlCl3	0.0081	0.023	0	0
AlF3	0.0130	0.034	0	0
Allene	0.0121	0.028	0	0
Aziridine	0.0092	0.022	0	0
BCl3	0.0112	0.045	0	0
Benzene	0.0101	0.027	0	0.0140
BF3	0.0123	0.043	0	0

Bicyclo-1-1-0-butane	0.0084	0.016	0	0
CCl2CCl2	0.0108	0.034	0	0.0156
CCl4	0.0106	0.026	0	0
CF2CF2	0.0132	0.041	0	0
CF3-CN	0.0136	0.034	0	0
CF4	0.0120	0.032	0	0
CH2CH-CN	0.0137	0.038	0	0.0087
CH2Cl2	0.0091	0.023	0	0
CH2F2	0.0118	0.029	0	0
CH3-CH2-CH2-Cl	0.0087	0.024	0	0
CH3-CH2-Cl	0.0086	0.023	0	0
CH3-CH2-O-CH3	0.0102	0.027	0	0
CH3-CH2-SH	0.0095	0.022	0	0
CH3-CN	0.0126	0.029	0	0
CH3-O-CH3	0.0102	0.026	0	0
CH3-O-NO	0.0213	0.073	0	0.0188
CH3-S-CH3	0.0095	0.022	0	0
CH3-SH	0.0096	0.021	0	0
CH3-SiH3	0.0100	0.019	0	0
CH3CFO	0.0147	0.049	0	0
CH3Cl	0.0081	0.021	0	0
CH3COCl	0.0147	0.046	0	0
CH3CONH2	0.0147	0.054	0	0
CH3COOH	0.0151	0.054	0	0
CH3NO2	0.0186	0.067	0	0.0266
CH4	0.0076	0.012	0	0
CHCl3	0.0100	0.024	0	0
Cl2	0.0090	0.022	0	0.0098
ClF	0.0129	0.032	0	0.0068
ClF3	0.0182	0.056	0	0.0125
ClNO	0.0217	0.062	0	0.0606
CO	0.0188	0.039	0	0

CO2	0.0183	0.047	0	0
CS	0.0255	0.050	0	0.0303
CS2	0.0200	0.050	0	0.0395
Cyanogen	0.0151	0.029	0	0.0468
Cyclobutane	0.0084	0.018	0	0
Cyclobutene	0.0102	0.029	0	0
Cyclopropane	0.0078	0.017	0	0
Cyclopropene	0.0100	0.029	0	0
Dimethylamine	0.0090	0.023	0	0
Dimethylsulfoxide	0.0158	0.047	0	0
Ethane	0.0079	0.014	0	0
Ethanol	0.0099	0.025	0	0
Ethenone	0.0168	0.046	0	0
Ethylene	0.0108	0.031	0	0
F2	0.0125	0.028	0	0.0153
F2O	0.0165	0.042	0	0
Furan	0.0135	0.043	0	0
Glyoxal	0.0164	0.049	0	0.0150
H2	0.0053	0.008	0	0
H2CO	0.0157	0.045	0	0
H2NNH2	0.0094	0.021	0	0
H2O	0.0102	0.022	0	0
HCF3	0.0123	0.031	0	0
HCl	0.0064	0.012	0	0
HCN	0.0144	0.028	0	0
HCOOCH3	0.0158	0.057	0	0
HCOOH	0.0168	0.054	0	0
HF	0.0102	0.018	0	0
HOCl	0.0120	0.026	0	0
HOOH	0.0127	0.025	0	0
Isobutane	0.0084	0.016	0	0
Isobutene	0.0100	0.031	0	0

Isopropyl-alcohol	0.0100	0.027	0	0
Ketene	0.0168	0.046	0	0
Li2	0.0112	0.027	0	0
LiF	0.0139	0.028	0	0
LiH	0.0070	0.014	0	0
Methanol	0.0100	0.023	0	0
Methylamine	0.0087	0.020	0	0
Methylene-cyclopropane	0.0101	0.031	0	0
N2	0.0134	0.026	0	0
Na2	0.0104	0.041	0	0.0157
NaCl	0.0060	0.017	0	0
NF3	0.0167	0.044	0	0
NH3	0.0084	0.019	0	0
NNO	0.0202	0.048	0	0
OCS-m1	0.0193	0.049	0	0
Oxirane	0.0113	0.028	0	0
Ozone	0.0274	0.075	0.59	0.1024
P2	0.0176	0.033	0	0.0521
PF3	0.0146	0.038	0	0
PH3	0.0137	0.022	0	0
Propane	0.0082	0.015	0	0
Propene-CS	0.0102	0.031	0	0
Propyne	0.0114	0.027	0	0
Pyridine	0.0119	0.034	0	0.0160
Pyrole	0.0112	0.031	0	0
SH2	0.0102	0.018	0	0
Si2H6	0.0129	0.024	0	0
SiCl4	0.0091	0.023	0	0
SiF4	0.0119	0.030	0	0
SiH4	0.0111	0.017	0	0
SiO	0.0264	0.055	0	0
SO2	0.0226	0.059	0	0.0238

Spiropentane	0.0084	0.019	0	0
Thiooxirane	0.0100	0.022	0	0
Thiophene	0.0131	0.037	0	0
Trans-1-3-butadiene	0.0113	0.035	0	0
Trans-butane	0.0084	0.016	0	0
Trans-ethylamine	0.0090	0.023	0	0
Trimethyl-amine	0.0096	0.027	0	0
Vinyl-chloride	0.0106	0.029	0	0
Vynil-fluoride	0.0124	0.029	0	0
1,3-cyclohexadiene	0.0108	0.034	0	0
1,3-DiFluorobenzene	0.0120	0.030	0	0.0080
1,4-DiFluorobenzene	0.0118	0.033	0	0.0188
2-methyl	0.0125	0.038	0	0
2,5-Dihydrothiophene	0.0112	0.029	0	0
3-methyl	0.0087	0.017	0	0
Acetic	0.0157	0.052	0	0
azulene	0.0116	0.042	0	0.0606
benzoquinone	0.0158	0.061	0	0.0300
c2f6	0.0127	0.038	0	0
C4H4N2	0.0115	0.028	0	0.0358
C4H6	0.0113	0.029	0	0
C4H6O	0.0133	0.040	0	0
C4H8O2	0.0117	0.033	0	0
C5H8	0.0109	0.033	0	0
C6H12	0.0088	0.017	0	0
C6H5-CH3	0.0100	0.027	0	0.0035
C6H5-NH2	0.0113	0.034	0	0
C6H5-OH	0.0116	0.034	0	0
cf3cl	0.0120	0.033	0	0
CH3_2CH-CHO	0.0128	0.048	0	0
CH3_2CH-CN	0.0112	0.029	0	0

CH3_2CH-O- CH_CH3_2	0.0102	0.031	0	0
CH3_3C-NH2	0.0092	0.025	0	0
CH3_3C-O-CH3	0.0102	0.029	0	0
CH3_3C-SH	0.0096	0.024	0	0
CH3-C_O_-CCH	0.0150	0.048	0	0.0090
CH3-C_O_-O- CH_CH3_2	0.0135	0.058	0	0
CH3-C_O_-OCH3	0.0146	0.057	0	0
CH3-CH_OCH3_2	0.0113	0.034	0	0
CH3-CH2-CH_CH3_- NO2	0.0155	0.068	0	0.0248
CH3-CH2-CO-CH2-CH3	0.0124	0.049	0	0
CH3-CH2-O-CH2-CH3	0.0101	0.028	0	0
CH3-CH2-S-S-CH2-CH3	0.0112	0.029	0	0
CH3-CHCH-CHO	0.0145	0.052	0	0.0096
CH3-CO-CH2-CH3	0.0129	0.049	0	0
Chlorobenzene	0.0102	0.026	0	0.0144
Cl2O2S	0.0182	0.061	0	0.0069
Cl2S2	0.0185	0.056	0	0.0131
cyclooctatetraene	0.0116	0.033	0	0
cyclopentane	0.0088	0.018	0	0
cyclopentanone	0.0129	0.051	0	0
dimethyl	0.0164	0.050	0	0
Fluorobenzene	0.0112	0.028	0	0.0049
n-Butyl	0.0088	0.024	0	0
n-heptane	0.0083	0.017	0	0
n-hexane	0.0086	0.016	0	0
N-methyl	0.0110	0.033	0	0
n-octane	0.0083	0.017	0	0
n-pentane	0.0085	0.016	0	0
Naphthalene	0.0100	0.032	0	0.0293

NC-CH2-CH2-CN	0.0130	0.029	0	0
Neopentane	0.0086	0.017	0	0
P4	0.0184	0.038	0	0
para-cyclohexadiene	0.0107	0.028	0	0
PCl3	0.0131	0.035	0	0
PCl5	0.0116	0.033	0	0
Perhydropyridine	0.0096	0.027	0	0
pf5	0.0125	0.037	0	0
POCl3	0.0143	0.044	0	0
pyrimidine	0.0146	0.045	0	0.0183
SCl2	0.0127	0.033	0	0
sf6	0.0128	0.032	0	0
SiCl2	0.0133	0.037	0	0.0106
SO3	0.0183	0.056	0	0.0138
t-butanol	0.0099	0.028	0	0
t-Butyl	0.0092	0.027	0	0
tetrahydrofuran	0.0104	0.028	0	0
Tetrahydropyran	0.0104	0.031	0	0
Tetrahydropyrrole	0.0096	0.026	0	0
Tetrahydrothiophene	0.0101	0.025	0	0
Tetrahydrothiopyran	0.0100	0.024	0	0
Tetramethylsilane	0.0093	0.020	0	0
alcl	0.012	0.026	0	0
alf	0.016	0.029	0	0
alh	0.014	0.026	0	0
alh3	0.008	0.015	0	0
b2h6	0.010	0.018	0	0
bf	0.016	0.030	0	0
bh	0.014	0.026	0.33	0
bh3	0.006	0.010	0	0
bhf2	0.013	0.043	0	0
c-hono	0.022	0.065	0	0.0214

c-n2h2	0.013	0.033	0	0.0118
ch2nh	0.012	0.034	0	0
ch3f	0.010	0.021	0	0
clcn	0.014	0.028	0	0
dioxirane	0.015	0.035	0	0
f2co	0.015	0.050	0	0
fccf	0.013	0.030	0	0
hccf	0.013	0.026	0	0
hcn	0.021	0.052	0	0
hcof	0.016	0.048	0	0
hnco	0.018	0.052	0	0
hnnn	0.020	0.054	0	0
hno	0.016	0.042	0.37	0.0200
hocn	0.015	0.033	0	0
hof	0.014	0.035	0	0
nh2cl	0.010	0.024	0	0
oxirene	0.014	0.032	0	0
s2o	0.023	0.061	0	0.0450
sih3f	0.011	0.023	0	0
t-hono	0.022	0.062	0	0.0203
t-n2h2	0.013	0.033	0	0
c2h5f	0.010	0.023	0	0
bn	0.072	0.197	1.36	0.0923
c2	0.038	0.085	1.27	0.1779
cl2o	0.015	0.044	0	0
foof	0.027	0.090	0	0.0812
s3	0.022	0.053	0.09	0.0685
s4-c2v	0.023	0.089	0.79	0.1518
clf5	0.017	0.054	0	0.0055
cloocl	0.019	0.058	0	0.0132
beta-lactim	0.013	0.045	0	0
borole	0.012	0.034	0	0

c2cl2	0.011	0.025	0	0
c2cl6	0.011	0.027	0	0
c2clh	0.012	0.026	0	0
ccl2o	0.015	0.047	0	0
cf2cl2	0.012	0.033	0	0
ch2clf	0.011	0.028	0	0
ch3ph2	0.012	0.024	0	0
cis-c2f2cl2	0.012	0.038	0	0
clcof	0.015	0.049	0	0
cyclobutadiene	0.012	0.040	0.21	0
cyclopentadiene	0.011	0.033	0	0
dioxetan2one	0.016	0.058	0	0
dioxetane	0.011	0.029	0	0
dithiotane	0.011	0.025	0	0
fno	0.022	0.062	0	0.0256
formamide	0.016	0.053	0	0
formic-anhydride	0.017	0.049	0	0
hclo4	0.019	0.062	0	0.0086
hoclo2	0.024	0.077	0	0.0094
hoclo	0.024	0.085	0	0.0083
n2o4	0.021	0.069	0	0.1193
nh2f	0.012	0.031	0	0
nh2oh	0.011	0.024	0	0
oxadiazole	0.018	0.063	0	0.0219
oxetane	0.010	0.029	0	0
silole	0.013	0.032	0	0.0075
tetrahydrane	0.009	0.017	0	0
trans-c2f2cl2	0.012	0.039	0	0

12. CCSD(T) DLPNO-CCSD(T) Correlation

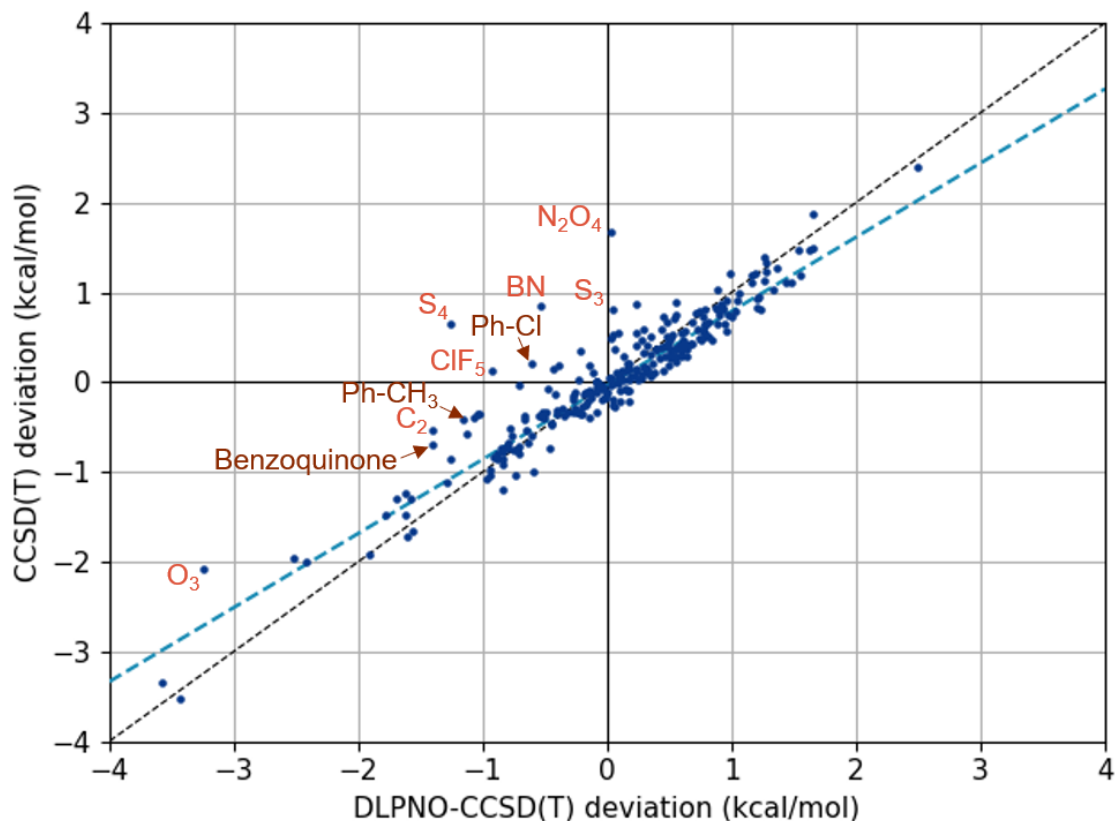


Figure S5: Correlation between DLPNO-CCSD(T) and CCSD(T) deviation of heat of formation from the reference value. DLPNO-CCSD(T) results show overall higher unsigned deviation than CCSD(T), as the line of best fit (blue dashed line) shows a smaller slope (0.83) than the 1:1 line (black dashed line). The coefficient of determination for the DLPNO-CCSD(T) correlation is $R^2 = 0.86$. The molecules with the top 10 largest differences between the CCSD(T) and DLPNO deviations for heat of formation are marked on the graph, where light red indicates multireference molecules (see Table S26) and dark red indicates single-reference molecules. These 10 molecules all above below the line $y = x$, which means that the DLPNO-CCSD(T) heat of formation is higher than the CCSD(T) heat of formation.

Despite the overall accuracy of DLPNO-CCSD(T), there are cases where it does not capture all of the correlation compared to CCSD(T) such as multireference molecules and molecules where electrons are strongly delocalized. The DLPNO-CCSD(T) and CCSD(T) results show a strong positive correlation with a coefficient of determination of the line of best fit $R^2 = 0.86$, as depicted in Figure S5 which plots CCSD(T) deviations against DLPNO-CCSD(T) deviations for the entire dataset. In the top 10 cases where DLPNO-CCSD(T) deviates from CCSD(T), 7 of them are from our MR subset of 10 molecules (refer to Table S26), and the remaining 3 are molecules with considerable electron delocalization. Table 3

in the main text lists these molecules in order of absolute atomization energy difference (or difference in deviation) of DLPNO-CCSD(T) and CCSD(T) methods. These cases possibly suggest components of correlation that DLPNO, as an approximation to CCSD(T), is unable to capture. Additionally, the largest deviations of DLPNO-CCSD(T) from CCSD(T) lie above the equivalence line (black dashed line), meaning that the atomization energy of DLPNO-CCSD(T) (opposite in sign to heat of formation) is lower than that of CCSD(T), i.e. the molecule single point energy (effectively, the correlation energy) is underestimated, even after accounting for differences in atomic energies.

13. AFQMC 0 Outliers

Table S28: Details (G2 and G3 set) for the outliers of AFQMC 0 protocol. Deviation from experimental heat of formation is listed in kcal/mol with statistical error in parentheses. After the first CI is run with an active space based on orbital maps to the atoms of the molecules (refer Table S4) that returns the ‘First CI AS’ listed, the second AS (shown here as ‘TZ final AS’ and ‘QZ final AS’, as the NOONs have a slight basis set dependency due to approximations such as the SHCI solver) is chosen from those orbitals from the first AS that have NOONs of between 0.01 and 1.99. The final number of determinants is determined by the number of determinants to get to 99.5% CI coefficient. Statistical errors are shown using parentheses.

Molecule	Dataset	Deviation	First CI AS	TZ final AS	QZ final AS	TZ final #dets	QZ final #dets
Bicyclo-1-1-0-butane	G2	-2.49(48)	8e+8e,16o	1e+1e,1o	1e+1e,1o	1	1
CLF3	G2, MR	2.42(65)	14e+14e,16o	1e+1e,2o	1e+1e,2o	2	2
F2	G2	-2.80(43)	7e+7e,8o	1e+1e,2o	1e+1e,2o	2	2
F2O	G2	-2.56(70)	10e+10e,12o	1e+1e,1o	1e+1e,1o	1	1
Li2	G2	-2.28(19)	1e+1e,2o	1e+1e,1o	1e+1e,1o	1	1
LiF	G2	3.38(39)	4e+4e,5o	1e+1e,1o	1e+1e,1o	1	1
OCS-m1	G2	3.25(67)	8e+8e,12o	1e+1e,1o	1e+1e,1o	1	1
Ozone	G2, MR	-5.05(51)	9e+9e,12o	2e+2e,3o	2e+2e,3o	3	3
Thiooxirane	G2	2.04(46)	7e+7e,12o	1e+1e,1o	1e+1e,1o	1	1
Trans-1-3-butadiene	G2	-2.03(55)	8e+8e,16o	1e+1e,1o	1e+1e,1o	1	1
1,3-cyclohexadiene	G3	-2.11(61)	12e+12e,24o	1e+1e,1o	1e+1e,1o	1	1
Acetic	G3	2.10(87)	17e+17e,28o	1e+1e,1o	1e+1e,1o	1	1
azulene	G3	2.65(74)	20e+20e,40o	3e+3e,5o	3e+3e,5o	12	11
C4H4N2	G3	-2.39(65)	13e+13e,24o	2e+2e,4o	2e+2e,4o	7	6
3-butyn-2-one	G3	-4.27(57)	11e+11e,20o	1e+1e,2o	1e+1e,2o	2	2
CH3-CH2-CO-CH2-CH3	G3	2.22(65)	13e+13e,24o	1e+1e,1o	1e+1e,1o	1	1
pyrimidine	G3	3.51(53)	13e+13e,24o	2e+2e,4o	1e+1e,3o	6	1

In Table S28, we list all the outliers from the G2 and G3 datasets for heat of formation, using the AFQMC 0 protocol, and their deviations from the experimental references in kcal/mol, alongside the active spaces of the first CI, and the second (and final) CI after applying the NOON cutoff. The final active spaces determine the number of determinants, which we pick as the number of determinants required to retain 99.5% of the CI weight. The final active spaces, and determinants chosen, for the TZ and QZ basis sets (see Section 2.6 for the exact "TZ" and "QZ" basis sets used) can be slightly different due to approximations such as the semistochastic heat bath, as well as basis set artefacts such as linear dependencies. Similarly, Table S29 shows the list of W4 molecules and their deviations.

Table S29: Details (W4 set) for AFQMC 0 outliers where after the first CI is run, the second AS is chosen from those orbitals from the first AS that have NOONs of between 0.01 and 1.99. The final number determinants is determined by the number of determinants to get to 99.5% CI coefficient. Refer to Table S28 for molecules in the G2 and G3 datasets.

Molecule	Dataset	Deviation	First CI AS	TZ final AS	QZ final AS	TZ final #dets	QZ final #dets
f2co	W4-11	2.32(62)	12e+12e,16o	1e+1e,1o	1e+1e,1o	1	1
hnco	W4-11	2.63(70)	7e+7e,12o	1e+1e,1o	1e+1e,1o	1	1
bn	W4-11, MR	-10.51(61)	4e+4e,8o	1e+1e,2o	1e+1e,2o	2	2
c2	W4-11, MR	-14.62(43)	4e+4e,8o	1e+1e,2o	1e+1e,2o	2	2
clf5	W4-17, MR	3.13(104)	21e+21e,24o	1e+1e,2o	1e+1e,1o	2	1
clcof	W4-17	3.00(72)	12e+12e,16o	1e+1e,1o	1e+1e,1o	1	1
cyclobutadiene	W4-17	-2.04(68)	8e+8e,16o	1e+1e,1o	1e+1e,1o	1	1
dioxetan3one	W4-17	3.04(80)	13e+13e,20o	1e+1e,1o	1e+1e,1o	1	1
hclo4	W4-17	4.16(82)	15e+15e,20o	1e+1e,2o	1e+1e,1o	1	1
hoclo2	W4-17	2.65(71)	12e+12e,16o	1e+1e,2o	1e+1e,1o	1	1
hoclo	W4-17	2.15(64)	9e+9e,12o	1e+1e,2o	1e+1e,1o	1	1
n2o4	W4-17, MR	-2.48(76)	17e+17e,24o	7e+7e,10o	7e+7e,10o	70	60
silole	W4-17	-2.19(52)	10e+10e,20o	1e+1e,2o	1e+1e,1o	2	1

References

- (1) Neugebauer, H.; Vuong, H. T.; Weber, J. L.; Friesner, R. A.; Shee, J.; Hansen, A. Toward Benchmark-Quality Ab Initio Predictions for 3d Transition Metal Electrocatalysts: A Comparison of CCSD (T) and ph-AFQMC. *J. Chem. Theory Comput.* **2023**, *19*, 6208–6225.
- (2) Rudsteyn, B.; Weber, J. L.; Coskun, D.; Devlaminck, P. A.; Zhang, S.; Reichman, D. R.; Shee, J.; Friesner, R. A. Calculation of metallocene ionization potentials via auxiliary field quantum Monte Carlo: Toward benchmark quantum chemistry for transition metals. *J. Chem. Theory Comput.* **2022**, *18*, 2845–2862.
- (3) Lee, J.; Pham, H. Q.; Reichman, D. R. Twenty Years of Auxiliary-Field Quantum Monte Carlo in Quantum Chemistry: An Overview and Assessment on Main Group Chemistry and Bond-Breaking. *J. Chem. Theory Comput.* **2022**, *18*, 7024–7042.
- (4) Martin, J. M. Ab initio total atomization energies of small molecules — towards the basis set limit. *Chem. Phys. Lett.* **1996**, *259*, 669–678.
- (5) Weber, J. L.; Vuong, H.; Devlaminck, P. A.; Shee, J.; Lee, J.; Reichman, D. R.; Friesner, R. A. A Localized-Orbital Energy Evaluation for Auxiliary-Field Quantum Monte Carlo. *J. Chem. Theory Comput.* **2022**, *18*, 3447–3459.

- (6) Wang, M.; He, X.; Taylor, M.; Lorpaiboon, W.; Mun, H.; Ho, J. Molecular Geometries and Vibrational Contributions to Reaction Thermochemistry Are Surprisingly Insensitive to the Choice of Basis Sets. *Journal of Chemical Theory and Computation* **2023**, *19*, 5036–5046, PMID: 37463146.
- (7) Bakowies, D.; von Lilienfeld, O. A. Density Functional Geometries and Zero-Point Energies in Ab Initio Thermochemical Treatments of Compounds with First-Row Atoms (H, C, N, O, F). *Journal of Chemical Theory and Computation* **2021**, *17*, 4872–4890, PMID: 34260240.
- (8) Martin, J. M. L.; de Oliveira, G. Towards standard methods for benchmark quality ab initio thermochemistry—W1 and W2 theory. *The Journal of Chemical Physics* **1999**, *111*, 1843–1856.
- (9) Semidalas, E.; Martin, J. M. L. Can G4-like composite Ab Initio methods accurately predict vibrational harmonic frequencies? *Molecular Physics* **2024**, *122*, e2263593.
- (10) Chan, B.; Ho, J. Simple Composite Approach to Efficiently Estimate Basis Set Limit CCSD(T) Harmonic Frequencies and Reaction Thermochemistry. *The Journal of Physical Chemistry A* **2023**, *127*, 10026–10031, PMID: 37970798.
- (11) Nelson, P. M.; Glick, Z. L.; Sherrill, C. D. Approximating large-basis coupled-cluster theory vibrational frequencies using focal-point approximations. *The Journal of Chemical Physics* **2023**, *159*, 094104.
- (12) Karton, A.; Daon, S.; Martin, J. M. W4-11: A high-confidence benchmark dataset for computational thermochemistry derived from first-principles W4 data. *Chem. Phys. Lett.* **2011**, *510*, 165–178.
- (13) Karton, A.; Sylvetsky, N.; Martin, J. M. L. W4-17: A diverse and high-confidence dataset of atomization energies for benchmarking high-level electronic structure methods. *J. Comput. Chem.* **2017**, *38*, 2063–2075.
- (14) Curtiss, L. A.; Raghavachari, K.; Redfern, P. C.; Pople, J. A. Assessment of Gaussian-2 and density functional theories for the computation of enthalpies of formation. *J. Chem. Phys.* **1997**, *106*, 1063–1079.

- (15) ACCESS Allocations: Exchange Calculator. https://allocations.access-ci.org/exchange_calculator (accessed 2024-04-30).
- (16) Lee, T. J.; Taylor, P. R. A diagnostic for determining the quality of single-reference electron correlation methods. *Int. J. Quantum Chem* **1989**, *36*, 199 – 207, Cited by: 1978; All Open Access, Green Open Access.
- (17) Janssen, C. L.; Nielsen, I. M. B. New diagnostics for coupled-cluster and Møller Plesset perturbation theory. *Chem. Phys. Lett.* **1998**, *290*, 423–430.
- (18) Pulay, P.; Hamilton, T. P. UHF natural orbitals for defining and starting MC-SCF calculations. *J. Chem. Phys.* **1988**, *88*, 4926–4933.
- (19) Lee, J.; Head-Gordon, M. Distinguishing artificial and essential symmetry breaking in a single determinant: approach and application to the C60, C36, and C20 fullerenes. *Phys. Chem. Chem. Phys.* **2019**, *21*, 4763–4778.
- (20) Langhoff, S. R.; Davidson, E. R. Configuration interaction calculations on the nitrogen molecule. *Int. J. Quantum Chem.* **1974**, *8*, 61–72.
- (21) Wang, J.; Manivasagam, S.; Wilson, A. K. Multireference Character for 4d Transition Metal-Containing Molecules. *J. Chem. Theory Comput.* **2015**, *11*, 5865–5872.
- (22) Weigend, F.; Ahlrichs, R. Balanced basis sets of split valence, triple zeta valence and quadruple zeta valence quality for H to Rn: Design and assessment of accuracy. *Phys. Chem. Chem. Phys.* **2005**, *7*, 3297.
- (23) Adamo, C.; Barone, V. Toward reliable density functional methods without adjustable parameters: The PBE0 model. *J. Chem. Phys.* **1999**, *110*, 6158–6170.